A theoretical and experimental study of atmospheric reactions of amines and their degradation products

Arne Joakim Coldevin Bunkan

2014

Dissertation for the degree of philosophiae doctor (PhD)

Department of Chemistry, Faculty of Mathematics and Natural Sciences
University of Oslo, Norway

Series of dissertations submitted to the
Faculty of Mathematics and Natural Sciences, University of Oslo
No. 1588

ISSN 1501-7710

Cover: Hanne Baadsgaard Utigard.
Printed in Norway: AIT Oslo AS.

Produced in co-operation with Akademika Publishing.
The thesis is produced by Akademika Publishing merely in connection with the thesis defence. Kindly direct all inquiries regarding the thesis to the copyright holder or the unit which grants the doctorate.

Abstract

Amine-based CO_2 capture has been proposed as a way of mitigating climate change. In this work, the fundamental processes governing the atmospheric gas phase chemistry of amines released from CO_2 capture have been studied using computational and experimental methods.

The reactions of amines, amides and imines with OH radicals have been studied with computational methods. The reactions are all characterized by strongly bound pre-reaction complexes and submerged barriers to hydrogen abstraction. Rate coefficients calculated from statistical rate theory show negative temperature dependencies and are in good agreement with experimental results where available.

It has been suggested that the climate effect of amine based CO_2 capture may be counteracted by the formation of N_2O as a minor product in the photo-oxidation of methylamine. Calculations in this work unambiguously show that N_2O is not a product in the photo-oxidation of methylamine.

The reaction rate coefficients for the OH radical reactions of *N*-methylformamide and *N,N*-dimethylformamide have been measured as a function of temperature and pressure by using the flash photolysis laser-induced fluorescence technique. The reactions are significantly slower than the corresponding amine reactions and show a negative temperature dependence. The study further reveals that the amides have a higher potential for nitramine and nitrosamine formation and that they may therefore constitute a previously undisclosed health risk.

Kinetic isotope effects for the OH radical reaction of HCN have been measured in a smog chamber through the use of FTIR spectroscopy. The measured values and calculated results confirm that the reaction, unlike the other reactions in this work, mainly occur through an addition channel.

The present work has contributed significantly to our understanding of the atmospheric reactions of the intermediates in the atmospheric degradation of methyl amines.

Preface

This work was carried out at the Centre for Theoretical and Computational Chemistry at the Department of Chemistry, University of Oslo during 2010-2014.

I would first like to thank my supervisor, Professor Claus Jørgen Nielsen, for all his support and encouragement throughout this work and for trusting me with the responsibility of lecturing. I am also grateful to my co-supervisors, Professor Einar Uggerud and Professor Trygve Helgaker for all helpful advice and good discussions.

I would further like to thank Professor Michael Pilling for introducing me to theoretical kinetics, the members of the CTCC and the physical chemistry group for creating an inspiring work environment, the other authors of the papers in this thesis for the work we have done together and Glenn and Martin for proofreading my thesis.

Professor Matthias Olzmann and the molecular physical chemistry group at Karlsruhe Institute of Technology are gratefully acknowledged. I had a wonderful year in Germany and this work would not have been the same without you.

Two persons who deserve special mention are Carl Otto Veidahl and Leif Thore Jelmert at Kristelig Gymnasium. Without you, I would not have studied chemistry in the first place.

Last, but not least, I would like to thank my friends and family for always being there for me.

List of papers

The thesis is based on the work presented in the following papers. A copy of each paper can be found at the end of the thesis.

I Onel, L.; Thonger, L.; Blitz, M. A.; Seakins, P. W.; Bunkan, A. J. C.; Solimannejad, M.; Nielsen, C. J. Gas-Phase Reactions of OH with Methyl Amines in the Presence or Absence of Molecular Oxygen. An Experimental and Theoretical Study. *The Journal of Physical Chemistry A* **2013**, *117*, 10736-10745.

II Nicovich, J. M.; Mazumder, S; Laine, P. L.: Wine, P. H.; Tang, Y.; Bunkan, A. J. C.; Nielsen, C. J. An experimental and theoretical study of the gas phase kinetics of atomic chlorine reactions with CH_3NH_2, $(CH_3)_2NH$, and $(CH_3)_3N$. *Physical Chemistry Chemical Physics* **2014**. *Submitted*

III Bunkan, A. J. C; Hetzler, J; Mikoviny, T; Wisthaler, A; Nielsen, C. J.; Olzmann, M. Experimental and theoretical study of the OH radical reactions with *N*-methylformamide and *N,N*-dimethylformamide. *Manuscript in preparation*

IV Bunkan, A. J. C.; Tang, Y. and Sellevåg, S. R. and Nielsen, C. J. Atmospheric Gas Phase Chemistry of CH_2=NH and HNC. A First-Principles Approach. *The Journal of Physical Chemistry A* **2014**, 118, 5279-5288.

V Maguta, M. M.; Aursnes, M. Bunkan, A. J. C.; Edelen, K.; Mikoviny, T; and Nielsen, C. J.; Stenstrøm, Y; Tang, Y; Wisthaler, A. Atmospheric Fate of Nitramines: An Experimental and Theoretical Study of the OH Reactions with CH_3NHNO_2 and $(CH_3)_2NNO_2$. *The Journal of Physical Chemistry A* **2014**, *118*, 3450-3462.

VI Bunkan, A. J. C.; Liang, C.-H.; Pilling, M. J.; Nielsen, C. J. Theoretical and experimental study of the OH radical reaction with HCN. *Molecular Physics* **2013**, *111*, 1589-1598.

Contents

Chapter 1

Introduction

In his new year speech in 2007, the Norwegian prime minister Jens Stoltenberg announced that the the gas power plant at Mongstad were to be constructed with a CO_2 capture facility, that all technology necessary would be developed within 7 years and that this great project were to be the Norwegian "moon landing" [1]:

> Vi må ta vårt ansvar. Klimautslippene må ned. Norge påtar seg en pionerrolle når vi har bestemt at gasskraftverket på Mongstad skal ha rensing av klimagassen CO2. Vi skal gjøre dette mulig. Da president Kennedy sa at amerikanerne skulle lande på månen innen 10 år, hadde ikke amerikanerne vært ute i verdensrommet. De kom til månen innen 10 år. De satte seg mål. Og de nådde målene. Vår visjon er at vi innen 7 år skal få på plass den teknologien som gjør det mulig å rense utslipp av klimagasser. Det blir et viktig gjennombrudd for å få ned utslippene i Norge, og når vi lykkes tror jeg verden vil følge etter. Dette er et stort prosjekt for landet. Det er vår månelanding."

At that time, very little was known about the possible environmental and health consequences of amine based CO_2 capture, hence several large research projects were initiated with the goal of providing fundamental knowledge about the processes necessary for a complete understanding of the risks and consequences of using amines for CO_2 capture. The literature on the atmospheric chemistry of amines was very scarce, with only a few measurements and studies of their OH radical reactions. The amines themselves are not particularly harmful, but there was concern that highly carcinogenic nitramines and nitrosoamines could be formed during their atmospheric degradation and in 2011, the Norwegian Institute of Public Health published a review,

"Health effects of amines and derivatives associated with CO_2 capture", reviewing available toxicology data for these compounds [2].

To ensure the public a negligible risk of cancer from exposure to nitramines and nitrosamines, the total amount of these compounds in air and water should be kept at very low levels and it is therefore essential to quantify all processes leading to nitramine and nitrosamine formation, including the actual emission rates, atmospheric transport, phase transfer, reaction kinetics and product distributions.

In this thesis, computational and experimental techniques have been applied to contribute to a fundamental understanding of the processes that dominate the gas phase chemistry of emissions from amine based CO_2 capture facilities.

1.1 The atmosphere

The earth's atmosphere is a complex chemical and physical system consisting of the main components nitrogen, oxygen and argon, as well as a large number of gases known as the atmospheric trace gases. The concentrations of the main components changes very little over time and are not influenced by human activity, whereas the trace gases are products of both natural and anthropogenic processes, and their concentrations show large spatial and temporal variation.

The earth's atmosphere is conveniently divided into several layers, of which the lowest is called the troposphere and reaches to the temperature inversion point, called the tropopause. The troposphere is only a small fraction of the total atmospheric volume, but accounts for 80% of its total mass and almost 99% of its water vapor. Because of the temperature inversion in the stratosphere, the mixing between the troposphere and the stratosphere is normally slow and only trace gases with lifetimes of several years enter the stratosphere. It is therefore sufficient to consider only the tropospheric chemistry of all but the most long-lived emitted trace gases.

1.2 Tropospheric processes

An important concept in atmospheric chemistry is the lifetime or atmospheric residence time, τ, of a molecule, defined as the average time a molecule remains in the atmosphere [3]. The lifetime can be expressed as the ratio of the amount of the compound present, m, to the loss rate, L.

$$\tau = \frac{m}{L} \tag{1.1}$$

There are in principle three different classes of processes that influence the life times of a trace gas emitted to the atmosphere: i) direct chemical loss, ii) photolysis and iii) deposition on particles, water droplets, and other surfaces. For most compounds, chemical loss trough reaction with the OH radical is the most important sink [4]. In the troposphere, OH radicals are mainly generated from photolysis of ozone in the presence of water:

$$O_3 + h\nu \rightarrow O(^1D) + O_2 \tag{1.2}$$

$$O(^1D) + H_2O \rightarrow 2OH \tag{1.3}$$

Other loss processes include reaction with chlorine atoms, ozone, and NO_3 radicals. OH radicals and chlorine atoms are only present in significant concentrations at daytime as they are generated photolytically and have short lifetimes. The NO_3 radical on the other hand, photolyzes rapidly and does therefore only constitute a significant sink at night [5].

The concentration of chlorine atoms is typically highest in marine areas and the concentration in the marine boundary layer has been reported to be 1-10 per cent of the OH concentration [6] with suggested average day time concentrations in the North Atlantic air mass of $6{\times}10^4$ cm^{-3} [7].

In order to compare the importance of the possible atmospheric sinks and to estimate the atmospheric residence times of the different trace gases, the following oxidant concentrations are assumed throughout this thesis: $[OH]_{24h} = 10^6$ cm^{-3}, $[O_3]_{24h} = 10^{12}$ cm^{-3}, $[Cl]_{12h} = 2 \times 10^3$ cm^{-3} and $[NO_3]_{12h} = 10^8$ cm^{-3}

1.3 Amines in the atmosphere

Amines in the atmosphere originate from a variety of sources including animal husbandry, food processing, marine sources and biomass burning [8]. However, with the proposed use of monoethanolamine (MEA) and other amines in post combustion carbon capture [9], the emissions are expected to increase. The emissions of the alkyl amines are also expected to increase as they are formed from degradation of larger amines during the capture/desorption process [10, 11].

1.3.1 Photo-oxidation of amines

The atmospheric degradation of amines is dominated by reaction with the OH radical [11] which occurs through abstraction from either a C-H site or a N-H site. Abstraction from a C-H site generally gives amides and imines as main products, and the main product from N-H abstraction is usually an imine. Depending on the NO_x concentrations, N centered imino radicals may also react to form nitramines and nitrosamines. It has also been suggested that photo-oxidation of methylamine might give N_2O as a product [12], and that eventual emissions of methylamine may therefore counteract the net climate effect of amine based CO_2 capture [13].

Figure 1.1 shows the main routes in the OH initiated photo-oxidation of dimethylamine. Abstraction from the amino group gives *N*-methylmethanimine as main product and *N,N*-nitrosodimethylamine and *N,N*-nitrodimethylamine as minor products, depending on the NO_x levels. Abstraction from the methyl groups gives *N*-methylmethanimine, *N*-methylformamide, formamide and methanimine as main products.

The reactions of aliphatic amines with OH radicals are very fast and their lifetimes with respect to the OH radical reaction are typically less than one day.

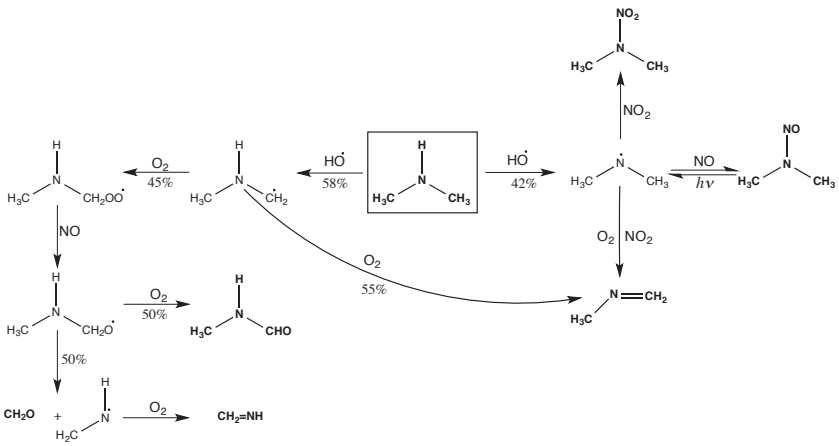

Figure 1.1: Main routes in the OH initiated photo-oxidation of dimethylamine. Adapted from Nielsen *et al.*, ref [14]

1.3.2 Imines

The main oxidation products of amines in the atmosphere are the imines [11]. Very little is known about the atmospheric chemistry of the imines and both gas phase oxidation and heterogenous processes may be important. There are no published studies on the OH radical reactions of imines, but there is a single study of the chlorine atom reaction reaction of *N*-methylmethanimine [15], showing the reaction to be fast with $k = (1.9 \pm 0.15) \times 10^{-11}$cm^3 molecule^{-1} s^{-1}. Inspection of available kinetic data [11] reveals that the reactions of chlorine atoms with nitrogen-containing VOCs in the atmosphere are, as a rough rule of thumb, a factor of 10 faster than the corresponding OH radical reaction. Assuming this also holds for the imines and that *N*-methylmethanimine is representative for imines, their lifetime respect to the OH radical reaction can therefore be assumed to be around 6 days.

1.3.3 Amides

In addition to being important high volume production chemicals, amides also constitute the other major group of atmospheric photo-oxidation products of amines. Their atmospheric chemistry was recently reviewed by Barnes *et al.* [16] The reactions with OH radicals are fast with typical atmospheric lifetimes of around 1 day and they give rise to some of the same photo-oxidation products as the amines, including nitramines and nitrosamines.

1.3.4 Nitrosamines

Nitrosamines have been reported to be minor photo-oxidation products of amines. They are known to be highly carcinogenic and the Norwegian Institute of Public Health has recommended that the total amount of nitramines and nitrosamines should not exceed 40 ng/L in drinking water or 0.3 ng/m^3, corresponding to around 0.1 ppt for dimethylnitrosamine, in air [2]. Since the nitrosamines photolyze rapidly, as already shown in Figure 1.1, they do not accumulate in the atmosphere [17, 18], but there is concern that they might rain out and end up in drinking water [19].

1.3.5 Nitramines

Nitramines are formed in the atmospheric photo-oxidation of amines, as illustrated for dimethylamine in Figure 1.1. Not much is known about the health effects of nitramines, but they are suspected to be both carcinogens and mutagens. Due to the lack of toxicity data, the Norwegian Institute of

Public Health has recommended that the nitramines should be included in the suggested maximum values for nitrosamines [2].

1.4 Objectives and research tasks

The overall goal of this work is to ontribute to the fundamental understanding of the elementary processes involved at the microscopic level and to develop detailed chemical mechanisms for the atmospheric photo-oxidation of amines emitted to air from industrial CO_2 capture plants. To achieve this, the following research objectives are defined:

- Contribute to our understanding of the elementary steps in the photo-oxidation of amines by studying the reactions of the methyl amines and their primary and secondary oxidation products with quantum chemical methods and statistical rate theory
- Increase our knowledge about the applicability of standard quantum chemical methods to the study of the atmospheric reactions of nitrogen containing trace gases by comparing experimental and theoretical results for a wide range of reactions
- Measure the rate coefficients of selected reactions relevant for the photo-oxidation of methyl amines

The strategy is to apply high level quantum chemistry methods to characterize the potential energy surfaces of all reactions in this study. The calculations are to be as accurate as possible, but still affordable for systems of real atmospheric interest. The quantum chemical calculations are to be linked to experimental data, when available, through the use of statistical rate theory. Only when the quantum chemical and kinetic methods are proven to be reliable for systems where experimental data is available, can they also be used with confidence to study reactions that are to difficult to measure experimentally.

1.5 Outline of the dissertation

The dissertation is organized as follows: In chapter 2 the fundamentals of quantum chemical methods used in this study is presented along with some practical considerations on how to choose the correct method for studying the kinetics and mechanisms of atmospheric radical reactions. In chapter 3, the basic principles of kinetics and statistical rate theory is discussed with

emphasis on methods applicable for describing the pressure dependence of unimolecular and complex forming bimolecular reactions. Chapter 4 deals with the experimental techniques used in this study, long path FTIR smog chamber and flash photolysis-laser induced fluorescence. Chapter 5 summarizes and discusses the papers on which this thesis is based. The first and second parts of the chapter deals with the primary sinks of the methyl amines. The OH radical reactions of the methyl amines and ethylamine are discussed in the first paper and chlorine atom reactions of the methyl amines in the second. The remaining papers are about the OH radical reactions of the primary and secondary photo-oxidation products of the amines. Conclusions and perspectives on future work are presented in chapter 6.

Chapter 2

Quantum chemical methods

This chapter concerns the quantum chemical methods used in this study. First a brief introduction to the general principles of quantum chemistry is given, then a short description of the methods and the basis sets used in this study, before some practical aspects of the performance and applicability of the methods are discussed.

2.1 General principles

At the heart of quantum chemistry is the non-relativistic, time-independent Schrödinger equation:

$$\hat{H}\Psi = E\Psi \tag{2.1}$$

where $\hat{H}$ is the Hamiltonian operator of the system, Ψ represents the wave function containing all information about the system, and E the molecular energy. As the Schrödinger equation can only be solved analytically for the simplest cases, like the hydrogen atom, approximations are necessary to describe systems of chemical interest. One simplification is the Born-Oppenheimer approximation where the movement of the electrons and the nuclei are considered to be separable and the Schrödinger equation is solved for the electrons, assuming fixed positions of the nuclei. The Born-Oppenheimer approximation is usually a very good approximation for ground states, but may be less reliable for excited states. Another important approximation is the separation of the electronic wave function in one electron wave functions, i.e. spin orbitals. The wave function expressed as the product of the individual one electron wave functions is known as the Hartree product, but this does not satisfy the requirement that the wave function must change sign when the coordinates of two fermions are interchanged.

This requirement can be fulfilled by writing the wave function as a Slater determinant, where all electrons appear in all spin orbitals:

$$\Phi_{SD} = \frac{1}{\sqrt{N!}} \begin{vmatrix} \chi_1(\mathbf{x}_1) & \chi_1(\mathbf{x}_2) & \cdots & \chi_1(\mathbf{x}_N) \\ \chi_2(\mathbf{x}_1) & \chi_2(\mathbf{x}_2) & \cdots & \chi_2(\mathbf{x}_N) \\ \vdots & \vdots & \ddots & \vdots \\ \chi_N(\mathbf{x}_1) & \chi_N(\mathbf{x}_2) & \cdots & \chi_N(\mathbf{x}_N) \end{vmatrix} \tag{2.2}$$

where $\chi_i(\mathbf{x}_j)$ denotes electron j in spin orbital i and χ_i is the combined spatial and spin orbital. When the wave function is expressed as a single Slater determinant and the energy is optimized variationally, we get the Hartree-Fock (HF) method which is the basis of most wave function based quantum chemical methods used today. In the HF method, the electrons only interact with the average of the other electrons and the equation for each one-electron orbital depends on the solution of the others. The equations are therefore solved iteratively until the new equations give rise to a sufficiently similar solution as the previous set of equations, *i.e.* the solution is self consistent. In practice, the wave function is expanded in a set of analytic functions representing atomic orbitals, called a basis set, and the coefficients of the expansion is determined variationally. By letting all electrons see only the average of the others, one typically recovers around 99% of the total energy of the system, but for the calculation of accurate reaction energies, molecular properties *etc.*, it is important to consider the remaining 1%, called the correlation energy [20].

The correlation energy, E_{corr} is mainly associated with the instantaneous movement of the electrons and it is defined as the difference between the exact non-relativistic energy of the system, E_{exact} and the energy of the HF method with the wave function expanded in an infinite basis set, called the HF limit, E_{HF}.

$$E_{\text{corr}} = E_{\text{exact}} - E_{\text{HF}} \tag{2.3}$$

Since the HF method gives the optimal one-determinant wave function in a given basis set, an improved description of the system must include more Slater determinants in what is called the configuration interaction (CI) expansion:

$$\Psi = a_0\Phi_{HF} + \sum_i a_i\Phi_i \tag{2.4}$$

The additional Slater determinants are constructed from the HF determinant by replacing occupied molecular orbitals by virtual ones, typically chosen as unoccupied HF orbitals. The methods accounting for the correlation energy are known as correlated methods and they mainly differ in how they

determine the coefficients a_i. The correlation energy can be conveniently divided into two contributions, static and dynamic correlation. When the coefficient a_0 in the CI expansion is close to unity and a large number of excited determinants each give a small contribution, the correlation energy is mostly related to the instantaneous Coulomb repulsion between the moving electrons, called dynamic correlation. When the correlation comes from near degeneracy between electron configurations, other determinants than Φ_{HF} also contribute significantly to CI expansion, the correlation is said to be static. There is no precise border between static and dynamic correlation, but most correlated methods account only for the dynamic correlation energy.

2.2 Methods

2.2.1 Møller-Plesset perturbation theory

One common method for calculating the correlation energy is Møller-Plesset perturbation theory [21], in which the zeroth order Hamiltonian is written as the sum over the Fock operators and the perturbation is the two-electron operators. The sum of the zeroth and first order energies is equal to the HF-energy, and the first improvement is therefore the second order energy. Møller-Plesset perturbation theory of second order, usually denoted MP2, recovers 80-90 % of the correlation energy and scales as N^5, where N is the number of basis functions, making it a cost efficient method. It is however not capable of calculating reaction energies to chemical accuracy [22]. Higher order varieties are available, but they are not as commonly used.

2.2.2 Coupled-cluster theory

A different approach for calculating the correlation energy is coupled cluster theory [23, 24] where the wavefunction is expressed as

$$\Phi_{CC} = e^{\hat{T}}\Phi_{HF} \tag{2.5}$$

where the cluster operator, $\hat{T}$, is defined as $\hat{T} = \hat{T}_1 + \hat{T}_2 + ... + \hat{T}_n$, n is the total number of electrons and $\hat{T}_i$ generates all possible excitations of order i from the HF determinant. The cost of the calculation increases rapidly with the number of electrons and the cluster operator is therefore usually truncated. Truncation after the $\hat{T}_2$ gives the Coupled Cluster Singles and Doubles (CCSD) [25] method and truncation after $\hat{T}_3$ gives the Coupled Cluster Singles Doubles and Triples (CCSDT) method [26–28]. The CCSD

method scales as N^6 and the CCSDT method scales as N^8 and the latter is therefore only applicable for the smallest molecules [29]. A common approximation is to treat the triple excitations with perturbation theory, giving the CCSD(T) [30] method. This method is sometimes referred to as the 'gold standard' of quantum chemistry [31]and is often capable of giving reaction energies within chemical accuracy [32], (loosely defined as within 1 kcal/mol = 4.184 kJ/mol).

A commonly used measure of the applicability of the coupled cluster methods is the T1-diagnostic of Lee and Taylor [33]. For closed shell molecules, coupled cluster results are considered reliable as long as the value of the T1-diagnostic is less than 0.02, while for open shell systems, 0.44 has been suggested as the limiting value [34]. Systems with higher values have significant multi-reference character and multi-configurational methods should be used instead.

2.2.3 Multi-configurational methods

Both Møller-Plesset perturbation theory and coupled cluster theory are based on the assumption that the wave function can be reasonably well described by a single electronic configuration. For systems like excited states, biradicals, and in bond breaking processes, it is often the case that more than one configuration play a significant role and it becomes necessary to use a multi-determinant wave function as the reference wave function. In the multi-configurational SCF (MCSCF) method, the wave function is expressed as a linear combination of several Slater determinants and both the orbitals and the configuration weights are optimized variationally.

Unlike in the HF method, the MCSCF method requires the user to select the configurations to be included in the calculations and the reliability of the method is strongly dependent of a balanced selection of configuration. A common way of choosing configurations to be included in the calculation is the complete active space (CASSCF) method [35, 36], where instead of individual configurations, a set of orbitals are selected and all possible excitations within this set is considered. A calculation with n electrons in m orbitals is denoted a CASSCF(n,m) calculation.

The CASSCF method provides a wave function that is qualitatively correct, but it does only to a very limited extent account for dynamical correlation. To obtain accurate energies, geometries, frequencies *etc.* it is therefore necessary to do a correlation treatment based on the CASSCF wave function. The most common correlated multi-reference methods are multi-reference configuration interaction singles and doubles (MRCI) and second order multi-reference perturbation theory (CASPT2) [37–39].

2.2.4 Density functional theory

A completely different approach to the problem of electron correlation is density functional theory where, instead of a wave function, the electron density, $\rho(\mathbf{r})$, is optimized [20]. The basis of modern DFT is the Hohenberg-Kohn theorem that states that the potential of a system is uniquely defined from its ground state electron density [40]. This reduces the problem from optimizing a $3N$ dimensional wave function where N is the number of electrons, to optimizing a 3 dimensional electron density. The energy of the system is described as a functional of the electron density, but unfortunately, the exact dependence of the exchange and correlation energy of the electron density is not known. Several different functionals are available and they differ in how they treat the exchange-correlation energy. One of the most common functionals is the combination of Becke's three parameter exchange functional with the correlation functional of Lee, Yang and Parr, giving the B3LYP functional. Although the B3LYP functional is widely used, it is not very good for radical kinetics as it systematically underestimates barrier heights [41]. Density functionals are often parameterized for a specific use, and a widely used functional for radical kinetics and thermochemistry is M06-2X [42]. Even with moderate basis sets does density functional theory offer a significant improved accuracy compared to the Hartree-Fock method at a similar cost [20], making it a very economic approach for most systems.

2.2.5 Basis sets

The set of mathematical functions used to construct the electronic wave function is called a basis set. The basis functions themselves typically represent atomic orbitals and the molecular orbitals are constructed as linear combinations of atomic orbitals. An obvious choice for the atomic orbitals is the Slater type orbital (STO) as they have the same functional form as the exact wave functions for the hydrogen atom where the radial distribution is described as an exponential decay. However, the two-electron integrals needed for the Coulomb and exchange operator do not have an analytic solution when STOs are used and numerical integration is therefore needed. A way of avoiding this problem is to use Gaussian functions as basis functions, which enables analytical solutions of the two-electron integrals. However, the Gaussian functions do not have the correct functional form, lacking the electron-density cusp at the nucleus and falling off too rapidly at large separations. To achieve the same accuracy as by using Slater type orbitals, the atomic orbitals may be approximated by a contraction of several Gaussian (primitive) functions.

The accuracy of a calculation will depend on the number of basis functions used to construct the wave function. The absolute minimum is to use one function for each atomic orbital, called a minimum basis set. This is inadequate for most purposes and larger basis sets are typically used. A basis set where each atomic orbital is described by two functions is called a double zeta basis set, a basis set with three functions per atomic orbital is called a triple zeta basis set *etc.* In a molecule, bonding primarily occurs between the valence orbitals, while the core orbitals are very similar to the orbitals in an isolated atom. It is therefore common to use several functions to describe each of the valence orbitals, while the core orbitals are described by a single basis function, giving a split valence basis set.

There are a large number of different basis sets available. The two most popular families of basis sets are the Pople and Dunning basis sets [29]. Pople's split valence basis sets include 3-21G, 6-31G and 6-311G, where the first number denotes the number of primitives contracted to describe a core orbital, while the numbers after the hyphen denotes the number of primitives used to describe the valence orbitals, i.e.,3-21G is a valence double zeta basis set that describes each core orbital as 3 contracted primitives and the valence orbitals are described by two functions of which one consists of two contracted primitives. The Pople basis sets can be extended by including basis functions of higher angular momentum, called polarization functions, and functions with small exponents, called diffuse functions. Polarization functions are essential for calculating electron correlation and should always be included, while diffuse functions are most important systems with loosely bound electrons.

The Dunning basis sets, the *correlation consistent polerized valence n-zeta* (cc-pVnZ) basis sets (n = D, T, Q, 5 or 6) [43, 44], are split valence basis sets optimized for calculation of electron correlation. The basis sets include polarization functions by default and can be augmented with diffuse functions. A very useful feature of the Dunning basis sets is that they converge to the basis set limit in a systematic fashion, allowing for extrapolation of the calculated energies. Several extrapolation schemes have been proposed, including the expression by Helgaker *et al.* [45, 46]

$$E_{XY} = \frac{E_X X^3 - E_Y Y^3}{X^3 - Y^3} \tag{2.6}$$

By doing two calculations with basis sets of cardinal number X and Y (X>Y), it is possible to extrapolate the correlation energy to the basis set limit. The accuracy of the extrapolation is typically much better than a single calculation using a basis set with cardinal number X+1 [22].

A different approach for calculating energies close to the basis set limit

is the use of explicitly correlated methods [47], where the wave function includes the inter-electronic distances. In this work, explicitly correlated coupled cluster singles and doubles with perturbative triples [48–50], denoted CCSD(T)-F12, has been used for calculating reaction energies and barriers.

2.3 Practical aspects

The "correct" choice of method for a problem depends on both the desired accuracy and the size of the system. It is known that for the smallest systems reaction energies can be calculated accurate to within a kJ/mol using coupled cluster theory with higher order excitations and large basis sets extrapolated to the basis set limit [51], but approaches this accurate are also too time consuming for application on most systems of chemical relevance.

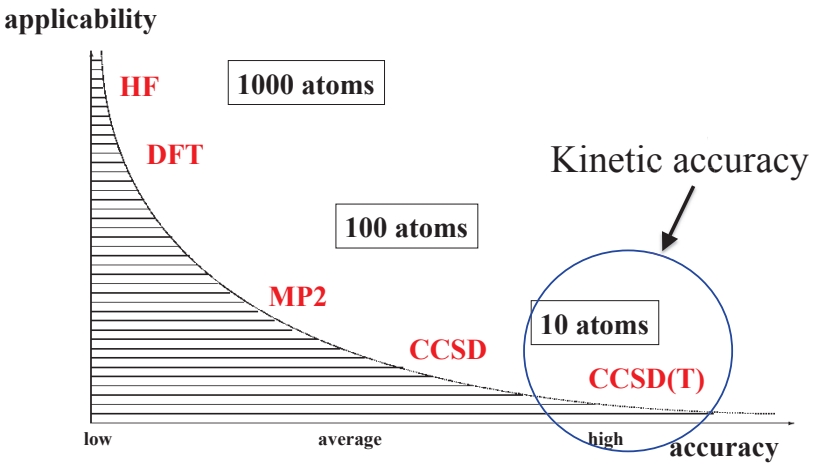

Figure 2.1: Schematic representation of the accuracy and applicability of quantum chemical methods. Adapted from [52].

In this work, the goal is the accurate determination of energies and reaction rate coefficients for radical reactions of amines and similar compounds in the troposphere. The application of computational methods for the study of tropospheric oxidation mechanisms was recently reviewed by Vereecken and Francisco [53]. The barrier height of a reaction enters the expression for the rate coefficient as an exponential term and the calculation of accurate rate coefficients is therefore strongly dependent on accurate reaction barriers. Assuming that the reaction barrier is the dominating error contribution in the

calculation of rate coefficients, predicting room temperature rate coefficients accurate to within a factor of ten require energy barriers accurate to within 5.7 kJ/mol and within a factor of two, so called kinetic accuracy, requires the barrier to be accurate to within 1.7 kJ/mol. It is clear that coupled cluster theory with large basis sets is absolutely necessary to achieve this accuracy. When single reference methods are applicable, reaction enthalpies accurate to within chemical accuracy can be obtained using CCSD(T)/cc-pCVTZ with all electrons correlated and by using basis set extrapolation [32]. This level of accuracy is applicable only for relatively small systems, as shown in figure 2.1. A common simplification is to use a cheaper method to optimize geometries and calculate frequencies, and then improve the energies using CCSD(T) with large basis sets. It should be noted that transition states in general are more challenging and high level methods can be necessary to obtain reliable geometries. Elm *et al.* [54] recently presented a study on the applicability of commonly applied quantum chemical methods to predict the kinetics of oxygenated trace gases with OH radicals. They found that MP2 or BHandHLYP structures and frequencies in conjunction with CCSD(T)-F12 single point calculations and Bell or Eckart tunneling yielded rate coefficients accurate within a factor of three, and that M06-2X with Bell or Eckart tunneling was capable of predicting rate coefficients accurate within a factor of 10 without any single point energy correction.

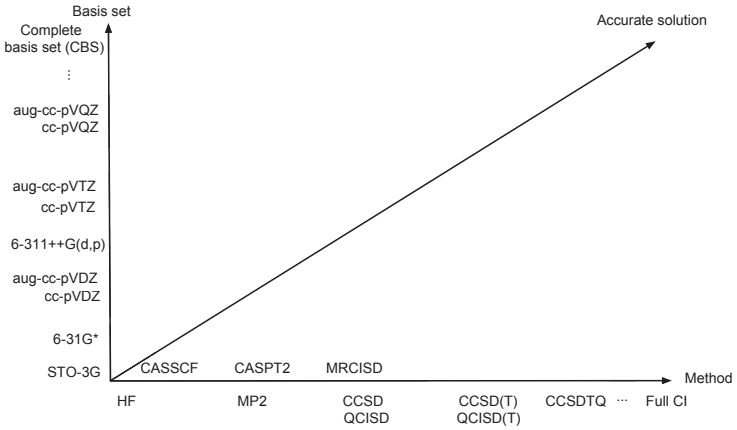

Figure 2.2: The two-dimensional chart of non-relativistic quantum chemistry.

Figure 2.2 shows a two dimensional representation of how both large basis sets and better treatment of electron correlation is necessary in order to im-

prove the accuracy of calculations in a systematic manner. In order to fully exploit the accuracy of correlated methods large basis sets are necessary, and it has been shown that CCSD(T) calculations do not give more accurate calculations than the best DFT functionals, unless at least a tripple zeta basis set is used. [55] The multi-reference methods are somewhat more difficult to place than the single-reference methods, as they do not offer a significant improvement compared with the corresponding single reference method in the absence of static correlation, but as long as suitable active spaces are chosen, their performance does not deteriorate when applied to system with a significant multi-reference character [22]. Transition states often have static correlation and multi-reference methods may be necessary both for geometries and energies [56]. An advantage of the CASPT2 method is that it can be applied to relatively large systems, as long as the multi-reference character can be sufficiently described by a small active space, and with the use of explicitly correlated CASPT2 [57], basis set convergence can be greatly accelerated.

Chapter 3

Chemical kinetics

This chapter is about the general principles and theory of chemical kinetics with emphasis on how reaction rate coefficients for gas phase reactions can be calculated as a function of pressure and temperature. First the basic principles of reaction kinetics are introduced, then unimolecular and complex forming bimolecular reactions are discussed along with the treatment of their pressure dependence and how simplified expressions can be obtained for the high and low pressure limits.

3.1 Fundamental principles

Chemical kinetics deals with the rate of change in a chemical system. For a general reaction,

$$a\mathrm{A} + b\mathrm{B} \rightarrow c\mathrm{C} + d\mathrm{D} \tag{3.1}$$

where a molecules of A react with b molecules of B to form c and d molecules of C and D, the rate of the reaction is given by:

$$r = -\frac{1}{a}\frac{\mathrm{d[A]}}{\mathrm{d}t} = -\frac{1}{b}\frac{\mathrm{d[B]}}{\mathrm{d}t} = \frac{1}{c}\frac{\mathrm{d[C]}}{\mathrm{d}t} = \frac{1}{d}\frac{\mathrm{d[D]}}{\mathrm{d}t} \tag{3.2}$$

The rate of the reaction is generally a function of the reactant concentrations, the product concentrations, temperature and pressure

$$r = f(T, p, [A], [B], [C], [D]) \tag{3.3}$$

called the rate law of the reaction, and can often be written as:

$$r = k(T, p)[A]^m[B]^n \tag{3.4}$$

The proportionality constant, $k(T, p)$, is called the rate coefficient and the exponents, n and m, are called the order of the reaction with respect to A and B respectively. The stoichiometric coefficients, a and b from equation 3.1 do not generally correspond to the reaction order, but do so for elementary reactions. The rate law describes the macroscopic change in a chemical system, but in order to predict the rate of chemical reactions, a microscopic view is necessary.

3.1.1 Reaction mechanisms

A key concept in chemical kinetics is the reaction mechanism. Although the rate law does not say how the reactions occur at the microscopic level, it is the consequence of a series of elementary reactions constituting the reaction mechanism of the overall reaction. An elementary reaction is a single reaction step without any intermediate and there are three different types, first the unimolecular reaction:

$$\mathrm{A} \rightarrow \mathrm{P} \tag{3.5}$$

the bimolecular reaction:

$$\mathrm{A} + \mathrm{B} \rightarrow \mathrm{P} \tag{3.6}$$

and the termolecular reaction:

$$\mathrm{A} + \mathrm{B} + \mathrm{C} \rightarrow \mathrm{P} \tag{3.7}$$

The number of particles in an elementary reaction is called the molecularity of the reaction and it is always equal to the order of the reaction for an elementary reaction, but not necessarily for other reactions.

3.1.2 Temperature dependence

It is often observed that the the rate coefficient of a reaction increases with temperature. The most commonly used empirical parametrization of $k(T)$ was proposed in 1884 by van't Hoff and is now known as the Arrhenius equation [58]

$$k(T) = Ae^{\frac{-E_a}{k_\mathrm{B}T}} \tag{3.8}$$

where A is called the pre-exponential factor, E_a the (Arrhenius) activation energy and R is the gas constant. A strongly simplified interpretation of the Arrhenius equation is that A is the collision frequency of the reactants in the case of a bimolecular reaction or the vibrational frequency of the dissociating bond in a unimolecular reaction, E_a corresponds to the minimum amount of energy required to react and $e^{\frac{-E_a}{k_\mathrm{B}T}}$ is the fraction of molecules having enough

energy to react at a given temperature, T. It should, however, be noted that the Arrhenius equation is a purely empirical description of the temperature dependence of reaction rates.

In the Arrhenius equation, both A and Ea are assumed to be independent of temperature and a plot of $\ln(k)$ against 1/T, called an Arrhenius plot, should give a straight line with slope Ea/R and $\ln(A)$ as intercept. Most reactions follow the Arrhenius equation quite well over limited temperature ranges, but deviations are not uncommon. Reactions giving curved Arrhenius plots are said to show non-Arrhenius behavior and are often caused by a change in reaction mechanism between different temperature regimes, tunneling at low temperatures or the presence of a short lived intermediate. A different equation to describe the temperature dependence of reaction rates was proposed by Harcourt and Esson

$$k(T) = AT^m \tag{3.9}$$

where A and m are empirical parameters. Since the parameters do not have any intuitive physical interpretation, it is much less used than the Arrhenius equation, although it often fits the experimental results better [58].

3.2 Unimolecular reactions

The simplest of the elementary reactions is the unimolecular reaction where a single reactant, A, reacts to form new products, P. The unimolecular reaction has the rate law:

$$-\frac{\mathrm{d[A]}}{\mathrm{d}t} = k_{uni}[\mathrm{A}] \tag{3.10}$$

where k is the reaction rate coefficient. It is often observed that k_{uni} is a function of both temperature and pressure. The first model to describe the pressure dependence of unimolecular reactions was the Lindemann-Hinshelwood mechanism where the reaction is assumed to occur through a vibrationally excited molecule, A*

$$\begin{gathered} \mathrm{A} + \mathrm{M} \underset{k_{-1}}{\overset{k_1}{\rightleftarrows}} \mathrm{A}^* + \mathrm{M} \\ \mathrm{A}^* \overset{k_2}{\rightarrow} \mathrm{P} \end{gathered} \tag{3.11}$$

where k_1 and k_{-1} are the rate coefficients for activation and deactivation by collision with another molecule, M. By applying the steady state approximation for A*, k_{uni} can be expressed as:

$$k_{uni} = \frac{k_1 k_2[\mathrm{M}]}{k_{-1}[\mathrm{M}] + k_2} \tag{3.12}$$

The Lindemann-Hinshelwood gives a qualitatively correct description of the observed pressure dependence of unimolecular reactions, although the predicted fall off is usually not quantitatively correct. In order to correctly predict the pressure dependence of a reaction it is necessary to consider the collisional energy transfer and reaction of the activated molecule at different energies, and the reaction rate can then be written:

$$\frac{\partial n(E_i)}{\partial t} = \mathrm{M} \sum_{j \neq i} \left[k_{ji} n(E_j) - k_{ji} n(E_i) \right] - k_i n(E_i) \tag{3.13}$$

where $n(E_i)$ is the population at energy level i, k_i is the reaction rate coefficient for energy level i, and k_{ij} and k_{ji} represent collisional energy transfer from level i to j and from j to i respectively. This equation is the simplest form of the master equation and its solution, $n(E_i)$, will depend on both temperature and pressure. In general, the rate of any unimolecular reaction can then be written as:

$$k(T,p) = \int_0^\infty k(E) n(E;T,p) \mathrm{d}E \tag{3.14}$$

In the high pressure limit, $n(E;T,p)$ corresponds to the Boltzmann distribution and k is independent of pressure, as predicted by Lindemann-Hinshelwood theory.

The unimolecular reaction is of great importance in atmospheric chemistry, not only because some trace gases react unimolecularly, but also because the rate of complex forming bimolecular reactions and association reactions are related to the rate of the reverse dissociation through the principle of detailed balance.

3.3 Complex-forming bimolecular reactions

Most reactions in the atmosphere are simple bimolecular reactions and are independent of pressure. In addition to these, some bimolecular reactions occur through a short lived intermediate. These reactions are called complex-forming bimolecular reactions [59]. Important examples include OH radical and chlorine atom reactions of olefins, carbonyl compounds and amines. The mechanism of such reactions can be written as:

$$\begin{array}{ccccc} \mathrm{A} + \mathrm{B} & \underset{k_{-1}}{\overset{k_1}{\rightleftarrows}} & \mathrm{AB}^* & \underset{k_{-2}}{\overset{k_2}{\rightleftarrows}} & \mathrm{C} + \mathrm{D} \\ & & {\scriptstyle k_M[M]}\downarrow\uparrow{\scriptstyle k_{-M}[M]} & & \\ & & \mathrm{AB} & & \end{array} \tag{3.15}$$

In the above equation AB* represents a short lived excited reaction intermediate that can either decompose to A and B, be stabilized to AB or react to form the products C and D. Since the kinetics of the reaction is governed by the competition between the unimolecular dissociation of AB to either A + B or C + D and collisional stabilization, the kinetics of complex-forming bimolecular reactions is closely related to the kinetics of unimolecular reactions.

When the back reaction of C and D can be neglected, the rate law of reaction 3.15 can be written as:

$$\begin{aligned}
\frac{\mathrm{d[A]}}{\mathrm{d}t} &= -k_1[\mathrm{A}][\mathrm{B}] + k_{-1}[AB^*] \\
\frac{\mathrm{d[AB^*]}}{\mathrm{d}t} &= k_1[\mathrm{A}][\mathrm{B}] - (k_{-1} + k_2 - k_M[M])[\mathrm{AB^*}] + \mathrm{k_{-M}[AB][M]} \\
\frac{\mathrm{d[AB]}}{\mathrm{d}t} &= k_M[\mathrm{AB^*}][\mathrm{M}] - k_{-M}[\mathrm{AB}][\mathrm{M}] \\
\frac{\mathrm{d[C]}}{\mathrm{d}t} &= k_2[\mathrm{AB^*}]
\end{aligned} \tag{3.16}$$

Assuming that the vibrationally excited complex, AB*, is in a steady state and that collisional reactivation can be neglected, the following expression is obtained for the effective overall rate coefficient.

$$k_{obs} = k_1 \frac{k_2 + k_M[M]}{k_{-1} + k_2 + k_M[M]} \tag{3.17}$$

From this expression, two limiting cases can be derived:

At very low pressures, the collision frequency is so low that collisional deactivation can be neglected and the reaction rate is independent of pressure.

$$k_0 = k_1 \frac{k_2}{k_{-1} + k_2} \tag{3.18}$$

Since it is assumed that no collisional stabilization takes place, it should also not be assumed that the energy is Boltzmann distributed in A* and equation 3.18 should be applied at the microcanonical level.

In the high pressure limit, k_M is very much larger than k_{-1} and k_2 and the formation of the complex becomes the rate determining step, yielding a pressure independent rate coefficient.

$$k_\infty = k_1 \tag{3.19}$$

Eq. 3.17 bears some similarity to eq. 3.12, but the rate of complex-forming bimolecular reactions typically shows an S-shaped falloff curve with

high and low pressure limits as described above, unlike unimolecular and association reaction that are pressure independent only in the high pressure limit. At intermediate pressures, the rate is pressure dependent and the transition between the two pressure regimes is described by the master equation. The following sections describe the principles for how the rate coefficient can be calculated for the different cases.

3.4 From potential energy surfaces to rate coefficients

Under the assumptions of classical mechanics, the time development of a system can be calculated when the positions and momenta of all particles as well as the potential energy function is known. It is therefore, in principle, possible to calculate how long it takes for a chemical system to react for a given set of initial conditions. The rate coefficient can then be expressed as the number of trajectories passing from the reactant space to the product space per time, divided by the number of trajectories left in the reactant space.

There are, however, some practical problems: i) The potential energy surface for a system consisting of N atoms is a 3N dimensional function and it is very demanding both to calculate the PES and to calculate trajectories on it, even with relatively cheap methods, for most systems of chemical relevance. ii) A trajectory represents a single possible initial condition. Any real chemical system will consist of an enormously large number of particles, each with its own set of initial conditions, and the number of trajectories needed to accurately represent a reaction will be prohibitively large. iii) The world is governed by quantum mechanics, not classical mechanics.

Since the number of trajectories needed to explicitly describe any chemical system is so enormous, it is clear that only the most probable behavoiur will be important. The problem may therefore be greatly simplified through the use of statistical mechanics. Several theories on how to calculate reaction rates from statistical mechanics have been proposed, and the most commonly used of these is transition state theory (TST).

3.5 Transition state theory

For simple bimolecular reactions that do not involve any intermediates and for unimolecular reactions in the high pressure limit TST is the standard method for calculating thermal rate coefficients [41, 60]. TST was developed

by Eyring [61], and Evans and Polanyi [62] independently and is based on the following assumptions:

1. The presence of a dividing surface/critical configuration between the reactant and the product parts of the phase space
2. That the transition state is in equilibrium with the reactants
3. That the motion through the critical configuration is separable from the other degrees of freedom in the reaction system
4. That the motion through the critical configuration can be treated using classical mechanics, *i.e.* quantum effects are ignored

The expression for the thermal rate coefficient in TST is:

$$k(T) = \frac{k_{\mathrm{B}}T}{h}\frac{Q^{\ddagger}(T)}{Q_R(T)}e^{\frac{-E_0}{k_{\mathrm{B}}T}} \tag{3.20}$$

where $Q^{\ddagger}(T)$ and $Q_R(T)$ represents the partition functions of the transition state and the reactants respectively and E_0 is the barrier height for the reaction.

The partition functions are obtained by summing over all possible energy levels, i, of the system:

$$Q(T) = \sum_i g_i e^{\frac{-E_i}{k_{\mathrm{B}}T}} \tag{3.21}$$

where g_i and E_i are the degeneracy and energy respectively of energy level i.

It is usually assumed that the different degrees of freedom are separable and the partition function is then expressed as a product of the contributions from electronic, vibrational, rotational and translational degrees of freedom:

$$Q_{tot}(T) = Q_{el}(T)Q_{vib}(T)Q_{rot}(T)Q_{trs}(T) \tag{3.22}$$

The translational partition function is calculated assuming that molecular translational motion is described by a quantum mechanical particle in a box and is therefore dependent of the molecular mass and the volume of the system, but it does not require any other information about the molecule.

$$Q_{trs}(T) = \left(\frac{2\pi M k_{\mathrm{B}}T}{h^2}\right)^{\frac{3}{2}} V \tag{3.23}$$

The rotational partition function requires only the moments of inertia of the molecule and is typically calculated assuming 3 separable, one dimensional rotors:

$$Q_{rot}(T) = \frac{\sqrt{\pi I_A I_B I_C}}{\sigma}\left(\frac{8\pi^2 k_B T}{h^2}\right)^{\frac{3}{2}} \tag{3.24}$$

In the harmonic approximation, the vibrational partition function is given by:

$$Q_{vib}(T) = \prod_i \left(\frac{1}{1 - e^{\frac{-h\nu_i}{k_B T}}}\right) \tag{3.25}$$

where the product is over all vibrational modes, i, and ν_i is the vibrational frequencies. Since there are no analytical expression that describes the spacing of the electronic energy levels of a molecule, explicit summation is necessary to calculate the exact electronic partition function. However, the electronic energy levels are so widely spaced that it is often sufficient to consider only the ground state and only rarely is it necessary to include more than the first one or two excited levels.

$$Q_{el}(T) = g_0 + g_1 e^{\frac{-E_1}{k_B T}} \tag{3.26}$$

The accuracy of TST depends strongly on the quality of the molecular parameters used, especially the energy barrier, and TST is therefore usually applied in conjunction with high level quantum chemical methods.

Equation 3.20 can also be expressed in a thermodynamic formulation,

$$k(T) = \frac{k_B T}{h} e^{\frac{\Delta^\ddagger S}{k_B}} e^{\frac{-\Delta^\ddagger H}{k_B T}} \tag{3.27}$$

where $\Delta^\ddagger S$ and $\Delta^\ddagger H$ represents the standard entropy and enthalpy of activation respectively. This form allows for easy comparison between TST and the Arrhenius equation and it is easily seen that the pre-exponential factor is related to the entropy of the transition state, and that the enthalpy does not correspond exactly to the activation energy.

3.6 The master equation

An implicit assumption in TST is that the collisional energy relaxation is fast on the timescale of reaction. This always true in the high pressure limit, but at intermediate pressures, reactions and relaxation may happen on the same time scale, and explicit consideration of collisional energy transfer through the master equation is necessary to predict the reaction rate. The master equation [63, 64] is a set of coupled differential equations that describe the

the time development of the energy levels of a system that may consist of one or more isomers.

$$\begin{aligned}\frac{dn_i(E)}{dt} = \omega \int_{E_{0_i}}^{\infty} P(E \leftarrow E')n_i(E')dE' - \omega n_i(E) \\ - \sum_{j \neq i}^{M} k_{ji}(E)n_i(E) + \sum_{j \neq i}^{M} k_{ij}(E)n_j(E) \\ - k_{Pi}(E)n_i(E) + K_{Ri}^{eq} k_{Ri}(E) \frac{\rho_i(E)e^{-\beta E}}{Q_i(T)} n_R n_m \\ - k_{Ri}(E)n_i(E) \end{aligned} \tag{3.28}$$

The first term describes the the population increase in $n_i(E)$ through collisional energy transfer from other energy grains, $n_i(E')$ in the same isomer, ω represents the Lennard-Jones collision frequency and $P(E \leftarrow E')$ is the probability that a collision results in a a transition from E' to E. The second term represents the loss of $n_i(E)$ by collisional deactivation. The third and fourth terms represents reaction between isomers i and j with reaction rate coefficients $k_{ji}(E)$ and $k_{ij}(E)$ respectively. The fifth term represents irreversible loss to products with rate coefficient k_{Pi}. The sixth and seventh term represent the rate off association of two bimolecular reactants and the dissociation back to reactants. $k_{Ri}(E)$ is the rate coefficient for dissociation to reactants R, K is the equilibrium constant between isomer i and the reactants and $Q_i(T)$ represents the rovibrational partition function for isomer i.

In this work $P(E \leftarrow E')$was calculated using an exponential down model

$$P(E \leftarrow E') = C(E')e^{-\frac{E'-E}{\langle \Delta E_{down} \rangle}} \tag{3.29}$$

where $E' > E$, $C(E')$ is a normalization constant and $\langle \Delta E_{down} \rangle$ is the average energy transferred per collision. The value of $\langle \Delta E_{down} \rangle$ is typically around RT (2.4 kJ mol⁻1 at room temeprature) and is either used as a parameter fitted to reproduce experimental data or experimental values for similar systems are used.

The master equation as described in equation 3.28 applies to a system with a continuos energy distribution. The rovibrational states of a molecule are not continuos, but their number is so large that it is impossible to treat them all explicitly. The energy scale is therefore divided into intervals, called energy grains and a discrete master equation is obtained. The discrete master equation is often written in matrix form:

$$\frac{d|w\rangle}{dt} = \mathbf{M}|w\rangle \tag{3.30}$$

where $|w\rangle$ is the population vector for the energy intervals in isomer i and $\mathbf{M}$ is the matrix describing energy transfer between the grains as well as reaction between the isomers. The master equation is solved by diagonalizing $\mathbf{M}$ and the solution is written as:

$$|w(t)\rangle = \mathbf{U}e^{\Lambda t}\mathbf{U}^{-1}|w(0)\rangle \tag{3.31}$$

where $|w(0)\rangle$ contains the initial conditions, $\mathbf{U}$ is the matrix containing the eigenvectors of $\mathbf{M}$ and Λ is a vector containing the corresponding eigenvalues.

The majority of the eigenvalues are large and correspond to energy transfer between the energy grains, while the eigenvalues corresponding to reaction between the isomers are much smaller. As long as the eigenvalues corresponding to chemical reactions are well separated from the other eigenvalues can phenomenological rate coefficients for reactions between all isomers be determined using the Bartis-Widom method [65, 66].

3.7 Specific rate coefficients

To calculate the pressure dependence of thermal rate coefficients it is necessary to calculate the microcanonical or specific rate coefficients, $k(E, J)$.

The general expression for the thermal rate coefficients is given by [63,64]:

$$k(E, J) = \frac{N(E, J)}{\mathrm{h}\rho(E)} \tag{3.32}$$

$N(E, J)$ represents the number of open reaction channels, or number of states or reaction channels available at a given energy and angular momentum, and $\rho(E)$ represents the density of states in the reactant at the same energy. The denominator, $\mathrm{h}\rho(E)$, can therefore be interpreted as the lifetime for a single reaction channel. The theories for the calculation of specific rate coefficients differ in the way they calculate the number of available reaction channels.

Figure 3.1 shows the two different types of reaction potentials [67]. When the potential has a well defined maximum along the reaction coordinate, it is called a Type I potential, the reaction has a tight transition state and the dependence of k on the angular momentum J is generally weak and often ignored. When there is no such maximum, the potential is of Type II and the reaction is said to have a loose transition state and the rate coefficient is strongly dependent on the angular momentum as well as the energy.

For the case of a tight transition state the specific rate coefficients are usually calculated using Rice-Ramsperger-Kassel-Marcus theory (RRKM-theory) [63]. RRKM theory is transition state theory applied to a microcanonical ensemble of the reactant molecule. The densities of states are typically evaluated by first calculating the rotational density of states by taking the inverse Laplace transform of the canonical partition function for the active rotational degrees of freedom, and then folding the vibrational density of states into it by using the Beyer-Swinehart algorithm [68].

For loose transition states several methods are available including the Statistical Adiabatic Channel Model (SACM) [69], Long Range Transition State Theory (LRTST) [70] and as well as different forms of Variational Transition State Theory (VTST) [41, 60]. In VTST, the transition state is optimized variationally by minimizing the rate coefficient. This can be done either at the canonical or the microcanonical level. LRTST is a limiting case of RRKM/TST where degrees of freedom for the transition state are taken to be like in the separated fragments, and the rate is then governed by long range electro static interactions and angular momentum conservation. This is usually a good approximation for reactions at low temperatures and for ion-molecule reactions, but less reliable at higher temperatures and shorter ranged potentials. The SACM model is in principle fundamentally different from methods based on TST as it does not make any reference to a transition state, instead the number of available adiabatic reaction channels are counted. SACM is also a quantum mechanical theory, whereas the other models are based on classical mechanics. In practice, however, much of the same formalism is used in both RRKM and SACM [63]

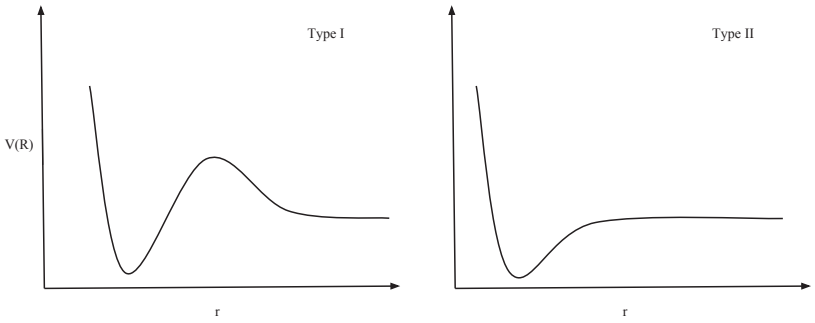

Figure 3.1: Schematic representation of the two types of reaction potentials. Left: Type 1 which corresponds to a tight transition state, Right: Type 2 which corresponds to a loose transition state.

3.7.1 Inverse Laplace transform

An alternative to the statistical rate theories is the use of the inverse Laplace transform (ILT) for calculating microcanonical rate coefficients [71] from canonical rate coefficients. Since the canonical rate coefficient can be written as a Laplace transform of the microcanonical rate coefficient,

$$k(T) = \frac{\int_0^\infty k(E)\rho_R(E)e^{\frac{-E}{k_B T}}\mathrm{d}E}{Q_R(T)} \tag{3.33}$$

it follows that when $k(T)$ can be represented by a modified Arrhenius expression:

$$k(T) = A\left(\frac{T}{T_0}\right)^n e^{\frac{-E_a}{k_B T}} \tag{3.34}$$

the microcanonical rate coefficients are given by:

$$k(E) = \frac{A(k_B T_0)^{-n}}{\rho_R(E)} L^{-1}\left[Q_R(T)e^{\frac{-E_a}{k_B T}}\right] \tag{3.35}$$

For a unimolecular reaction Equation 3.35 becomes:

$$k(E) = \frac{A(k_B T_0)^{-n}}{\rho_R(E)\Gamma(n)} \int_0^\infty \rho_R(E-\tau)(\tau - E_a)^{n-1}u(\tau - Ea)\mathrm{d}\tau \tag{3.36}$$

while for bimolecular reactions, the translational degrees of freedom must also be included:

$$\begin{aligned} k(E) = &\frac{A(k_B T)^{-n}}{\rho_R(E)\Gamma(n+1.5)}\left(\frac{2\pi\mu}{h^2}\right)^{\frac{3}{2}} \int_0^\infty \rho_R(E-\tau) \\ &\times (\tau - E_a - \Delta U_{0K})^{n+0.5}u(\tau - Ea - \Delta U_{0K})\mathrm{d}\tau \end{aligned} \tag{3.37}$$

The ILT technique is in principle applicable for any reaction which can be accurately described by a modified Arrhenius expression, but it is particularly useful for barrier-less association reactions as $k(E)$ can be calculated from high pressure experimental data or simple capture rate expressions like LRTST. It should be noted that the method is only exact as long as $k(T)$ is valid over the entire temperature range, and that the quality of the calculated $k(E)$s depend strongly on the quality of the Arrhenius parameters.

3.8 Kinetic isotope effects

The observed ratio in the reaction rate of two isotopologues is called the kinetic isotope effect (KIE) and is expressed as the ration of the reaction rate coefficients of the two isotopologues:

$$KIE = \frac{k_{light}}{k_{heavy}} \tag{3.38}$$

where k_{light} and k_{heavy} represent the rate coefficient of the light and heavier isotopologue respectively. A KIE larger than one is called a normal KIE and KIE smaller than one is then an inverse KIE.

Different reaction mechanisms give rise to different KIEs and they are therefore a useful tool to gain insight in to the mechanism of a reaction [72]. The KIE is usually larger when the reaction involves the substituted atom. The electronic potential energy surface of the reaction is not influenced by isotopic substitution, but the zero point vibrational energy changes and a heavier isotopologue will therefore have a lower vibrational energy.

For direct abstraction reactions the bond being broken is often significantly weakened in the transition state and the difference in zero point energy will therefore be smaller in the transition state than in the reactants. If the bond being broken includes the substituted atom, the energy barrier will be larger for the heavier isotopologue, resulting in a lower reaction rate than for the lighter one. The largest KIEs are often observed for direct hydrogen abstractions, with KIE larger than 3 being common. KIE larger than 7 have been observed and is a clear indicator of tunneling. If the reaction proceeds through a pre-reaction adduct and with a submerged barrier, both the capture step and the abstraction step will influence the reaction rate. Since the KIE for the capture step is close to unity and the reaction rate is less sensitive to changes in the zero point energy, smaller KIEs are observed than for direct abstractions. For association reactions, the difference in zero point energy plays a less important role and the KIE is also influenced by the the competition between back reaction and collisional stabilization of the adduct. The KIEs for addition reactions are smaller than for abstraction reactions and it is sometimes observed that the heavier isotopologue reacts faster.

Since all processes have a characteristic KIE, atmospheric trace gases may be enriched or depleted in certain isotopes. If the KIEs for the potential sources and sinks of a trace gas are well characterized, it is possible to trace its source and estimate the relative importance of the different sinks, making isotope analysis a highly useful tool in atmospheric science.

Chapter 4

Experimental methods

In this chapter, the experimental techniques used in the study are presented. The following experiments have been performed:

- The OH radical reaction of *N*-methyl formamide and *N,N*-dimethylformamide have been studied using the laser-induced fluorescence technique (LIF). Rate coefficients for the reactions have been measured as a function of temperature and pressure with helium as bath gas. The experiments were performed in the group of Professor Matthias Olzmann at Karlsruhe Institute of Technology.

- Kinetic isotope effects for the OH radical reaction of hydrogen cyanide have been measured using the relative rate technique using FTIR detection. The experiments were performed in the IR spectroscopy laboratory at the University of Oslo.

4.1 Laser-induced fluorescence

The laser induced fluorescence technique is based on using a laser to generate fluorescence in a radical species and by monitoring the decay of this fluorescence signal the decay of the radical species can be determined. In this work, LIF has used along with flash photolysis of a radical precursor to generate OH radicals, which were then monitored using LIF.

4.1.1 Principles

Fluorescence is the spontaneous, spin allowed emission from a specific rovibrational state of an excited electronic state to a lower electronic state. In

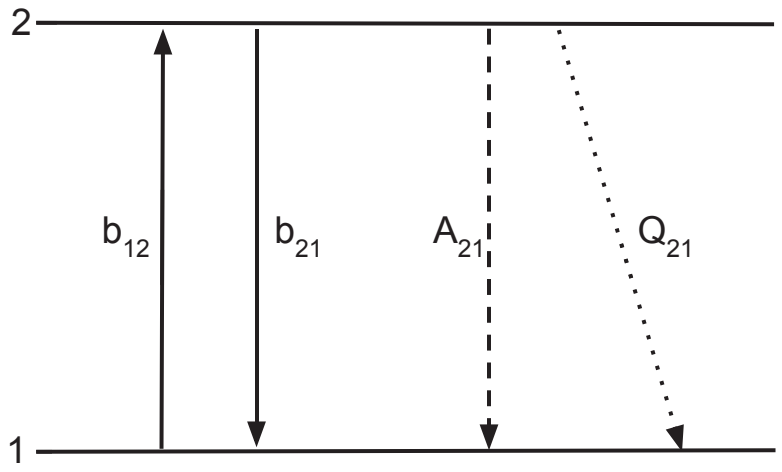

Figure 4.1: Simplified two-level system used to describe the principles of laser-induced fluorescence.

the laser induced fluorescence (LIF) technique the monitored radical is electronically excited using a laser and the fluorescence signal is detected. If the emitted radiation is at the same wavelength as the absorption it is called resonant LIF. In non-resonant LIF the emission is red shifted relative to the absorbed light. It is generally more practical to do non-resonant LIF as stray light from the excitation laser can then easily be filtered out.

The principles of LIF can be explained using a simplified two-level system as shown in Figure 4.1.

A_{21} is the Einstein coefficient of spontaneous emission, Q_{21} is the pseudo-first-order rate coefficient of radiation-less loss processes, b_{12} and b_{21} are the pseudo-first-order rate coefficients for the absorption and induced emission and are related to the corresponding Einstein coefficients, B_{ij} through

$$b_{ij} = B_{ij} I_\nu \tag{4.1}$$

where I_ν denotes the intensity of the incoming laser light. The population numbers of two states, N_1 and N_2 can then be described by:

$$\frac{\mathrm{d}N_2}{\mathrm{d}t} = -\frac{\mathrm{d}N_2}{\mathrm{d}t} = N_1 b_{12} - N_2(b_{21} + A_{21} + Q_{21}) \tag{4.2}$$

Assuming that all molecules are in the ground state before the excitation laser pulse the fluorescence intensity can be expressed as:

$$F \propto N_1(t=0)\frac{A_{21}B_{21}}{B_{12}+B_{21}}\frac{1}{1+\frac{I_{sat}}{I_\nu}} \tag{4.3}$$

where I_{sat} is a characteristic spectral intensity, defined from the ratio of spontaneous to induced processes:

$$I_{sat} = \frac{A_{21}+Q_{21}}{B_{12}+B_{21}} \tag{4.4}$$

Two limiting cases can be derived, for $I_\nu \ll I_{sat}$:

$$F \propto N_1(t=0)\frac{A_{21}B_{21}}{B_{12}+B_{21}}\frac{I_\nu}{I_{sat}} \tag{4.5}$$

and for $I_\nu \gg I_{sat}$:

$$F \propto N_1(t=0)\frac{A_{21}B_{21}}{B_{12}+B_{21}} \tag{4.6}$$

It is clear from equation 4.6 that a high laser intensity is desirable as the fluorescence signal will then be unaffected by fluctuations in the laser intensity. It should be noted that this simplified model is insufficient to describe absolute intensities, but as all measurements in this work was done under pseudo-first-order, only the ratio of intensities $I(t)/I(0)$ is needed to describe the kinetics of the systems.

4.1.2 Experimental setup

The experiments were performed in a coolable quasi-static reactor shown in Figure 4.2 [73]. The reaction cell is T shaped, has an inner volume of 640 cm^3 and is enclosed in a steel mantel that can be evacuated to prevent condensation of water vapour on the windows and to improve thermal insulation. The beams of the photolysis and excitation lasers run antiparallel coaxially through the cell and the fluorescence signal is measured orthogonally to the laser beams using a photomultiplier (PMT, Hamamatsu).

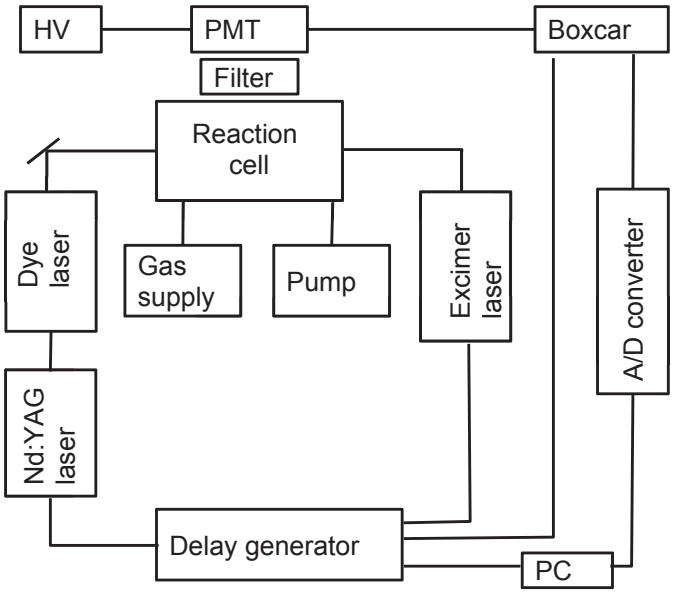

Figure 4.2: Schematic representation of the experimental setup used in the absolute rate measurements.

An excimer laser (Coherent CompexPro 102) operated with KrF at 248 nm was used as the photolysis laser and the OH radicals were excited using a frequency doubled Nd:YAG (Continuum Powerlite 7010) pumped dye laser (Lambda Physik FL3002) operating with Rhodamine 6G and frequency doubled to 281.9 nm.

The mixtures of the OH precursors, t-BuOOH and acetyl acetone, were prepared and stored as diluted mixtures in helium in stainless steel gas cyl-

inders. The reactant amide was brought into the gas phase by letting helium flow through a gas wash bottle filled with the relevant amide. The saturated gas mixture was then mixed with the precursor and bath gas through calibrated mass flow controllers. Concentrations of the different amides were then calculated from their respective vapour pressures.

The gas flow was regulated to be fast enough to prevent a buildup of reaction products in the reaction/detection zone, but still slow enough not to compete with the loss reactions of the OH radical.

In the experiments, the decay of OH radicals in a large excess of the reactant amide is measured. All measurements were done under first order conditions and the OH signal then decays exponentially with a pseudo-first-order rate coefficient k'.

$$\frac{I}{I_0} = e^{-k't} \tag{4.7}$$

By measuring k' at different concentrations of the reactant amide, under otherwise identical conditions, the bimolecular rate coefficient can be extracted as the slope of k' plotted against the reactant concentration. This process is then repeated at different temperatures and pressures to give $k(T, p)$.

4.2 Relative rate measurements

The kinetic isotope effects for the OH radical reaction of HCN were measured using the relative rate technique. This is a conceptually very simple technique that is widely used to determine the rate coefficient of bimolecular reactions relative to already known reaction rates.

4.2.1 Principles

For two competing reactions of A and B with a third species X:

$$\mathrm{A} + \mathrm{X} \xrightarrow{\mathrm{k_A}} \mathrm{P} \tag{4.8}$$

$$\mathrm{B} + \mathrm{X} \xrightarrow{\mathrm{k_B}} \mathrm{P} \tag{4.9}$$

As long as the reactants A and B only react with the same reactant X and that none of them are regenerated, it can be shown that the relative rate, k_A/k_B is given by:

$$\ln \frac{[A_0]}{[A_t]} = \frac{k_A}{k_B} \ln \frac{[B_0]}{[B_t]} \tag{4.10}$$

where $[A_0]$, $[A_t]$, $[B_0]$ and $[B_t]$ represent the concentrations of A and B at times equal 0 and t respectively. In the experiments, A and B represented the lighter and heavier isotopologue of HCN respectively.

The relative rate technique is only applicable when accurate rate coefficients for the reference reaction are available. In the case of kinetic isotope effects it is the relative rate itself that is determined and the method is therefore particularly suited for this.

4.2.2 Experimental setup

The experiments were performed in a 250 L electropolished stainless steel reaction cell equipped with a White type mirror system with a 120 m optical path length for ro-vibrationally resolved FTIR spectroscopy. The reaction cell is equipped with UV lamps mounted in a quartz tube inside the cell. All experiments were carried out in 1013 ± 20 hPa synthetic air (AGA) at 298±2 K. The infrared spectra were recorded with a Bruker IFS 66v/S FTIR spectrometer equipped with an InSb detector cooled with liquid nitrogen.

Hydroxyl radicals were generated by photolysis of ozone in the presence of hydrogen using a Phillips TUV 30W lamp (λ_{max}~ 254 nm):

$$\mathrm{O_3} + \mathrm{h}\nu \rightarrow \mathrm{O}(^1\mathrm{D}) + \mathrm{O_2} \tag{4.11}$$

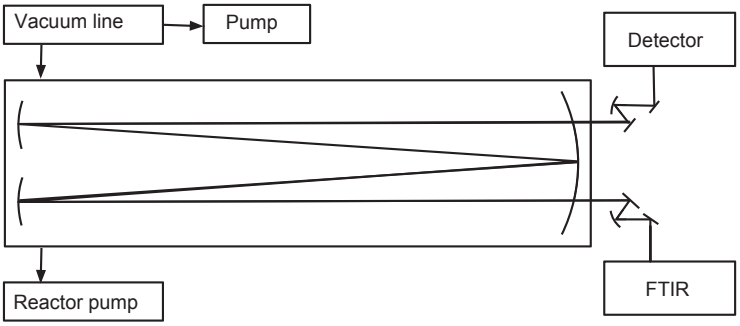

Figure 4.3: Schematic representation of the reaction cell used for the relative rate measurements.

$$O(^1D) + H_2 \rightarrow OH + H \tag{4.12}$$

$$H + O_3 \rightarrow OH + O_2 \tag{4.13}$$

$$H + O_2 + M \rightarrow HO_2 + M \tag{4.14}$$

$$HO_2 + O_3 \rightarrow OH + 2O_2 \tag{4.15}$$

$$HO_2 + HO_2 \rightarrow H_2O_2 + O_2 \tag{4.16}$$

$$H_2O_2 + h\nu \rightarrow 2OH \tag{4.17}$$

$$OH + H_2 \rightarrow H + H_2O \tag{4.18}$$

$$OH + O_3 \rightarrow HO_2 + O_2 \tag{4.19}$$

$$OH + H_2O_2 \rightarrow HO_2 + H_2O \tag{4.20}$$

$$OH + HO_2 \rightarrow H_2O + O_2 \tag{4.21}$$

This method generates OH radicals not only in the ground state, but also in excited vibrational states [74–76]. However, the mixing ratios of O_2 and N_2 are five orders of magnitude larger than those of the HCN isotopologues and it can safely be assumed that these react exclusively with OH in the vibrational ground state.

Chapter 5

Results and discussion

This chapter summarizes experimental and calculated results that are given in the attached papers. In addition some unpublished results are discussed.

5.1 The OH radical reactions of amines

Paper I: Onel, L.; Thonger, L.; Blitz, M. A.; Seakins, P. W.; Bunkan, A. J. C.; Solimannejad, M.; Nielsen, C. J. Gas-Phase Reactions of OH with Methyl Amines in the Presence or Absence of Molecular Oxygen. An Experimental and Theoretical Study. *The Journal of Physical Chemistry A* **2013**, 117, 10736-10745.

This paper presents a computational and experimental study of the OH radical reaction of methylamine (MA), dimethylamine (DMA), trimethylamine (TMA) and ethylamine (EA). The work was performed in collaboration with the group of Professor Paul Seakins at the University of Leeds and all experiments were conducted by them.

Several authors have studied these reactions, both experimentally [14, 17, 77–82], and by computational methods [83, 84]. The reactions are very fast, show negative temperature dependencies and no pressure dependence, and the atmospheric lifetimes of the amines with respect to reaction with OH radicals will be less than one day.

The OH radical reactions of MA, DMA, TMA and EA were studied with quantum chemical methods and statistical rate theory. Stationary points on the potential energy surfaces were characterized with MP2/aug-cc-pVTZ calculations and the energies of the stationary points were improved with CCSD(T*)-F12a/aug-cc-pVTZ and CCSD(T) with basis set extrapolation with the aug-cc-pVTZ and aug-cc-pVQZ basis sets. The results of the cal-

culations are shown in Figure 5.1. The potential energy surfaces for all reactions show relatively stable pre-reaction complexes and submerged barriers for the hydrogen abstraction reactions. The overall kinetics of the amine OH reactions may therefore be influenced by both the formation of the pre-reaction complexes and the tight transition states for the hydrogen abstraction reactions. Rate coefficients were calculated using a two transition state model [85], assuming no collisional relaxation of the pre-reaction complexes.

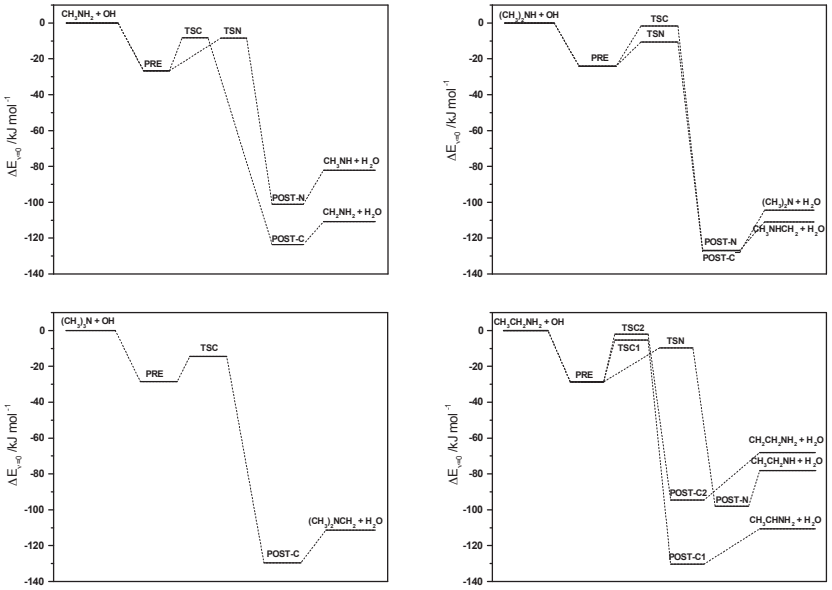

Figure 5.1: Stationary points on the potential energy surfaces of the OH radical reactions of the methyl amines and ethylamine. The results are from CCSD(T*)-F12a/aug-cc-pVTZ//MP2/aug-cc-pVTZ calculations.

The calculated rate coefficients are shown in Figure 5.2 along with experimental values from the University of Leeds as well as values from the literature. The agreement between the calculated and experimental rate coefficients is very good, with the largest deviations being smaller than a factor of two. The calculated branching ratios, shown in Table 5.1, differ significantly from both experimental values and from previous theoretical studies. In order to examine the reason for this discrepancy, the sensitivity of the calculated branching ratios to the barrier heights was tested by shifting the energy barriers of the different reaction paths for MA by 4 kJ/mol in

Table 5.1: Available branching ratios(/%C-H abstraction) for methyl amines + OH reactions

	MA	DMA	EA	
Calculated[a]	47	22	18	This work
Calculated[b]	74	-	-	Tian *et al.* [84]
Calculated[c]	80	48	98	Galano & Alvarez-Idaboy [83]
FTIR[d]	-	63 ±5	-	Lindley *et al.* [86]
PTR-ToF-MS[e]	75 ±5	58 ±5	81 ±1	Nielsen *et al.* [14]
LIF[f]	76 ± 8	59 ±7	49 ±6	Onel *et al.* [82]

[a]CCSD(T*)-F12a/aug-cc-pVTZ//MP2/aug-cc-pVTZ, microcanonical steady-state TST
[b]CCSD(T)/6-311++G(2d,2p)//CCSD/6-31G(d), VTST with small curvature tunneling
[c]CCSD(T)/6-311++G(2d,2p)//BHandHLYP/6-311++G(2d,2p),VTST
[d]End product analysis with Long path FTIR in smog chamber
[e]End product analysis with PTR-ToF-MS in smog chamber
[f]Laser-induced fluorescence of radical intermediates

opposite directions. By raising the barrier to C-H abstraction while lowering the barrier to N-H abstraction by 4 kJ mol^{-1}, a branching ratio of 9C : 91N and a rate coefficient of 4.9×10^{-11} cm^3 molecule^{-1} s^{-1} were predicted, while the reverse adjustment resulted in a branching ratio of 89C : 11N and a rate coefficient of 3.7×10^{-11} cm^3 molecule^{-1} s^{-1}. It should also be noted that all barriers are below the entrance energy and collisional stabilization is not included, tunneling is also excluded from the model, which might contribute to the underestimation of the C-H abstraction channels.

The good agreement between the calculated and experimental reaction rates is to a certain extent caused by the submerged barriers, which makes the overall rate coefficients less sensitive to variations in the barrier heights. The same is not the case for the calculated branching ratios as even minor changes in the barrier height causes large changes. It seems clear that the sensitivity of the branching ratios to the calculated barriers is so strong that the calculation of accurate values is beyond the current level of accuracy for standard quantum chemical methods.

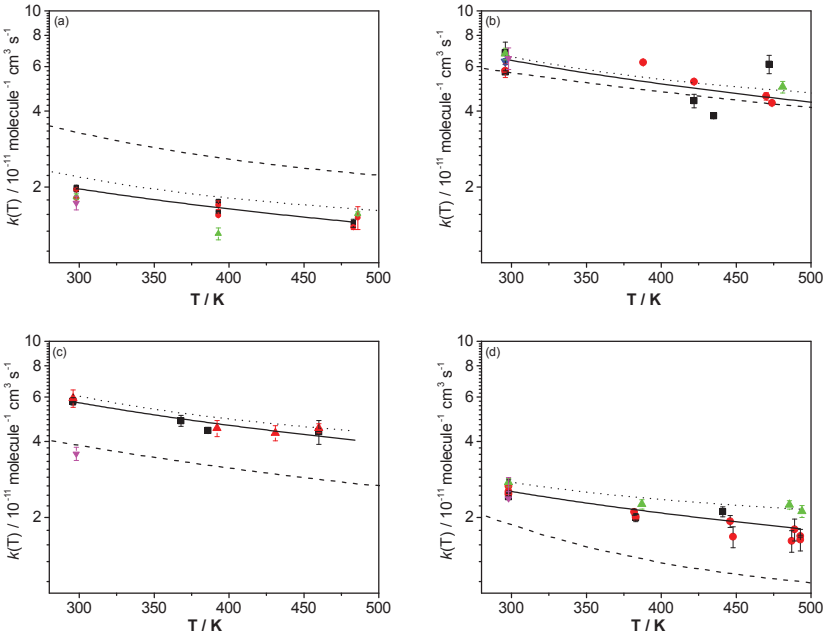

Figure 5.2: Calculated and experimental rate coefficients for the reaction of OH radicals with (a) methylamine, (b) dimethylamine, (c) trimethylamine and (d) ethylamine. Symbols: black ■, OH, N2 bath gas; red ▲, OD, N2 bath gas; red ●, OH, N2/O2 bath gas; green ▲, OD, N2/O2 bath gas; blue ▼, OD, He bath gas; pink ▼, data of Carl and Crowley at 298 K [79]. Full line, Harcourt-Esson fit to experimental data from this work; dotted line, parametrized data from Atkinson et al. [77,78]; dashed line, theoretical prediction.

5.2 The chlorine atom reactions of amines

Paper II: Nicovich, J. M.; Mazumder, S; Laine, P. L.: Wine, P. H.; Tang, Y.; Bunkan, A. J. C.; Nielsen, C. J. An experimental and theoretical study of the gas phase kinetics of atomic chlorine reactions with CH_3NH_2, $(CH_3)_2NH$, and $(CH_3)_3N$. *Physical Chemistry Chemical Physics* **2014**. *Submitted*

In the previous section we saw that the OH radical reactions of small aliphatic amines are very fast, indicating that OH radicals constitute their main sink and that the atmospheric residence times are only a few hours. If the chlorine atom reactions are fast enough, they may be of importance in areas of high chlorine concentrations and it is therefore important to know also the branching ratios. This paper presents an experimental and theoretical study of the chlorine atom reactions of MA, DMA and TMA. The work was done in cooperation with Professor Paul Wine and co-workers at Georgia Institute of Technology. All experiments were performed by them.

The reactions were studied using similar methods as for the OH reactions. Geometries and frequencies of the stationary points on the potential energy surfaces were calculated using MP2/cc-pVTZ and the energies were improved with CCSD(T)-F12a calculations. Figure 5.3 shows the results of the calculations. The potential energy surfaces are characterized by very strongly bound pre reaction adducts and submerged barriers. The strongly bound adducts are caused by an interaction between the lone pair on nitrogen and the radical orbital of the chlorine atom, forming a two-center three-electron bond [87].

Rate coefficients for the reactions were calculated based on the potential energy surfaces shown in Figure 5.3 by assuming a microcanonical steady state and no collisional stabilization for the pre-reaction complexes. The results are in excellent agreement with the values measured at Georgia Tech. The reactions are independent of temperature and pressure, and extremely fast with rates even exceeding the predicted hard sphere collision rate. The reason for this is thought to be the long range two-center three-electron interaction of the nitrogen lone pair with the Cl atom to form the exceptionally strongly bound pre reaction adducts as shown in figure 5.3 and that the barriers to hydrogen abstraction are so low that they have very little influence on the overall reaction rate.

The branching ratios were calculated to 9C:91N and 0C:100N for MA and DMA respectively. The branching ratio for MA was also measured to be 48C:52N (no experimental uncertainty given) by Rudic *et al.* [88], who also studied the reaction with G2//MP2/6-311G(d,p). The calculated potential energy surface in this work is in good agreement with the results from Rudic

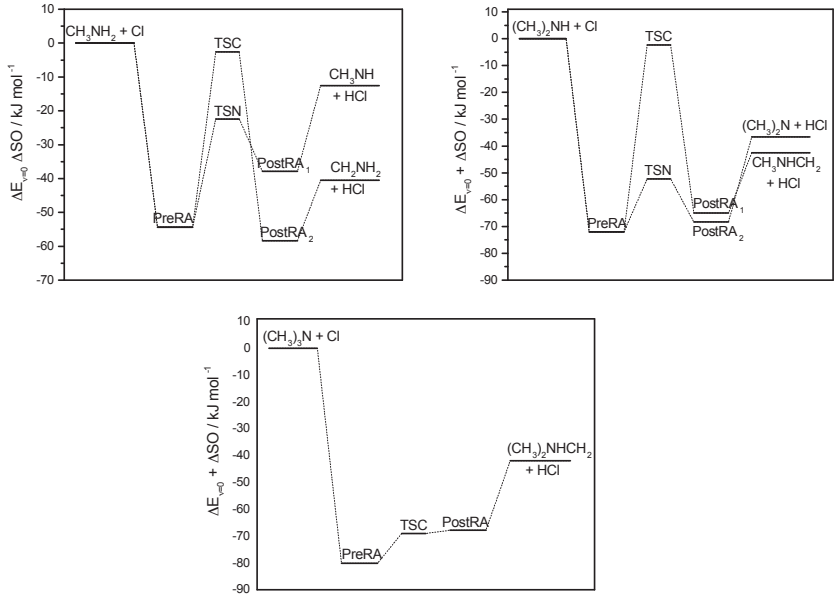

Figure 5.3: Stationary points on the potential energy surfaces of the chlorine atom reactions of the methyl amines. The results are from CCSD(T)-F12a/aug-cc-pVTZ//MP2/cc-pVTZ calculations.

et al., but the calculated and experimental branching ratios differ somewhat. However, since the translational energy in the experiments was around 2000 cm^{-1}, corresponding to a translational temperature of ≈ 2900 K and the calculated C-H abstraction yield increases from 9% at 298 K to 22% at 600 K, the calculations and the experiments may still be in reasonable agreement with each other. The sensitivity of the calculated room temperature branching ratios to the barrier heights was tested as for the OH reactions by shifting the barriers by 4 kJ/mol in opposite directions. Raising the barriers for C-abstraction and lowering the barrier for N-abstraction in MA gave 1C:99N, while the opposite change resulted in 40C:60N. The maximum change in the overall rate coefficient was 7%. For DMA, the shift in barrier heights resulted in no change in the calculated branching ratio and only 1% change in the overall reaction rate. It should be noted that since the model assumes no collisional stabilization and that all transition states are below the entrance energy, no tunneling is included in the model. This is unlikely to be of any importance for the overall reaction rate, but it could influence the relative

yield of the C-H abstraction channels. The effect should, however, be much smaller that that of the shift in the barrier heights.

The calculations indicate that the N-H abstraction reactions play a larger role in the chlorine atom reactions than in the OH radical reactions, although the calculated branching ratio for the MA reaction does have a large uncertainty and the calculations seem to overestimate the importance of the N-H abstraction channels for both chlorine atom and OH radical reactions. For DMA, N-H abstraction seems to be the dominating reaction path, even when allowing for a significant uncertainty in the calculated barriers.

Based on the quantum chemical results and the kinetic data, it seems clear that reaction with chlorine atoms may constitute an important sink of amines in some marine areas, especially for MA for which the chlorine atom reaction is almost 20 times faster than the corresponding OH radical reaction. An important consequence of this is that a larger fraction will react through N-H abstraction, leading to a larger potential for nitramine and nitrosamine formation than expected from considering only the OH radical reaction.

5.3 The OH radical reactions of amides

Paper III: Bunkan, A. J. C; Hetzler, J; Mikoviny, T; Wisthaler, A; Nielsen, C. J.; Olzmann, M. Experimental and theoretical study of the OH radical reactions with *N*-methylformamide and *N,N*-dimethylformamide. *Manuscript in preparation*

This section presents a kinetic and mechanistic study of the OH radical reactions of *N*-methylformamide (MF) and *N,N*-dimethylformamide (DMF). Amides have been identified as major photo-oxidation products of all amines studied [11], and MF and DMF have been reported as major degradation products of dimethylamine and trimethylamine respectively. Barnes *et al.* [16] have presented a review on the atmospheric chemistry of amides and proposed mechanisms for their atmospheric degradation.

The OH radical reactions of MF and DMF were studied using experimental and theoretical methods. Figure 5.4 shows stationary points on the potential energy surfaces calculated with CCSD(T*)-F12a/aug-cc-pVTZ//MP2/aug-cc-pVTZ. The potential energy surfaces show the same characteristics as for the corresponding amine reactions with relatively stable pre reaction adducts and submerged barriers for hydrogen abstraction.

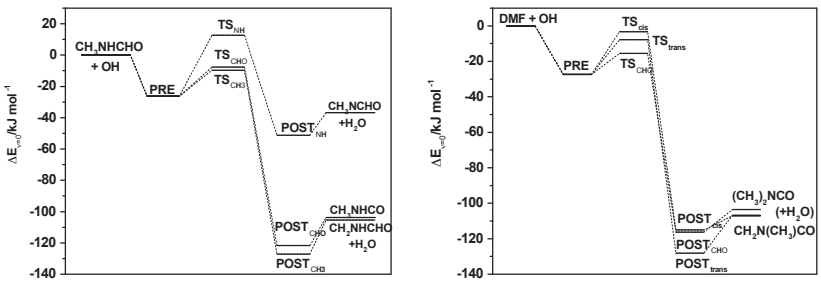

Figure 5.4: Stationary points on the potential energy surfaces of the OH radical reactions of the *N*-methylformamide and *N,N*-dimethylformamide. The results are from CCSD(T*)-F12a/aug-cc-pVTZ//MP2/aug-cc-pVTZ calculations.

Rate coefficients for the OH radical reactions of MF and DMF were measured with laser-induced fluorescence in a slow flow system as a function of temperature from 260 K to 295 K at different pressures. Both reactions show negative temperature dependencies and the reaction of DMF shows no pres-

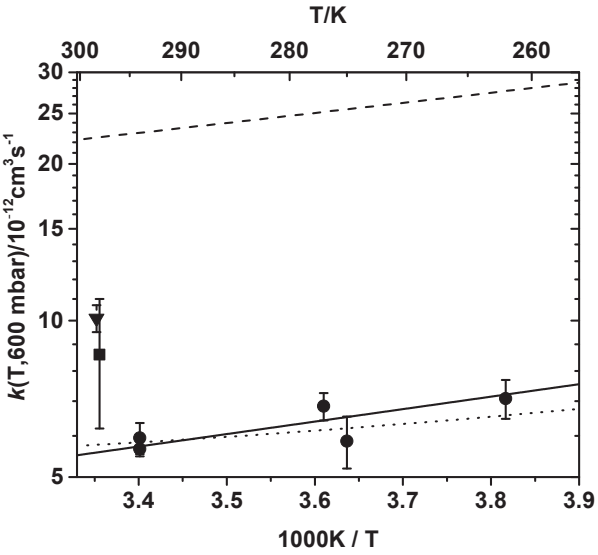

Figure 5.5: Temperature dependence of the measured reaction rate coefficients for MF + OH. ●: This work in 600 mbar helium,▼: Borduas et al. in 1000 mbar air, [89], ■: Solignac et al. in 1000 mbar air, Ref [90]. The full curve represents an Arrhenius fit, the dashed line the predicted rate coefficient from master equation calculations based on the CCSD(T)-F12a//MP2 calculations and the dotted line represents the calculated rate coefficient with the barrier heights adjusted to best reproduce the experimental values.

sure dependence but a very weak positive pressure dependence is observed for MF.

In order to examine why this weak pressure dependence is observed for MF but not for DMF, the kinetics of the reactions were modeled using a master equation model as implemented in MESMER [91]. The calculations indicate a very small positive pressure dependence for both reactions, although significantly larger for MF than for DMF. The calculated rate coefficients are somewhat larger than the observed values, but excellent agreement can be achieved with only moderate adjustment of the reaction barriers. The results for MF and DMF are shown in Figures 5.5 and 5.6 respectively.

Based on the measured rate coefficients and assuming $[OH]_{24h}=10^6$ molecule cm^{-3}, the atmospheric lifetimes of MF and DMF with respect to reac-

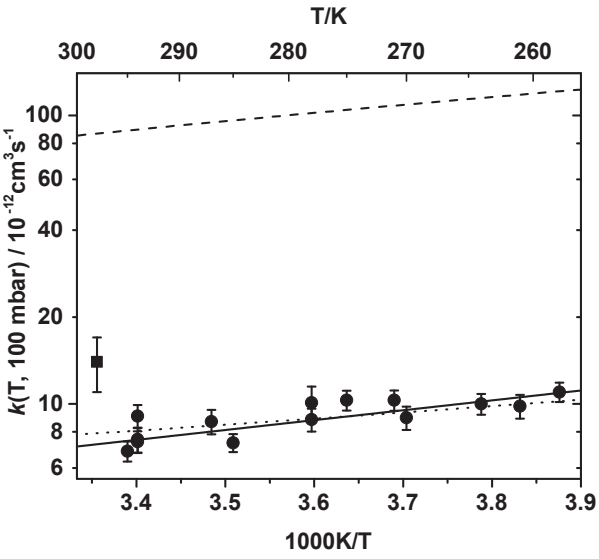

Figure 5.6: Temperature dependence of the measured reaction rate coefficients for DMF + OH. ●: This work at 100 mbar in helium, ■: Solignac et al. in 1000 mbar air, Ref [90]. The full curve represent an Arrhenius fit, the dashed line the predicted rate coefficient from master equation calculations based on the CCSD(T)-F12a//MP2 calculations and the dotted line represents the calculated rate coefficient with the barrier heights adjusted to best reproduce the experimental values.

Table 5.2: Available kinetic data for alkyl amide + OH reactions[a]

Amide	$k(298K)/10^{-12}$cm^{3}s^{-1}	Ea / kJ mol^{-1}	Reference
Formamide	4.44±0.46		[89]
N-methylformamide	5.7±1.7	-4.6	This work
	8.6±2.4		[90]
	10.6 ±0.6		[89]
N,N-dimethylformamide	14±3		[90]
	8.5±2.6	-6.6	This work
Acetamide	3.5±1.0		[16]
	0.8±0.4		[89]
N-methylacetamide	11±3		[16]
	5.2	-4.1	[92]
	5.42±0.19		[89]
N,N-dimethylacetamide	13.6	-5.2	[92]
	19±3		[90]
Propanamide	1.78 ±0.43		[89]
N-methylpropanamide	7.6	-3.3	[92]
N,N-dimethylpropanamide	20.7	-4.3	[92]

[a]Uncertainties given by the autors

tion with OH radicals are expected to be 1 $^1/_2$ to 2 days. Since the amides react slower than amines with OH radicals and have higher dipole moments, they may deposit on water droplets and particles to a larger extent than the amines.

Table 5.2 shows the available kinetic data for alkylamide + OH reactions. The rate coefficients from this work fit nicely in with the trend that the larger amides react faster than the smaller ones and that the activation energy increases with length of the alkyl chain and decreases with the number of methyl groups. The values from this work are also somewhat lower than the values reported by Solignac *et al.* [90], but within the combined error bars. Somewhat more surprising is the fact that the relative measurements (Solignac *et al.* [90], Barnes *et al.* [16], and Borduas *et al.* [89]) systematically give higher rate coefficients than the absolute measurements (This work and Koch *et al.* [92]). A possible explanation for this discrepancy is the different nature of the experiments. In the relative measurements, the removal rate of the amide is measured relative to a reference with a known rate coefficient and any additional process that removes the amide will give a higher observed reaction rate unless the extra loss is corrected for, as done by both Solignac *et al.* and Barnes *et al.*, but not by Borduas *et al.* In addition, any systematic error in the reference reaction rate, will influence the result, unless two or more references are used, as done by Solignac *et al.* and Barnes *et al.* In

the flow experiments, the measured quantity is the loss rate of OH radicals to reaction under pseudo first order conditions, so a process that removes reactant amide will make the observed reaction rate lower than the actual rate.

The products of the photooxidation of MF and DMF were detected by proton-transfer-reaction time-of-flight mass spectrometry (PTR-ToF-MS) in a series of experiments by Armin Wisthaler. Based on the observed product time profiles, the quantum chemical calculations and master equation modeling of the initial reactions and hot reaction intermediates, photo-oxidation mechanisms are proposed.

Figure 5.7 shows the major pathways in the atmospheric photo-oxidation of MF. The dominant product observed in the product study is methyl isocyanate and minor products include *N*-formylformamide and *N*-methylnitramine. In addition methanimine was observed in traces. Barnes *et al.* reported methyl isocyanate and N-formylformamide as major products in the MF photooxidation, but since calibrated reference spectra were not available, accurate product yields were not determined. Based on reactivity trends, they suggested that 50% of the reaction proceed through hydrogen abstraction from the methyl group. Borduas *et al.* studied the reaction under NO_x-free conditions and report methyl isocyanate as the major product with a yield of 36-40%, and only trace amounts of *N*-formylformamide. In addition they observed 15% formamide, but state that the how it is formed remains unclear.

Figure 5.8 shows the major pathways in the DMF photooxidation. The observed main products are $CH_3N(CHO)_2$, $(CH3)_2NC(O)OONO_2$ and *N,N*-dimethylnitramine. In addition, *N*-methylmethanimine and *N,N*-dimethylnitrosamine are observed as minor products. Barnes *et al.* reported $CH_3N(CHO)_2$ as the major product in the photo-oxidation of DMF, with unquantified amounts of $(CH3)_2NC(O)OONO_2$ as a minor product and no mention of any imines, nitramines or nitrosamines. Since these compounds are formed in small amounts, depending on the NO_x concentration, it is likely that they were formed in the experiments, but never reached the detection limit of the FTIR spectrometer.

Based on the product study, it is clear that both MF and DMF give rise to several harmful products and may have an even higher potential for nitramine and nitrosamine formation than the corresponding amines.

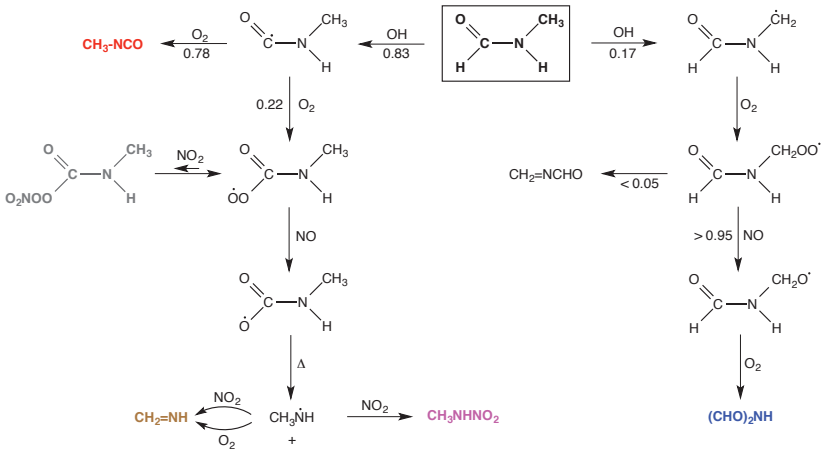

Figure 5.7: Simplified mechanism for atmospheric photo-oxidation of *N*-methylformamide. The branching ratios stem from the PTR-ToF-MS experiments and have estimated uncertainties of ± 0.05

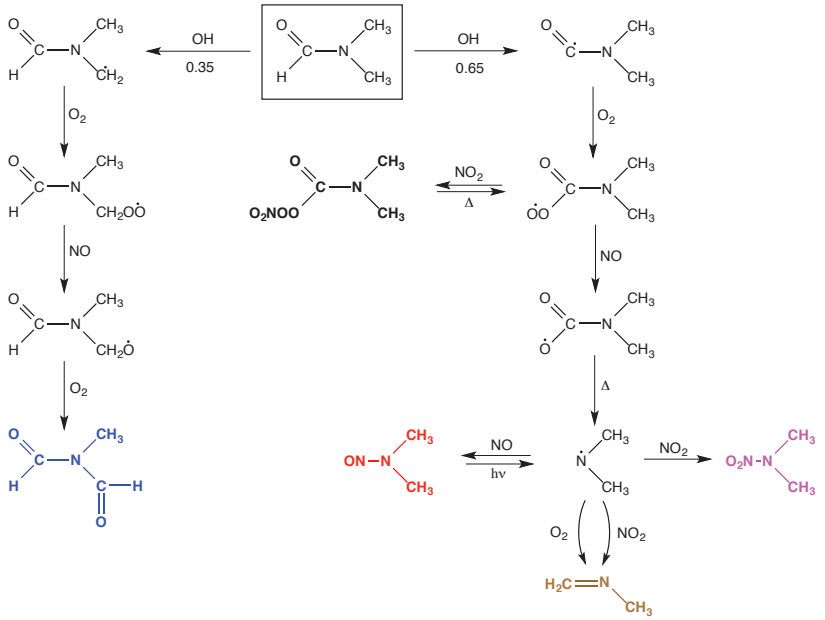

Figure 5.8: Simplified mechanism for atmospheric photo-oxidation of *N,N*-dimethylformamide. The branching ratios stem from the PTR-ToF-MS experiments and have estimated uncertainties of ± 0.05

5.4 The atmospheric chemistry of methanimine

Paper IV: Bunkan, A. J. C.; Tang, Y. and Sellevåg, S. R. and Nielsen, C. J. Atmospheric Gas Phase Chemistry of CH_2=NH and HNC. A First-Principles Approach. *The Journal of Physical Chemistry A* **2014**, 118, 5279-5288.

Methanimine has been reported to constitute 90 % of the primary degradation products in the photo-oxidation of methylamine [14], but despite its obvious importance, virtually nothing is known about its atmospheric chemistry. This paper presents a computational study of the atmospheric reactions of methanimine and its degradation products.

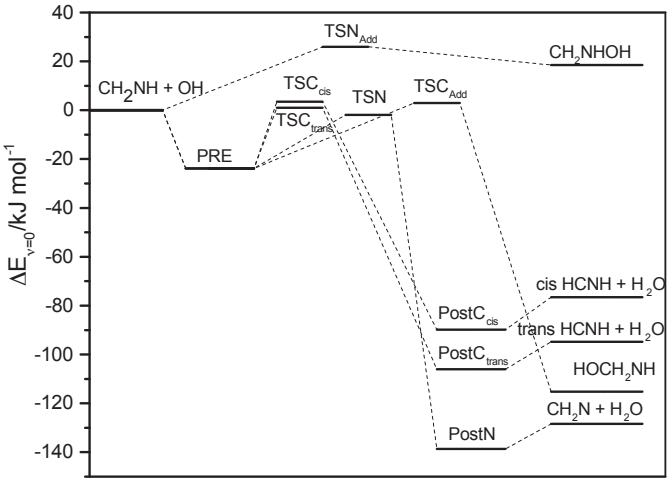

Figure 5.9: Stationary points on the potential energy surface of the OH radical reaction of methanimine. Results from CCSD(T)/cc-pV(TQ)Z//CCSD(T)/cc-pVTZ calculations.

The reaction of methanimine with OH radicals has been studied with high level computational methods. Stationary points on the potential energy surface, shown in Figure 5.9, were characterized by CCSD(T)/cc-pVTZ calculations and the single point energies of the stationary points were improved with CCSD(T)/cc-pVQZ calculations and basis set extrapolation. The potential energy surface has many similarities to those of the corresponding amine and amide reactions with a stable pre-reaction adduct and low bar-

riers for hydrogen abstraction. Unlike the amines and amides, which have barriers significantly below zero, the barriers for hydrogen abstraction from methanimine are all close to zero and there is also an addition route that may be important.

The T1 diagnostic [33] values for the saddle points are in the range 0.035 to 0.040, indicating that they may have significant multi-reference character. The reactions were therefore also studied by using CASPT2 in different basis sets and an active space consisting of the minimum set of orbitals necessary to describe the reaction, 3 electrons in 3 orbitals for the addition channel and 5 electrons in 5 orbitals for the hydrogen abstraction reactions. In addition, larger active spaces were also studied. The CASSCF calculations give occupation numbers of around 1.975 for the bonds being formed and broken in the hydrogen abstractions and 1.90 for the addition reactions. The results from the CCSD(T) and the CASPT2 calculations are very similar, and the barrier heights resulting from CCSD(T)/cc-pV(TQ)Z calculations based on the CASPT2 and CCSD(T) geometries are in excellent agreement. It is therefore reasonable to assume that the potential multi-reference character of the saddle points does not seriously affect the coupled cluster results.

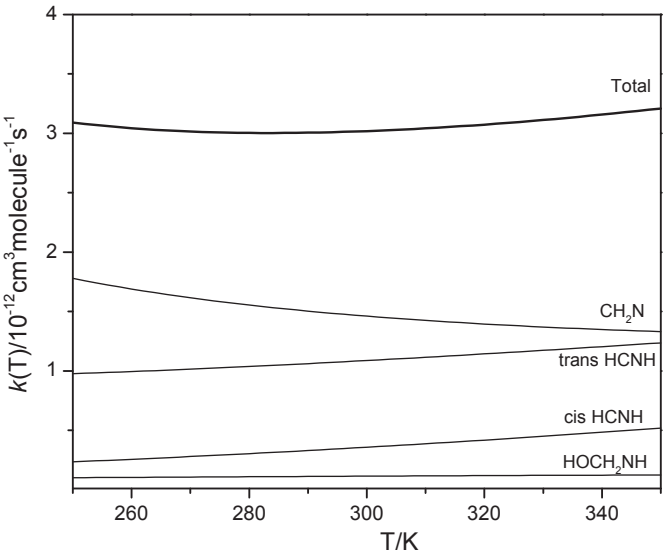

Figure 5.10: Calculated rate coefficients for the individual reaction paths as well as the overall rate of the CH_2NH + OH reaction at 1 bar.

Rate coefficients and branching ratios for the CH_2NH + OH reaction were calculated by using a master equation model as implemented in MESMER [91].

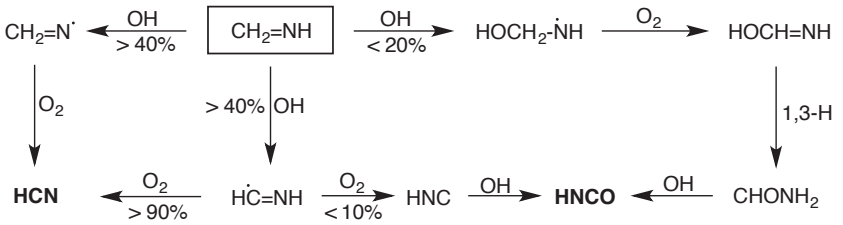

Figure 5.11: Simplified mechanism for atmospheric photo-oxidation of methanimine.

The calculated rate coefficient as well as contributions from the individual reaction channels are shown in Figure 5.10. The reaction is predicted to be significantly slower than the corresponding amine reaction and the dominating reaction paths are the formation of CH_2N and trans HCNH, with cis HCNH and $HOCH_2NH$ as minor products. CH_2N, cis HCNH and trans HCNH are all expected to react with O_2 in the atmosphere giving HCN and possibly also minor amounts of HNC, while $HOCH_2NH$ is expected to form formamide. Based on the calculated branching ratios, a simplified degradation scheme for the atmospheric photo-oxidation of methanimine is proposed, as shown in Figure 5.11.

HNC + OH

The OH radical reaction of HNC was studied at the same level of theory as for methanimine. The reaction proceeds through a highly energized intermediate, HNCOH, that can react further by direct hydrogen atom loss, as shown in Figure 5.12, while the barrier to hydrogen abstraction is too high to be of any importance in the atmosphere. Master equation modeling reveals that the reaction is very fast, independent of pressure and that the dominating product is isocyanic acid. It has been suggested that if HNC is a product of methylamine photo-oxidation and it reacts through hydrogen abstraction to form the cyano radical, it might result in the formation of N_2O [12]. Since the quantum chemical calculations unambiguously show that neither HCN nor HNC react to form the cyano radical, it can be concluded that N_2O is not a product of methylamine photo-oxidation.

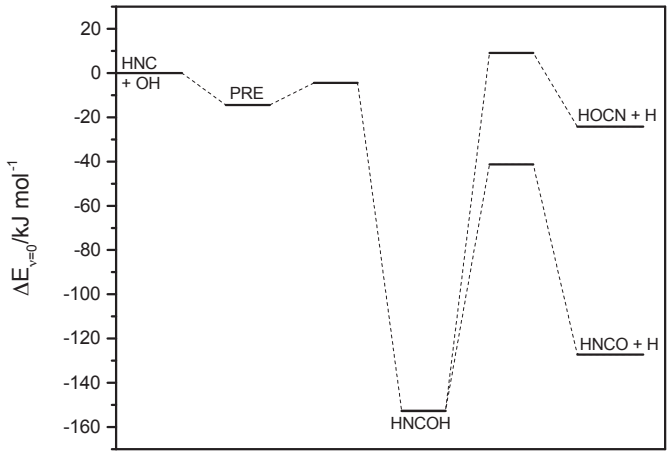

Figure 5.12: Stationary points on the potential energy surface of the OH radical reaction of HNC. Results from CCSD(T)/cc-pV(TQ)Z//CCSD(T)/cc-pVTZ calculations.

5.5 The OH radical reaction of nitramines

Paper V: Maguta, M. M.; Aursnes, M. Bunkan, A. J. C.; Edelen, K.; Mikoviny, T; and Nielsen, C. J.; Stenstrøm, Y; Tang, Y; Wisthaler, A. Atmospheric Fate of Nitramines: An Experimental and Theoretical Study of the OH Reactions with CH_3NHNO_2 and $(CH_3)_2NNO_2$. *The Journal of Physical Chemistry A* **2014** *118* (19), 3450-3462.

This paper presents an experimental and theoretical study of the kinetics and mechanisms of the OH radical reactions of *N*-methylnitramine and *N,N*-dimethylnitramine. The FTIR experiments were performed by Mihayo Musabila Maguta and are included in his PhD thesis. PTR-ToF-MS experiments were done by Armin Wisthaler.

N-methylnitramine and *N,N*-dimethylnitramine are formed as minor products in the photo-oxidation of methylamine and dimethylamine respectively, but not much is known about their atmospheric chemistry. There is only one previous study of the OH radical reaction of *N,N*-dimethylnitramine [18]. The reactions proceed through hydrogen abstraction, mainly from the methyl groups, and are significantly slower than the corresponding amine reactions.

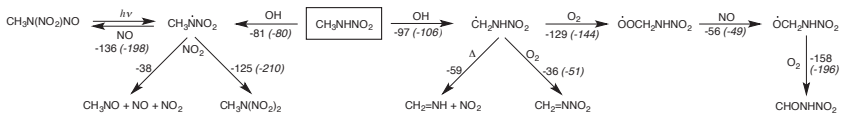

Figure 5.13: Major reaction pathways in the atmospheric photo-oxidation of *N*-methylnitramine. Reaction enthalpies from G4 calculations are given. The numbers in parenthesis are for the corresponding amine reactions.

Figure 5.13 shows the main routes in the atmospheric photo-oxidation of *N*-methylnitramine. Based on the quantum chemical calculations, it is clear that hydrogen abstraction from the methyl group is the dominating reaction pathway. The resulting radical, CH_2NHNO_2 is formed with a considerable amount of internal energy and its fate is governed by competition between unimolecular dissociation and collisional stabilization followed by bimolecular reaction with O_2 to form a peroxy radical. The competition between the two processes was examined using a master equation model. The calculations indicate that unless a very large amount of the reaction enthalpy is deposited in the water molecule, direct dissociation to form CH_2NH and NO_2 dominates at all relevant pressures, but if the water molecule is formed with two energy quanta in the OH stretching vibration, the calculations predict a dissociation yield of 7 %. If a peroxy radical is formed, it is formed with a large excess

of internal energy, and may either react unimolecularly, giving HO_2 and CH_2NNO_2 or bimolecularly following collisional stabilization. In the master equation for the chemically activated peroxy radical, the competition between unimolecular reaction to form HO_2 and collisional stabilization followed by reaction with NO was found to be strongly pressure dependent with an HO_2 yield of only 4 % at 1 bar.

The FTIR product study barely shows any sign of products. This is probably because all expected products are more reactive than *N*-methylnitramine and are therefore only present in small amounts. The PTR-ToF-MS experiments, on the other hand, does show significant amounts of HCN and it is therefore concluded that methanimine is indeed the dominant product in *N*-methylnitramine photo-oxidation.

For *N,N*-dimethylnitramine, the situation is somewhat simpler as there is only one possible hydrogen abstraction route, as shown in Figure 5.14. Master equation modeling reveals that the $CH_3N(NO_2)CH_2$ radical will dissociate immediately to NO_2 and CH_3NCH_2 if formed with enough energy to overcome the dissociation barrier and that a significant amount will dissociate, even if the two quanta of the reaction enthalpy is deposited in the water molecule. The theoretical predictions are supported by the observation of a nitro compound in the FTIR experiments and peaks corresponding to *N*-methyl-*N*-nitroformamide and *N*-methylmethanimine in the PTR-ToF-MS experiments.

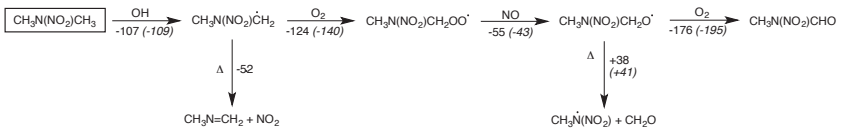

Figure 5.14: Major reaction pathways in the atmospheric photo-oxidation of *N,N*-dimethylnitramine. Reaction enthalpies from G4 calculations are given. The numbers in parenthesis are for the corresponding amine reactions.

Methanimine and N-methylmethanimine constitute the main products in the OH initiated photo-oxidation of *N*-methylnitramine and *N,N*-dimethylnitramine respectively. Other products include *N*-nitroamides, but the yields are yet to be determined.

5.6 The OH radical reaction of HCN

Paper VI: Bunkan, A. J. C.; Liang, C.-H.; Pilling, M. J.; Nielsen, C. J. Theoretical and experimental study of the OH radical reaction with HCN. *Molecular Physics* **2013** *111* , 1589-1598.

Based on the computational study of methanimine it seems clear that HCN will constitute a major degradation product of methanimine and therefore also of methylamine. The atmospheric chemistry of HCN has been studied by several authors [93–113] and it is well established that its main source is biomass burning [109] and that ocean uptake constitute its main sink, with reaction with OH radicals constituting an additional, minor sink [107]. There are several studies of the OH radical reaction of HCN, both experimental [114–118] and theoretical [119–123]. The OH radical reaction of HCN

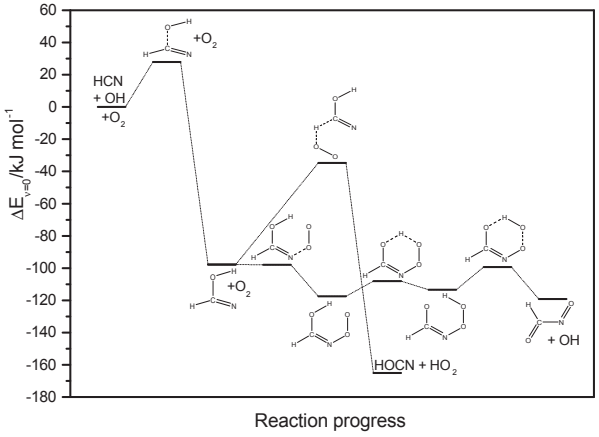

Figure 5.15: Stationary points on the potential energy surface of the OH radical reaction of HCN in the presence of oxygen. Results from CCSD(T)/aug-cc-pV(TQ)Z//MP2/aug-cc-pVQZ calculations.

in the presence of oxygen was studied with experimental and computational methods. Stationary points on the potential energy surfaces were characterized by MP2 calculations in different basis sets and the single point energies were improved by CCSD(T)/aug-cc-pVQZ calculations and basis set extrapolation. In addition, the geometry for the initial reaction was calculated

with CCSD/aug-cc-pVTZ. The results from the CCSD(T)/aug-cc-pV(TQ)Z calculations are shown in Figure 5.15.

The ^{13}C and ^{14}N kinetic isotope effects for the OH radical reaction of HCN were measured in a stationary gas mixture with long path FTIR detection. Both isotope effects are inverse and the measured values are 0.9733 ± 0.0024 and 0.9840 ± 0.0032.

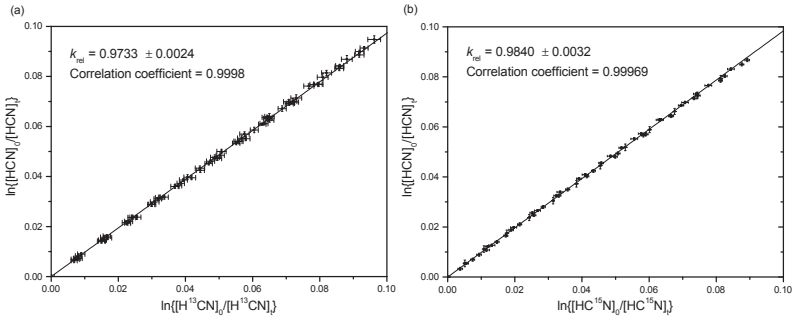

Figure 5.16: Relative rate plots from the measurements of the kinetic isotope effects for the OH radical reaction of HCN. The calculated uncertainty is 2σ from the linear regression and the uncertainties of the individual data points are the combined uncertainty of the spectral fitting procedure and a 0.1% error in the optical accuracy of the spectrometer.

Rate coefficients for the initial reaction were calculated using a master equation model with Eckart tunneling. The barrier height and the collisional energy transfer parameter were fitted to reproduce experimental values from Strekowski [118] and the results are shown in Figure 5.17. The agreement between the experimental and calculated values is very good and only small adjustments of the barrier height were necessary to reproduce the experimental results. Tunneling makes a small, but noticable contribution and the difference in fitted barrier heights for the models with and without tunneling is around 1 kJ/mol, corresponding to roughly a factor of 1.5 change in the reaction rate. It should be noted that the Eckart model is a relatively simple model and that it has a tendency to overestimate the tunneling contribution.

The kinetic isotope effects were calculated using the same master equation model as for the absolute reaction rates, but the agreement is less satisfactory. The calculations predict normal isotope effects for both ^{13}C and ^{14}N while the experiments give inverse kinetic isotope effects. The reason for this is not clear, but it is likely that the harmonic oscillator model is inadequate

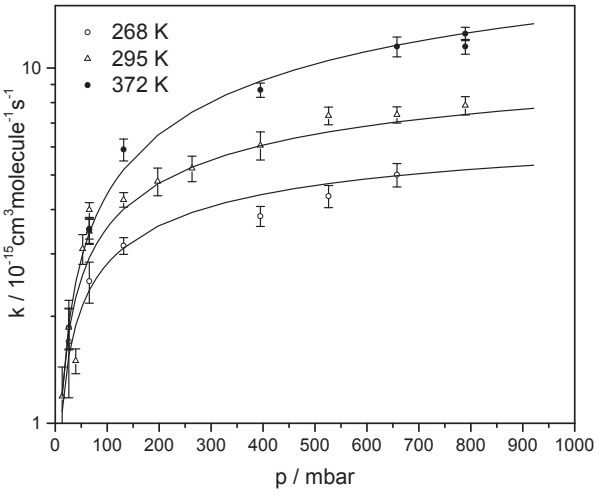

Figure 5.17: Rate coefficients for the OH radical reaction of HCN. The data points are from Strekowski [118] and the curves represent the best fit of the master equation model with Eckart tunneling, and $\langle \Delta E_{down} \rangle$ was allowed to vary with temperature, and barrier height of 14.3 kJ mol^{-1}

to describe small changes in the vibrational density of states from isotopic substitutions accurately.

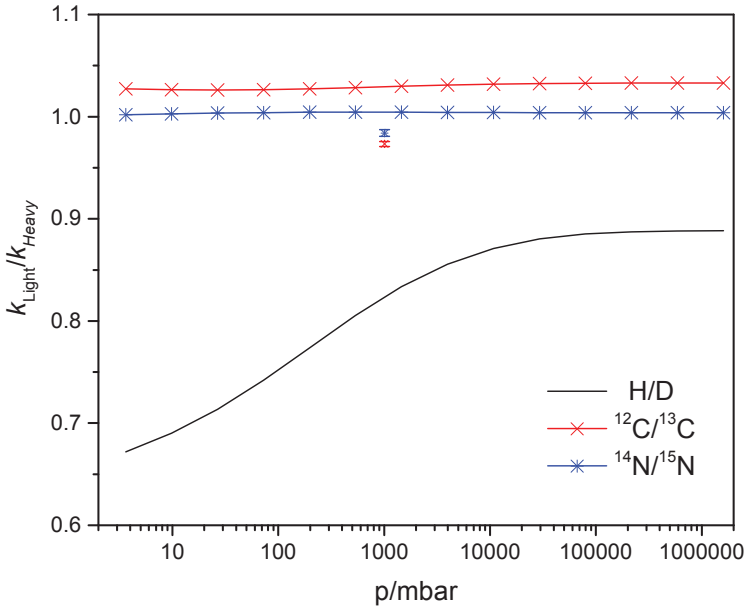

Figure 5.18: Calculated kinetic isotope effects for the OH radical reaction of HCN along with experimental values for the ^{13}C and ^{15}N isotope effects

5.7 The OH radical reaction of formamide

Formamide constitutes the second most abundant oxidation product of methylamine [11] and a minor oxidation product of methanimine. Barnes *et al.* [16] unsuccessfully attempted to measure the rate coefficient of its OH radical reaction and reported isocyanic acid as the main product of formamide photooxidation. Borduas *et al.* [89] recently published an experimental and theoretical study of the OH radical reactions of amides, and reported the first experimental rate coefficient for the reaction.

Along with the kinetic measurements for *N*-methylformamide and *N,N*-dimethyl-formamide described in paper III, measurement of the rate coefficient for the OH radical reaction of formamide was attempted. The experiments were abandoned due to a dependence of the measured rate coefficients on the photolysis laser intensity, indicating that secondary radical chemistry was taking place in the cell. Measurements were also attempted in the smog chamber in Oslo, but due to severe wall effects, no kinetic information could be extracted from the experiments. The smog chamber experiments did, however, confirm isocyanic acid as the only observed product. As an alternative to the experiments, high level quantum chemical calculations were performed.

As for the reactions of *N*-methylformamide and *N,N*-dimethylformamide, geometry optimization and frequency calculations for the stationary points on the potential energy surfaces were done at the MP2/aug-cc-pVTZ level and single point energies were improved by CCSD(T*)-F12a/aug-cc-pVTZ calculations. The calculations indicate that the only relevant reaction channel under atmospheric conditions is abstraction from the carbonyl site. The stationary points of this reaction path were therefore studied at the same level as for the methanimine reaction described in paper IV, with geometries and frequencies from CCSD(T)/cc-pVTZ calculations, and single point energies improved by CCSD(T)/cc-pVQZ calculations and basis set extrapolation according to the scheme by Helgaker *et al.* [45, 46]. The coupled cluster and MP2 calculations were performed in Molpro [124, 125] and Gaussian [126] respectively.

The potential energy surface for the OH radical reaction of formamide, shown in Figure 5.19, displays not only similar features as the potential energy surfaces for methylamine and methanimine, but is also very similar to the corresponding reaction of acetaldehyde [127] with hydrogen abstraction from the carbonyl site having a submerged barrier, while the other abstraction channel and addition to the double bond both have moderate barriers. It can unambiguously be concluded that abstraction from the carbonyl site is the dominating reaction and that the resulting $OCNH_2$ radical reacts

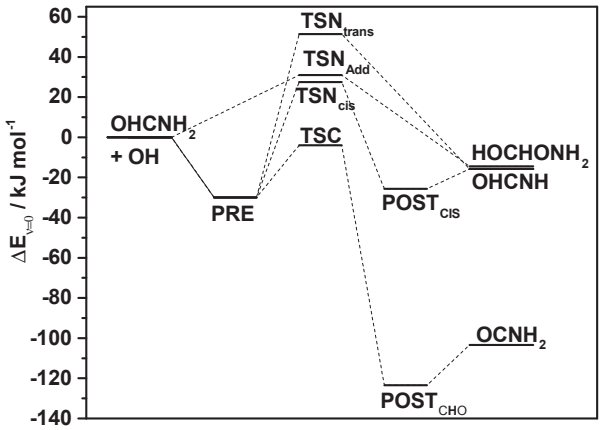

Figure 5.19: Potential energy surface for the OH radical reaction of formamide. Results from CCSD(T*)-F12a/aug-cc-pVTZ//MP2/aug-cc-pVTZ level of theory.

quickly with O_2 to form isocyanic acid as the by far dominant product. The calculated energies in this work are in fair agreement with the results from G3X-K//M06-2X/6-31G(2df,p) calculations performed by Borduas *et al.*, although they report a slightly positive barrier for abstraction from the C-H site, whereas the high-level calculations in this work predict a barrier of -4 kJ mol^{-1}.

Rate coefficients for the overall reaction were calculated in the same manner as for the reaction of methanimine + OH. Capture rate coefficients for formation of the pre reaction complexes were calculated from long range transition state theory based on experimental dipole moments from the NIST database [128], while specific rate coefficients for the inner transition states were calculated with RRKM theory, based on rovibrational data from the CCSD(T)/cc-pVTZ calculations. The torsional mode of the OH fragment in the transition state for abstraction from the carbonyl group was treated as a hindered internal rotor with a rotational potential calculated at the BHandHLYP/aug-cc-pVDZ level of theory.

The calculated rate coefficient for the OH reaction of formamide is in good agreement with the experimental value from Borduas *et al.*, as shown in Figure 5.20, although a factor of three lower. It should be noted that

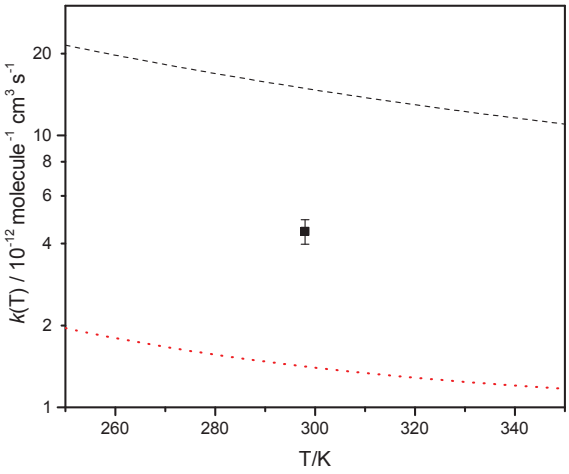

Figure 5.20: Rate coefficients for the OH radical reaction of formamide. Black dashed line: theoretical estimate based on CCSD(T*)-F12a/aug-cc-pVTZ//MP2/aug-cc-pVTZ, red dotted line: theoretical estimate based on CCSD(T)/cc-pV(TQ)Z/CCSD(T)//cc-pVTZ calculations, ■: experimental value from Borduas *et al.* [89]

Borduas *et al.* only employed one reference compound in their relative rate experiments, and any systematic error in the reference rate coefficient will then influence the measured rate coefficient. Further, the given uncertainty of ±10% is one standard deviation of three or more reproducible experiments and does not include any uncertainty of the reference compound. Although the authors state that no wall loss of formamide was observed, they also report that isocyanic acid was observed as a sole product, but with a yield of only 17-19%. It is therefore possible that the measurement is influenced by wall loss of formamide.

5.8 What can we learn from high level calculations?

The general topic of this work is the OH radical reactions of amines, imines and amides, and all reactions have been studied using quantum chemical methods and statistical rate theory. As mentioned in Chapter 2 and 3, the calculation of rate coefficients within 'kinetic accuracy' requires the energy barriers accurate within 2 kJ/mol as well as highly accurate partition functions. Such accuracy is available only for the smallest systems in this work, and the reactions have therefore been studied with less accurate methods. To assess the accuracy of the calculations, a high level case study was performed on the atmospherically relevant pathways of the OH radical reactions of methylamine, methanimine and formamide. Most of the calculations for methanimine are published in paper IV, while the calculations for methylamine and formamide are yet unpublished.

5.8.1 Potential energy surfaces

Stationary points on the potential energy surfaces were characterized at the CCSD(T)/cc-pVTZ level. Single point energies of the stationary points were improved CCSD(T)/cc-pVQZ calculations and basis set extrapolation after the scheme by Helgaker *et al.* [45, 46]. The coupled cluster calculations were performed in Molpro [124, 125].

From the potential energy surfaces, shown in Figure 5.21, some similarities are immediately clear. All three reaction systems are characterized by a deep pre reaction potential well, all reactions have barriers close to the entrance energies and they all have strongly exothermic hydrogen abstraction reactions. The Hammond postulate states that when the transition state is close to an intermediate in energy, the geometries will also be very similar. This is evident in the OH radical reactions studied here which are characterized by very early transition states, with reacting C-H and N-H bonds being stretched by as little as 3-5 pm in the transition state structures. The O-H bonds being formed are, on the other hand, 30-50 pm longer than in the stable water molecule.

Some differences are also evident. For both methylamine and methanimine all hydrogen abstraction channels are strongly exothermic and have barriers close to or below zero. For formamide, the situation is analogous to the reaction of OH radicals with acetaldehyde [127], with hydrogen abstraction from the carbonyl site having a submerged barrier, while the other abstraction channel and addition to the double bond both have

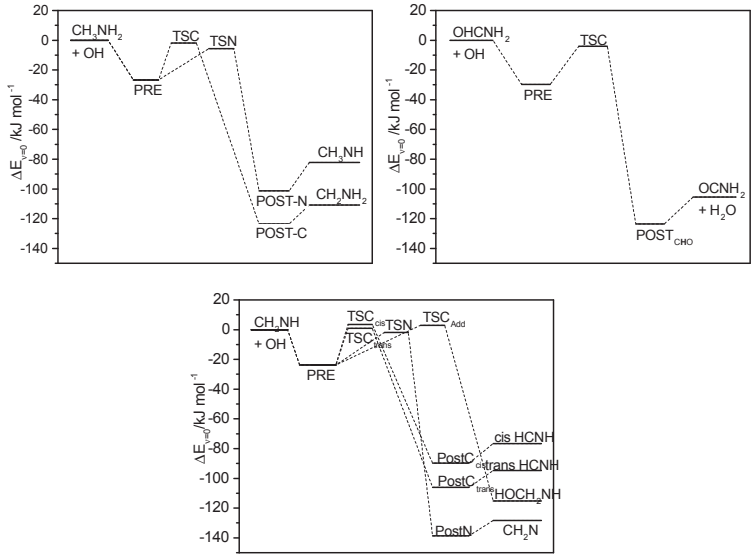

Figure 5.21: Energies of the stationary points of the atmospherically relevant pathways of the OH radical reactions of methylamine, methanimine and formamide.

moderate barriers, as described in the previous section. For methylamine, the CCSD(T)/cc-pV(TQ)Z//CCSD(T)/cc-pVTZ calculations give barriers of -1.9 and -5.6 kJ mol^{-1} for abstraction from the methyl and amino site, respectively. This is slightly higher than predicted by the CCSD(T)-F12a/aug-cc-pVTZ//MP2/aug-cc-pVTZ calculations published in paper I, where the barriers are -8.2 and -8.4 kJ mol^{-1} respectively. For formamide, the barrier to abstraction from the carbonyl site is calculated to be -4.0 kJ mol^{-1} at the CCSD(T)/cc-pV(TQ)Z//CCSD(T)/cc-pVTZ level of theory while CCSD(T)-F12a/aug-cc-pVTZ//MP2/aug-cc-pVTZ calculations predict a barrier of -10.8 kJ mol^{-1}. Since the barrier height for the OH radical reaction of formamide was underestimated at the CCSD(T*)-F12a/aug-cc-pVTZ//MP2/aug-cc-pVTZ level of theory, it is reasonable to suspect that it may also be the case for the reactions of MF and DMF for which no higher level calculations are available.

5.8.2 Kinetics

In order to compare calculated rate coefficients and branching ratios for the reactions, the kinetics were modeled using a similar master equation model as employed for the OH radical reactions of methanimine in paper IV and for formamide in the previous section. For methylamine and formamide, a very slight pressure dependence with a change of 9 % in the rate coefficients for formamide and 4% for methylamine over the range 50-1000 mbar is predicted, while a somewhat larger change is calculated for methanimine due to the adduct forming channel. This effect was observed for *N*-methylformamide and should be possible to measure for formamide as well, although it is unlikely to be of any atmospheric importance.

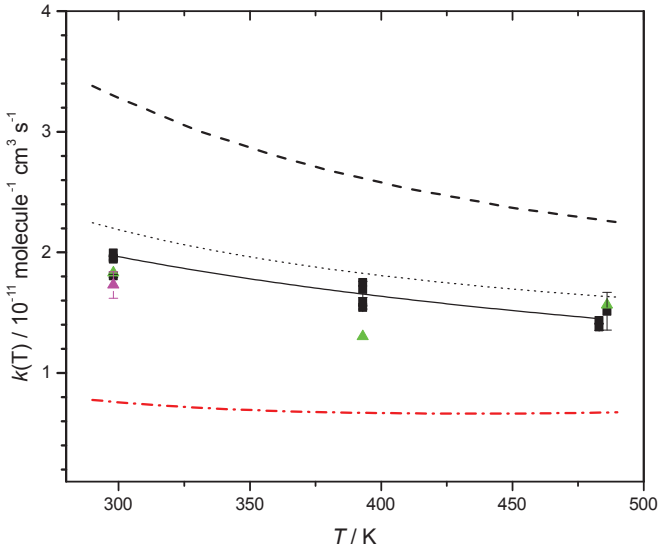

Figure 5.22: Calculated and experimental rate coefficients for the reaction of OH radicals with methylamine. Symbols: black ■, OH, N2 bath gas; red ●, OH, N2/O2 bath gas; green ▲, OD, N2/O2 bath gas; pink ▼, data of Carl and Crowley at 298 K. Full line, Harcourt-Esson fit to experimental data from this work; black dotted line, parametrized data from Atkinson et al. [77, 78]; black dashed line, theoretical prediction based on CCSD(T*)-F12a/aug-cc-pVTZ//MP2/aug-cc-pVTZ described in paper I; red dash-dot line, theoretical prediction based on CCSD(T)/cc-pV(TQ)Z calculations.

To illustrate the differences between the employed levels of theory, rate coefficients for the OH radical reaction of methylamine are shown in Figure 5.22. The high level calculations predict values are lower than the experimental values while the CCSD(T*)-F12a/aug-cc-pVTZ//MP2/aug-cc-pVTZ calculations, presented in paper I, predict higher values. The same is observed for formamide (Figure 5.20), and the CCSD(T*)-F12a/aug-cc-pVTZ//MP2/aug-cc-pVTZ calculations presented in paper III also overestimated the measured rate coefficients for MF and DMF. The reason for this is not entirely clear, but inspection of the optimized geometries reveal that the MP2 calculations systematically predict smaller O-H distances than the CCSD(T) calculations in all hydrogen-abstraction transition states examined, except for abstraction at the N site in MA. The branching ratio obtained in the high-level calculations for the methylamine reaction is in worse agreement with the experiments than the results presented in paper I. Apparently both the calculations presented in paper I and the previous computational studies [83, 84] represent cases where calculations give the right answer, but maybe not for the right reason.

The effect of tunneling was tested by including Eckart tunneling in the master equation model. For MA, there is no significant effect in either the rate coefficient or the branching ratio, but for formamide, an increase in the rate coefficient of around 10 % is predicted. For methanimine tunneling has a large effect on the abstraction leading to cis HCNH, nearly doubling the overall reaction rate, but it also makes the master equation eigenvalues for reactions approach the eigenvalues for collisional energy transfer, making the results less reliable. It is nevertheless concluded that tunneling may be important when there are positive barriers, but that it can otherwise be ignored without much loss of accuracy for the reactions of nitrogen containing VOCs with OH radicals.

Since the master equation models based on the CCSD(T)/cc-pV(T)Q)Z//CCSD(T)/cc-pVTZ calculations underestimate the rate coefficients for both methylamine and formamide, and since the calculations indicate that tunneling may be important, it is reasonable to suspect that the reaction rate is also underestimated for methanimine. This is, however, difficult to confirm without accurate kinetic measurements.

Chapter 6

Concluding remarks

The overall goal of this study was to contribute to the fundamental understanding of the gas phase photo-oxidation of amines. The mechanisms of amine photo-oxidation are in many aspects similar to those of hydrocarbons, with the first step being formation of (amino) alkyl radical through hydrogen abstraction by the OH radical. While both the alkyl and the amino alkyl radical may react with O_2 to form a peroxy radical, only the amino alkyl radical may undergo hydrogen abstraction to give HO_2 and an unsaturated compound which may either react with OH radicals, or deposit on surfaces and hydrolyze. Furthermore, there are no important routes in hydrocarbon photooxidation analogous to nitramine or nitrosamine formation. In summary, while hydrocarbons are mainly oxidized to carbonyl compounds, the amines are mainly oxidized to imines, with nitro, nitroso and carbonyl compounds constituting minor products.

The reactions of OH radicals and chlorine atoms with methylamine, dimethylamine and trimethylamine as well as the OH radical reaction of ethylamine have been studied using quantum chemical methods in conjunction with statistical rate theory. The reaction kinetics are dominated by the formation of very stable pre-reaction van der Waals adducts and submerged barriers. The calculated rate coefficients are in good agreement with the experimental values, but the calculation of accurate branching ratios was proven to require more accurate barrier heights than those available from (today's) applicable quantum chemical methods. The calculations indicate that the chlorine reactions have a higher potential for nitramine and nitrosamine formation than the corresponding OH reactions. Accurate determination of the branching ratios for methylamine and dimethylamine, as well as rate coefficients and branching ratios for larger amines is clearly needed.

The kinetics of the reactions of OH radicals with *N*-methylformamide and *N,N*-methylformamide were studied using flash photolysis coupled with laser

induced fluorescence in addition to quantum chemical and master equation methods. The reactions show weak negative temperature dependencies and they are significantly slower than the corresponding amine reactions. The product study reveals that the amides also have a larger nitramine and nitrosamine formation potential than amines and may therefore constitute a previously undisclosed health risk that may actually be of more concern than amine emissions from carbon capture.

An experimental study of the reaction of OH radicals with methanimine was attempted, but was abandoned due to rapid polymerization of the methanimine in the reaction cell. The reaction was instead studied using highly accurate quantum chemical methods in conjunction with a master equation model. The reaction is predicted to be significantly slower than the corresponding reaction of methylamine and HCN was found to be the main product with HNCO as a minor product. A possible intermediate in the photo-oxidation of methanimine is HNC which was found to react very quickly with OH radicals giving HNCO as dominant product. It is also concluded that N_2O is not a product of methylamine photo-oxidation as previously suggested.

The competition between collisional stabilization and unimolecular reaction of the chemically activated intermediates in the photo-oxidation of *N*-methylnitramine and *N,N*-dimethylnitramine was studied using a master equation model. Direct dissociation to form an imine and NO_2 was found to be the main fate of the nitramino radicals formed in the reactions of the nitramines with OH radicals.

Kinetic isotope effects for the OH radical reaction of HCN were measured using long path FTIR spectroscopy and were supported by quantum chemical calculations and master equation modeling. The study confirms that the reaction occur through the formation of an adduct.

Finally, in order to assess the accuracy of the employed theoretical methods, the reactions of methylamine, methanimine and formamide with OH radicals were studied by employing high level quantum chemical methods and compared with both experimental data and computational results from this work.

The reactions of the alkyl amines with OH radicals are now to a large degree understood, but there are several unresolved questions. The atmospheric fate of imines is still largely unknown and the reaction of *N*-methylmethanimine with OH radicals is an obvious candidate for further examination. Another important issue that needs to be addressed is whether the main sink of imines is gas phase reactions, or if uptake on water droplets and particles dominate. In the latter case the imine will hydrolyze resulting in amines or alternatively NH_3.

Bibliography

[1] J. Stoltenberg. New year speech, January 2007. http://www.regjeringen.no/en/archive/Stoltenbergs-2nd-Government/Office-of-the-Prime-Minister/taler-og-artikler/2007/statsministerens-nyttarstale-2007.html?id=440349.

[2] M. Låg, B Lindeman, Instanes C., Brunborg G., and Schwarze P. Health effects of amines and derivatives associated with CO_2 capture. Technical report, Norwegian Institute of Public Health, 2011.

[3] D. J. Jacob. *Introduction to Atmospheric Chemistry*. Princeton University Press, 1999.

[4] B.J. Finlayson-Pitts and J.N. Jr. Pitts. *Atmospheric chemistry. Fundamentals and experimental techniques*. Wiley, Jan 1986.

[5] R. P. Wayne, I. Barnes, P. Biggs, J. P. Burrows, C. E. Canosa-Mas, J. Hjorth, G. Le Bras, G. K. Moortgat, D. Perner, G. Poulet, G. Restelli, and H. Sidebottom. The nitrate radical: Physics, chemistry, and the atmosphere. *Atmospheric Environment. Part A. General Topics*, 25(1):1 – 203, 1991.

[6] O. W. Wingenter, B. C. Sive, N. J. Blake, D. R. Blake, and F.S . Rowland. Atomic chlorine concentrations derived from ethane and hydroxyl measurements over the equatorial Pacific Ocean: Implication for dimethyl sulfide and bromine monoxide. *Journal of Geophysical Research-Atmospheres*, 110(D20), 2005.

[7] O. W. Wingenter, M. K. Kubo, N. J. Blake, T. W. Smith, D. R. Blake, and F. S. Rowland. Hydrocarbon and halocarbon measurements as photochemical and dynamical indicators of atmospheric hydroxyl, atomic chlorine, and vertical mixing obtained during Lagrangian flights. *Journal of Geophysical Research-Atmospheres*, 101(D2):4331–4340, 1996.

[8] X. Ge, A. S. Wexler, and S. L. Clegg. Atmospheric amines – part I. a review. *Atmospheric Environment*, 45(3):524 – 546, 2011.

[9] A. B. Rao and E. S. Rubin. A technical, economic, and environmental assessment of amine-based CO_2 capture technology for power plant greenhouse gas control. *Environmental Science & Technology*, 36(20):4467–4475, 2002.

[10] C. Gouedard, D. Picq, F. Launay, and P.-L. Carrette. Amine degradation in CO_2 capture. I. a review. *International Journal of Greenhouse Gas Control*, 10(0):244 – 270, 2012.

[11] C. J. Nielsen, H. Herrmann, and C. Weller. Atmospheric chemistry and environmental impact of the use of amines in carbon capture and storage (CCS). *Chemical Society Reviews*, 41:6684–6704, 2012.

[12] G. W. Schade and P. J. Crutzen. Emission of aliphatic amines from animal husbandry and their reactions: Potential source of N2O and HCN. *Journal of Atmospheric Chemistry*, 22(3):319–346, 1995.

[13] DY. Lee and A. S. Wexler. Atmospheric amines – Part III: Photochemistry and toxicity . *Atmospheric Environment*, 71(0):95 – 103, 2013.

[14] C. J. Nielsen, B. D'Anna, A. Aursnes, A. Boreave, R. Bossi, A. J. C. Bunkan, M. Glasius, A. M. K. Hansen, M. Hallquist, K. Kristensen, T. Mikoviny, M. M. Maguta, M. Müller, Q. Nguyen, J. Westerlund, K. Salo, H. Skov, Y. Stenstrøm, and A. Wisthaler. Summary report: photo-oxidation of methylamine, dimethylamine and trimetahylamine, climit project no. 201604 NILU OR 2/2011, isbn 978-82-425-2357-0, nilu, 2011.

[15] Y. G. Lazarou and P. Papagiannakopoulos. Kinetic studies of the reactions of atomic chlorine with N-methylmethylenimine and 1,3,5-trimethylhexahydro-1,3,5-triazine. *The Journal of Physical Chemistry*, 97(17):4468–4472, 1993.

[16] I. Barnes, G. Solignac, A. Mellouki, and K. H. Becker. Aspects of the atmospheric chemistry of amides. *ChemPhysChem*, 11(18):3844–3857, 2010.

[17] J. N. Pitts, D. Grosjean, K. Van Cauwenberghe, J. P. Schmid, and Dennis R. Fitz. Photooxidation of aliphatic amines under simulated atmospheric conditions: formation of nitrosamines, nitramines, amides,

and photochemical oxidant. *Environmental Science & Technology*, 12(8):946–953, 1978.

[18] E. C. Tuazon, W. P. L. Carter, R. Atkinson, A M. Winer, and J. N. Pitts. Atmospheric reactions of N-nitrosodimethylamine and dimethylnitramine. *Environmental Science & Technology*, 18(1):49–54, 1984.

[19] S. P. Mezyk, W. J. Cooper, K. P. Madden, and D. M. Bartels. Free radical destruction of N-nitrosodimethylamine in water. *Environmental Science & Technology*, 38(11):3161–3167, 2004.

[20] F. Jensen. *Introduction to Computational Chemistry*. Wiley, 2 edition, 2006.

[21] C. Møller and M. S. Plesset. Note on an approximation treatment for many-electron systems. *Physical Review*, 46(7):618–622, 1934.

[22] T. Helgaker, P. Jørgensen, and J. Olsen. *Molecular Electronic Structure Theory*. Wiley, 1 edition, 2000.

[23] J. Čížek. On the correlation problem in atomic and molecular systems. calculation of wavefunction components in ursell-type expansion using quantum field theoretical methods. *The Journal of Chemical Physics*, 45(11):4256–4266, 1966.

[24] J. Čížek. On the use of the cluster expansion and the technique of diagrams in calculations of correlation effects in atoms and molecules. *Advances in Chemical Physics*, pages 35–89, 1969.

[25] G. D. Purvis and R. J. Bartlett. A full coupled-cluster singles and doubles model - the inclusion of disconnected triples. *The Journal of Chemical Physics*, 76(4):1910–1918, 1982.

[26] J. Noga and R. J. Bartlett. The full CCSDT model for molecular electronic-structure. *Journal of Chemical Physics*, 86(12):7041–7050, 1987.

[27] G. E. Scuseria and T. J. Lee. Comparison of coupled-cluster methods which include the effects of connected triple excitations. *The Journal of Chemical Physics*, 93(8):5851–5855, 1990.

[28] J. D. Watts and R. J. Bartlett. The coupled-cluster single, double, and triple excitation model for open-shell single reference functions. *The Journal of Chemical Physics*, 93(8):6104–6105, 1990.

[29] C. J. Cramer. *Essentials of Computational Chemistry*. Wiley, 2 edition, 2004.

[30] K. Raghavachari, G. W. Trucks, J. A. Pople, and M. Head-Gordon. A fifth-order perturbation comparison of electron correlation theories. *Chemical Physics Letters*, 157(6):479 – 483, 1989.

[31] C. J. Cramer. *Essentials of Computational Chemistry*. Wiley, 2 edition, 2004. Page 226.

[32] T. Helgaker, T.A. Ruden, P. Jorgensen, J. Olsen, and W. Klopper. A priori calculation of molecular properties to chemical accuracy. *Journal of physical organic chemistry.*, 17(11):913–933, 2004.

[33] T. J. Lee and P. R. Taylor. A diagnostic for determining the quality of single-reference electron correlation methods. *International Journal of Quantum Chemistry*, (23):199–207, 1989.

[34] J. C. Rienstra-Kiracofe, W. D. Allen, and H. F. Schaefer. The C_2H_5 + O_2 reaction mechanism: High-level ab initio characterizations. *The Journal of Physical Chemistry A*, 104(44):9823–9840, 2000.

[35] B. O. Roos, P. R. Taylor, and P. E.M. Siegbahn. A complete active space SCF method (CASSCF) using a density matrix formulated super-CI approach. *Chemical Physics*, 48(2):157 – 173, 1980.

[36] K. Ruedenberg, M. W. Schmidt, M. M. Gilbert, and S.T. Elbert. Are atoms intrinsic to molecular electronic wavefunctions? I. the FORS model. *Chemical Physics*, 71(1):41 – 49, 1982.

[37] K Andersson, P. A. Malmqvist, B. O. Roos, A.J. Sadlej, and K Wolinski. 2nd-order perturbation-theory with a CASSCF reference function. *The Journal of Physical Chemistry*, 94(14):5483–5488, 1990.

[38] K Andersson, P. A. Malmqvist, and B. O. Roos. 2nd-order perturbation-theory with a complete active space self-consistent field reference function. *The Journal of Chemical Physics*, 96(2):1218–1226, 1992.

[39] H.-J. Werner. Third-order multireference perturbation theory the CASPT3 method. *Molecular Physics*, 89(2):645–661, 1996.

[40] P. Hohenberg and W. Kohn. Inhomogeneous electron gas. *Physical Review*, 136:B864–B871, 1964.

[41] A. Fernandez-Ramos, J. A. Miller, S. J. Klippenstein, and D. G. Truhlar. Modeling the kinetics of bimolecular reactions. *Chemical Reviews*, 106(11):4518–4584, 2006.

[42] Y. Zhao and D. G. Truhlar. The M06 suite of density functionals for main group thermochemistry, thermochemical kinetics, noncovalent interactions, excited states, and transition elements: two new functionals and systematic testing of four M06-class functionals and 12 other functionals. *Theoretical Chemistry Accounts*, 120(1-3):215–241, 2008.

[43] T. H. Dunning. Gaussian basis sets for use in correlated molecular calculations. I. the atoms boron through neon and hydrogen. *The Journal of Chemical Physics*, 90(2):1007–1023, 1989.

[44] R. A. Kendall, T. H. Dunning, and R. J. Harrison. Electron-affinities of the 1st-row atoms revisited - systematic basis-sets and wave-functions. *The Journal of Chemical Physics*, 96(9):6796–6806, 1992.

[45] T. Helgaker, W. Klopper, H. Koch, and J. Noga. Basis-set convergence of correlated calculations on water. *The Journal of Chemical Physics*, 106(23):9639–9646, 1997.

[46] A. Halkier, T. Helgaker, P. Jørgensen, W. Klopper, H. Koch, J. Olsen, and A. K. Wilson. Basis-set convergence in correlated calculations on Ne, N_2 and H_2O. *Chemical Physics Letters*, 286(1-3):243–252, 1998.

[47] W. Kutzelnigg and W. Klopper. Wave functions with terms linear in the interelectronic coordinates to take care of the correlation cusp. I. general theory. *The Journal of Chemical Physics*, 94(3):1985–2001, 1991.

[48] J. Noga, W. Kutzelnigg, and W. Klopper. CC-R12, a correlation cusp corrected coupled-cluster method with a pilot application to the Be_2 potential curve. *Chemical Physics Letters*, 199(5):497 – 504, 1992.

[49] T. B. Adler, G. Knizia, and H.-J. Werner. A simple and efficient CCSD(T)-F12 approximation. *The Journal of Chemical Physics*, 127(22):221106, 2007.

[50] G. Knizia, T. B. Adler, and H-J. Werner. Simplified CCSD(T)-F12 methods: Theory and benchmarks. *The Journal of Chemical Physics*, 130(5):054104, 2009.

[51] A. Tajti, P. G. Szalay, A. G. Császár, M. Kállay, J. Gauss, E. F. Valeev, B. A. Flowers, J. Vázquez, and J. F. Stanton. HEAT: High accuracy extrapolated ab initio thermochemistry. *The Journal of Chemical Physics*, 121(23):11599–11613, 2004.

[52] J. Gauss. Lecture notes. Winter School in Theoretical Chemistry, Helsinki, 2013.

[53] L. Vereecken and J. S. Francisco. Theoretical studies of atmospheric reaction mechanisms in the troposphere. *Chemical Society Reviews*, 41:6259–6293, 2012.

[54] J. Elm, S. Jorgensen, M. Bilde, and K. V. Mikkelsen. Ambient reaction kinetics of atmospheric oxygenated organics with the OH radical: a computational methodology study. *Physical Chemistry Chemical Physics*, 15:9636–9645, 2013.

[55] Jingjing Zheng, Yan Zhao, and Donald G. Truhlar. The DBH24/08 database and its use to assess electronic structure model chemistries for chemical reaction barrier heights. *Journal of Chemical Theory and Computation*, 5(4):808–821, 2009.

[56] Lawrence B. Harding, Stephen J. Klippenstein, and Ahren W. Jasper. Ab initio methods for reactive potential surfaces. *Physical Chemistry Chemical Physics*, 9:4055–4070, 2007.

[57] T. Shiozaki and H.-J. Werner. Communication: Second-order multireference perturbation theory with explicit correlation: CASPT2-F12. *The Journal of Chemical Physics*, 133(14):141103, 2010.

[58] K Laidler. *Chemical Kinetics*. Harper & Row, Publishers, 3 edition, 1987.

[59] J. Troe. The Polanyi lecture. The colourful world of complex-forming bimolecular reactions. *Journal of the Chemical Society, Faraday Transactions*, 90:2303–2317, 1994.

[60] D. G. Truhlar, B. C. Garrett, and S. J. Klippenstein. Current status of transition-state theory. *The Journal of Physical Chemistry*, 100(31):12771–12800, 1996.

[61] H Eyring. The activated complex in chemical reactions. *The Journal of Chemical Physics*, 3(2):107–115, 1935.

[62] M. G. Evans and M. Polanyi. Some applications of the transition state method to the calculation of reaction velocities, especially in solution. *Transactions of the Faraday Society*, 31:875–894, 1935.

[63] R. G. Gilbert and S. C. Smith. *Theory of unimolecular and recombination reactions*. Blackwell Scientific Publications, 1 edition, 1990.

[64] K. A. Holbrook, M.J. Pilling, and S.H. Robertson. *Unimolecular Reactions*. Wiley, 1996.

[65] J. A. Miller and S. J. Klippenstein. Master equation methods in gas phase chemical kinetics. *The Journal of Physical Chemistry A*, 110(36):10528–10544, 2006.

[66] J. T. Bartis and B. Widom. Stochastic models of interconversion of 3 or more chemical species. *The Journal of Chemical Physics*, 60(9):3474–3482, 1974.

[67] E. V. Waage and B. S. Rabinovitch. Centrifugal effects in reaction rate theory. *Chemical Reviews*, 70(3):377–387, 1970.

[68] T. Beyer and D. F. Swinehart. Algorithm 448: Number of multiply-restricted partitions. *Communications of the ACM*, 16(6):379–, 1973.

[69] M. Quack and J. Troe. Specific rate constants of unimolecular processes II. adiabatic channel model. *Berichte der Bunsengesellschaft für physikalische Chemie*, 78(3):240–252, 1974.

[70] Y Georgievskii and S. J. Klippenstein. Long-range transition state theory. *The Journal of Chemical Physics*, 122(19), 2005.

[71] W. Forst. Unimolecular rate theory test in thermal reactions. *The Journal of Physical Chemistry*, 76(3):342–348, 1972.

[72] M. S. Johnson, K. L. Feilberg, P. von Hessberg, and O. J. Nielsen. Isotopic processes in atmospheric chemistry. *Chemical Society Reviews*, 31:313–323, 2002.

[73] S. Nasterlack. *Bestimmung von Ausbeuten bei komplexbildenden bimolekularen Reaktionen mittels laserinduzierter Fluoreszenz*. PhD thesis, University of Karlsruhe, 2004.

[74] P. M. Aker and J. J. Sloan. The initial product vibrational-energy distribution in the reaction between $O(^1D_2)$ and H_2. *The Journal of Chemical Physics*, 85(3):1412–1417, 1986.

[75] G. E. Streit, G. Z. Whitten, and H. S. Johnston. Fate of vibrationally excited hydroxyl radicals, HO (v ≤ 9), in stratosphere. *Geophysical Research Letters*, 3(9):521–523, 1976.

[76] Y. L. Huang, Y. K. Gu, C. S. Liu, X. F. Yang, and Y. S. Tao. The nascent product vibrational-energy distribution of the reaction $O(^1D)+H_2$ by the grating selection chemical-laser technique. *Chemical Physics Letters*, 127(5):432–437, 1986.

[77] R. Atkinson, R. A. Perry, and J. N. Pitts. Rate constants for the reaction of the OH radical with CH_3SH and CH_3NH_2 over the temperature range 299-426 K. *The Journal of Chemical Physics*, 66(4):1578–1581, 1977.

[78] R. Atkinson, R. A. Perry, and J. N. Pitts. Rate constants for the reactions of the OH radical with $(CH_3)_2NH$, $(CH_3)_3N$, and $C_2H_5NH_2$ over the temperature range 298–426 K. *The Journal of Chemical Physics*, 68(4):1850–1853, 1978.

[79] S. A. Carl and J. N. Crowley. Sequential two (blue) photon absorption by NO_2 in the presence of H_2 as a source of OH in pulsed photolysis kinetic studies: Rate constants for reaction of OH with CH_3NH_2, $(CH_3)_2NH$, $(CH_3)_3N$, and $C_2H_5NH_2$ at 295 K. *The Journal of Physical Chemistry A*, 102(42):8131–8141, 1998.

[80] C. J. Nielsen, B. D'Anna, R. Bossi, A. J. C. Bunkan, L. Dithmer, M. Glasius, M. Hallquist, A. M. K. Hansen, A. Lutz, K. Salo, M. M. Maguta, Q. Nguyen, T. Mikoviny, M. Müller, H. Skov, Y. Sarrasin, E. Stenstrøm, J. Tang, Y. Westerlund, and A. Wisthaler. Atmospheric degradation of amines (ADA). ISBN 978-82-992954-7-5, http://urn.nb.no/URN:NBN:no 30510, University of Oslo, 2012.

[81] L. Onel, M. A. Blitz, and P. W. Seakins. Direct determination of the rate coefficient for the reaction of OH radicals with monoethanol amine (MEA) from 296 to 510 K. *The Journal of Physical Chemistry Letters*, 3(7):853–856, 2012.

[82] L. Onel, M. Blitz, M. Dryden, L. Thonger, and P. Seakins. Branching ratios in reactions of OH radicals with methylamine, dimethylamine, and ethylamine. *Environmental Science & Technology*, 48(16):9935–9942, 2014.

[83] Annia Galano and J. Raul Alvarez-Idaboy. Branching ratios of aliphatic amines + OH gas-phase reactions: A variational transition-state theory

study. *Journal of Chemical Theory and Computation*, 4(2):322–327, 2008.

[84] W. Tian, W. Wang, Y. Zhang, and W. Wang. Direct dynamics study on the mechanism and the kinetics of the reaction of CH_3NH_2 with OH. *International Journal of Quantum Chemistry*, 109(7):1566–1575, 2009.

[85] E. E. Greenwald, S. W. North, Y. Georgievskii, and S. J. Klippenstein. A two transition state model for radical-molecule reactions: A case study of the addition of OH to C_2H_4. *The Journal of Physical Chemistry A*, 109(27):6031–6044, 2005.

[86] C. R.C. Lindley, J. G. Calvert, and J. H. Shaw. Rate studies of the reactions of the $(CH_3)_2N$ radical with O_2, NO, and NO_2. *Chemical Physics Letters*, 67(1):57 – 62, 1979.

[87] I. Fourré and B. Silvi. What can we learn from two-center three-electron bonding with the topological analysis of ELF? *Heteroatom Chemistry*, 18(2):135–160, 2007.

[88] S. Rudic, C. Murray, J. N. Harvey, and A. J. Orr-Ewing. The product branching and dynamics of the reaction of chlorine atoms with methylamine. *Physical Chemistry Chemical Physics*, 5:1205–1212, 2003.

[89] N. Borduas, G. da Silva, J. G. Murphy, and J. P. D. Abbatt. Experimental and theoretical understanding of the gas phase oxidation of atmospheric amides with OH radicals: Kinetics, products, and mechanisms. *The Journal of Physical Chemistry A*, 2014. 10.1021/jp503759f.

[90] G. Solignac, A. Mellouki, G. Le Bras, I. Barnes, and Th. Benter. Kinetics of the OH and Cl reactions with N-methylformamide, N,N-dimethylformamide and N,N-dimethylacetamide. *Journal of Photochemistry and Photobiology A: Chemistry*, 176(1–3):136 – 142, 2005.

[91] D. R. Glowacki, C.-H. Liang, C. Morley, M. J. Pilling, and S. H. Robertson. MESMER: An open-source master equation solver for multi-energy well reactions. *The Journal of Physical Chemistry A*, 116(38):9545–9560, 2012.

[92] R. Koch, W.-U. Palm, and C. Zetzsch. First rate constants for reactions of OH radicals with amides. *International Journal of Chemical Kinetics*, 29(2):81–87, 1997.

[93] P. H. Wine, R. S. Strekowski, M. Nicovich, M. L. McKee, G. Chen, and D. D. Davis. Atmospheric chemistry of HCN. Presented at National Meeting of the American Chemical Society, Boston, MA, 2002.

[94] M. T. Coffey and A. Goldman. Atmospheric hydrogen-cyandide absorption near 14μm. *Applied Optics*, 20(20):3480–3481, 1981.

[95] B. Carli, F. Mencaraglia, and A. Bonetti. New assignments in the submillimeter emission-spectrum of the stratosphere. *International Journal of Infrared and Millimeter Waves*, 3(3):385–394, 1982.

[96] C. P. Rinsland, M. A. H. Smith, P. L. Rinsland, A. Goldman, J. W. Brault, and G. M. Stokes. Ground-based infrared spectroscopic measurements of atmospheric hydrogen-cyanide. *Journal of Geophysical Research-Oceans and Atmospheres*, 87(NC13):1119–1125, 1982.

[97] R. J. Cicerone and R. Zellner. The atmospheric chemistry of hydrogen-cyanide(HCN). *Journal of Geophysical Research-Oceans and Atmospheres*, 88:689–696, 1983.

[98] J. M. Lobert, D. H. Scharffe, W. M. Hao, and P. J. Crutzen. Importance of biomass burning in the atmospheric budgets of nitrogen-containing gases. *Nature*, 346(6284):552–554, 1990.

[99] C. P. Rinsland, E. Mahieu, R. Zander, M. R. Gunson, R. J. Salawitch, A. Y. Chang, A. Goldman, M. C. Abrams, M. M. Abbas, M. J. Newchurch, and F. W. Irion. Trends of OCS, HCN, SF_6, $CHClF_2$, (HCFC-22) in the lower stratosphere from 1985 and 1994 atmospheric trace molecule spectroscopy experiment measurements near 30 degrees N latitude. *Geophysical Research Letters*, 23(17):2349–2352, 1996.

[100] Y. Kondo, S. Kawakami, M. Koike, D. W. Fahey, H. Nakajima, Y. Zhao, N. Toriyama, M. Kanada, G. W. Sachse, and G. L. Gregory. Performance of an aircraft instrument for the measurement of NO_y. *Journal of Geophysical Research-Atmospheres*, 102(D23):28663–28671, 1997.

[101] J. Schneider, V. Burger, and F. Arnold. Methyl cyanide and hydrogen cyanide measurements in the lower stratosphere: Implications for methyl cyanide sources and sinks. *Journal of Geophysical Research-Atmospheres*, 102(D21):25501–25506, 1997.

[102] C. P. Rinsland, A. Goldman, F. J. Murcray, T. M. Stephen, N. S. Pougatchev, J. Fishman, S. J. David, R. D. Blatherwick, P. C. Novelli,

N. B. Jones, and B. J. Connor. Infrared solar spectroscopic measurements of free tropospheric CO, C_2H_6, and HCN above Mauna Loa, Hawaii: Seasonal variations and evidence for enhanced emissions from the southeast Asian tropical fires of 1997-1998. *Journal of Geophysical Research-Atmospheres*, 104(D15):18667–18680, 1999.

[103] J. G. Goode, R. J. Yokelson, D. E. Ward, R. A. Susott, R. E. Babbitt, M. A. Davies, and W. M. Hao. Measurements of excess O_3, CO_2, CO, CH_4, C_2H_4, C_2H_2, HCN, NO, NH_3, HCOOH, CH_3COOH, HCHO, and CH_3OH in 1997 alaskan biomass burning plumes by airborne fourier transform infrared spectroscopy (AFTIR). *Journal of Geophysical Research-Atmospheres*, 105(D17):22147–22166, 2000.

[104] Q. B. Li, D. J. Jacob, I. Bey, R. M. Yantosca, Y. J. Zhao, Y. Kondo, and J. Notholt. Atmospheric hydrogen cyanide (HCN): Biomass burning source, ocean sink? *Geophysical Research Letters*, 27(3):357–360, 2000.

[105] C. P. Rinsland, E. Mahieu, R. Zander, P. Demoulin, J. Forrer, and B. Buchmann. Free tropospheric CO, C_2H_6, and HCN above central europe: Recent measurements from the Jungfraujoch station including the detection of elevated columns during 1998. *Journal of Geophysical Research-Atmospheres*, 105(D19):24235–24249, 2000.

[106] M. O. Andreae and P. Merlet. Emission of trace gases and aerosols from biomass burning. *Global Biogeochemical Cycles*, 15(4):955–966, 2001.

[107] Q. B. Li, D. J. Jacob, R. M. Yantosca, C. L. Heald, H. B. Singh, M. Koike, Y. J. Zhao, G. W. Sachse, and D. G. Streets. A global three-dimensional model analysis of the atmospheric budgets of HCN and CH_3CN: Constraints from aircraft and ground measurements. *Journal of Geophysical Research-Atmospheres*, 108(D21), 2003.

[108] H. B. Singh, L. Salas, D. Herlth, R. Kolyer, E. Czech, W. Viezee, Q. Li, D. J. Jacob, D. Blake, G. Sachse, C. N. Harward, H. Fuelberg, C. M. Kiley, Y. Zhao, and Y. Kondo. In situ measurements of HCN and CH_3CN over the pacific ocean: Sources, sinks, and budgets. *Journal of Geophysical Research-Atmospheres*, 108(D20), 2003.

[109] A. Kleinbohl, G. C. Toon, B. Sen, J. F. L. Blavier, D. K. Weisenstein, R. S. Strekowski, J. M. Nicovich, P. H. Wine, and P. O. Wennberg. On the stratospheric chemistry of hydrogen cyanide. *Geophysical Research Letters*, 33(11), 2006.

[110] H. C. Pumphrey, C. J. Jimenez, and J. W. Waters. Measurement of HCN in the middle atmosphere by EOS MLS. *Geophysical Research Letters*, 33(8):4, 2006.

[111] P. H. Wine, R. S. Strekowski, J. M. Nicovich, M. L. McKee, A. Kleinbohl, G. C. Toon, B. Sen, J.-F. L. Blavier, D. K. Weisenstein, and P. O. Wennberg. The OH + HCN reaction: Kinetics, mechanism, and role in atmospheric chemistry. Presented at the 19th International Symposium on Gas Kinetics; Orleans, France, 2006.

[112] H. C. Pumphrey, C. Boone, K. A. Walker, P. Bernath, and N. J. Livesey. Tropical tape recorder observed in HCN. *Geophysical Research Letters*, 35(5), 2008.

[113] A. Lupu, J. W. Kaminski, L. Neary, J. C. McConnell, K. Toyota, C. P. Rinsland, P. F. Bernath, K. A. Walker, C. D. Boone, Y. Nagahama, and K. Suzuki. Hydrogen cyanide in the upper troposphere: GEM-AQ simulation and comparison with ACE-FTS observations. *Atmospheric Chemistry and Physics*, 9(13):4301–4313, 2009.

[114] L. F. Phillips. Pressure-dependence of rate of reaction of OH with HCN. *Chemical Physics Letters*, 57(4):538–539, 1978.

[115] L. F. Phillips. Rate of reaction of oh with HCN between 298K and 563K. *Australian Journal of Chemistry*, 32(12):2571–2577, 1979.

[116] B. Fritz, K. Lorenz, W. Steinert, and R. Zellner. Laboratory kinetic investigations of the tropospheric oxidation of selected industrial emissions. *In Physico-Chemical Behavior of Atmospheric Pollutants, Proceedings of the Second European Symposium, Varese, Italy, 29 Sep.-1 Oct. 1981*, pages 192–202, 1982.

[117] B. Fritz, K. Lorenz, W. Steinert, and R. Zellner. Rate of oxidation of hydrogen cyanide by hydroxyl radicals at lower temperatures. *Oxidation Communications*, 6(1-4):363–70, 1984.

[118] R. Strekowski. *Laser Flash Photolysis Studies of Some $O(^1D_2)$ and $OH(X^2\Pi)$ Reactions of Atmospheric Interest*. PhD thesis, Georgia Institute of Thechnology, May 2001.

[119] A. Palma, E. Semprini, F. Stefani, and A. Talamo. Extensive ab initio study of the OH+HCN reaction: Low lying electronic states of the stationary points on the ^{2}A' surface. *The Journal of Chemical Physics*, 105(12):5091–5098, 1996.

[120] C. Y. Wang, S. W. Zhang, and Q. S. Li. Ab initio study of rate constants of the reaction: HCN+OH → CN+H_2O. *Theoretical Chemistry Accounts*, 108(6):341–346, 2002.

[121] A. Galano. Mechanism of OH radical reactions with HCN and CH_3CN: OH regeneration in the presence of O_2. *Journal of Physical Chemistry A*, 111(23):5086–5091, 2007.

[122] W. A. Shapley and G. B. Bacskay. Ab initio quantum chemical studies of the formaldiminoxy (CH_2NO) radical: 1. isomerization reactions. *The Journal of Physical Chemistry A*, 103(23):4505–4513, 1999.

[123] W. A. Shapley and G. B. Bacskay. Ab initio quantum chemical studies of the formaldiminoxy (CH_2NO) radical: 2. dissociation reactions. *The Journal of Physical Chemistry A*, 103(23):4514–4524, 1999.

[124] H.-J. Werner, P. J. Knowles, G. Knizia, F. R. Manby, M. Schütz, P. Celani, T. Korona, R. Lindh, A. Mitrushenkov, G. Rauhut, K. R. Shamasundar, T. B. Adler, R. D. Amos, A. Bernhardsson, A. Berning, D. L. Cooper, M. J. O. Deegan, A. J. Dobbyn, F. Eckert, E. Goll, C. Hampel, A. Hesselmann, G. Hetzer, T. Hrenar, G. Jansen, C. Köppl, Y. Liu, A. W. Lloyd, R. A. Mata, A. J. May, S. J. McNicholas, W. Meyer, M. E. Mura, A. Nicklass, D. P. O'Neill, P. Palmieri, D. Peng, K. Pflüger, R. Pitzer, M. Reiher, T. Shiozaki, H. Stoll, A. J. Stone, R. Tarroni, T. Thorsteinsson, and M. Wang. Molpro, version 2012.1, a package of ab initio programs, 2012.

[125] H.-J. Werner, P. J. Knowles, G. Knizia, F. R. Manby, and M. Schütz. Molpro: a general purpose quantum chemistry program package. *WIREs Computational Molecular Science*, 2:242–253, 2012.

[126] M. J. Frisch, G. W. Trucks, H. B. Schlegel, G. E. Scuseria, M. A. Robb, J. R. Cheeseman, G. Scalmani, V. Barone, B. Mennucci, G. A. Petersson, H. Nakatsuji, M. Caricato, X. Li, H. P. Hratchian, A. F. Izmaylov, J. Bloino, G. Zheng, J. L. Sonnenberg, M. Hada, M. Ehara, K. Toyota, R. Fukuda, J. Hasegawa, M. Ishida, T. Nakajima, Y. Honda, O. Kitao, H. Nakai, T. Vreven, J. A. Montgomery, Jr., J. E. Peralta, F. Ogliaro, M. Bearpark, J. J. Heyd, E. Brothers, K. N. Kudin, V. N. Staroverov, R. Kobayashi, J. Normand, K. Raghavachari, A. Rendell, J. C. Burant, S. S. Iyengar, J. Tomasi, M. Cossi, N. Rega, J. M. Millam, M. Klene, J. E. Knox, J. B. Cross, V. Bakken, C. Adamo, J. Jaramillo, R. Gomperts, R. E. Stratmann, O. Yazyev, A. J. Austin, R. Cammi,

C. Pomelli, J. W. Ochterski, R. L. Martin, K. Morokuma, V. G. Zakrzewski, G. A. Voth, P. Salvador, J. J. Dannenberg, S. Dapprich, A. D. Daniels, Ö. Farkas, J. B. Foresman, J. V. Ortiz, J. Cioslowski, and D. J. Fox. Gaussian09 Revision D.01. Gaussian Inc. Wallingford CT 2009.

[127] B. D'Anna, V. Bakken, J. A. Beukes, C. J. Nielsen, K. Brudnik, and J. T. Jodkowski. Experimental and theoretical studies of gas phase NO_3 and OH radical reactions with formaldehyde, acetaldehyde and their isotopomers. *Physical Chemistry Chemical Physics*, 5:1790–1805, 2003.

[128] NIST Computational Chemistry Comparison and Benchmark Database, NIST Standard Reference Database Number 101 Release 16a, August 2013, Editor: Russell D. Johnson III http://cccbdb.nist.gov/.

Appendix A

List of abbreviations

CASPT2	Complete Active Space Perturbation Theory to 2nd order
CASSCF	Complete Active Space Self Consistent Field
CCSD	Coupled Cluster Singles and Doubles
CCSD(T)	Coupled Cluster Singles and Doubles with perturbative Triples
DFT	Density Functional Theory
EGME	Energy Grained Master Equation
FTIR	Fourier Transform Infrared Spectroscopy
HF	Hartree-Fock theory
G3	Gaussian 3 theory
G4	Gaussian 4 theory
GTO	Gaussian Type Orbital
ILT	Inverse Laplace Transform
IRC	Intrinsic Reaction Coordinate
KIE	Kinetic Isotope Effect
LIF	Laser-Induced Fluorescence
LRTST	Long Range Transition State Theory
MCSCF	Multiconfigurational SCF
ME	Master Equation
MPn	Møller Plesset Perturbation theory to nth order
RRKM	Rice-Ramsperger-Kassel-Marcus theory
SACM	Statistical Adiabatic Channel Model
SCF	Self Consistent Field
STO	Slater Type Orbital
TS	Transition State
TST	Transition State Theory
VOC	Volatile Organic Compound
VTST	Variational Transition State Theory
ZPE	Zero Point Energy

Appendix B

Presentations

Additional papers

Simakov, A.; Sekiguchi, O.; Bunkan, A. J. C.; Uggerud, E. Energetics and Mechanisms for the Unimolecular Dissociation of Protonated Trioses and Relationship to Proton-Mediated Formaldehyde Polymerization to Carbohydrates in Interstellar Environments. *Journal of the American Chemical Society* **2011**, 133, 20816– 20822

Møllendal, H.; Samdal, S; Bunkan, A. J. C.; Guillemin J.-C. Synthesis and Microwave Spectrum of Vinyl Isoselenocyanate (H2C=CHNCSe), a Compound with a Quasilinear CNCSe Chain. *The Journal of Physical Chemistry A* **2012**, 116, 4074-4081.

Simakov, A.; Miller, G. B. S.; Bunkan, A. J. C.; Hoffmann, M. R.; Uggerud, E. The dissociation of glycolate-astrochemical and prebiotic relevance. *Physical Chemistry Chemical Physics* **2013**, 15, 16615-16625.

Conference talks

Bunkan, A. J. C; Hetzler, J; Nielsen, C. J., Olzmann, M. Kinetics of the reactions of OH radicals with *N*-methylformamide and *N,N*-dimethylformamide. 23rd International Symposium on Gas Kinetics, Szeged, Hungary, 20. - 25. July 2014

Bunkan, A. J. C.; Nielsen, C. J. What is so special about the atmospheric chemistry of amines, imines and amides? The Eleventh Informal Conference on Atmospheric and Molecular Science, Helsingør, Denmark, 14. - 15. August 2014

Posters

Bunkan, A. J. C.; Tang, Y.; Sellevåg, S. R.; Nielsen, C. J. Atmospheric chemistry of methyleneimine. 4th EuCheMS Chemistry Congress, Prague, Czech Republic, 26. - 30. August 2012,

Bunkan, A. J. C.; Nielsen, C. J. Kinetics of the OH radical reaction of CH_2NH. 8th International Conference on Chemical Kinetics, 8. - 12. July 2013, Seville, Spain

Bunkan, A. J. C; Hetzler, J; Nielsen, C. J., Olzmann, M. Kinetics of the reactions of OH radicals with *N*-methylformamide and *N,N*-dimethylformamide. Bunsentagung 2014, Hamburg, Germany, 29. - 31. May 2014,

Popular science

Bunkan, A. J. C. Hvorfor er luften så ren? *Kjemi* 4, 2014

Paper I

Onel, L.; Thonger, L.; Blitz, M. A.; Seakins, P. W.; Bunkan, A. J. C.; Solimannejad, M.; Nielsen, C. J. Gas-Phase Reactions of OH with Methyl Amines in the Presence or Absence of Molecular Oxygen. An Experimental and Theoretical Study. *The Journal of Physical Chemistry A* **2013**, *117*, 10736-10745.

Paper II

Nicovich, J. M.; Mazumder, S; Laine, P. L.: Wine, P. H.; Tang, Y.; Bunkan, A. J. C.; Nielsen, C. J. An experimental and theoretical study of the gas phase kinetics of atomic chlorine reactions with CH_3NH_2, $(CH_3)_2NH$, and $(CH_3)_3N$. *Physical Chemistry Chemical Physics* **2014**.
Submitted

PCCP

RSCPublishing

ARTICLE

An experimental and theoretical study of the gas phase kinetics of atomic chlorine reactions with CH_3NH_2, $(CH_3)_2NH$, and $(CH_3)_3N$†

Cite this: DOI: 10.1039/x0xx00000x

Received 00th January 2012,
Accepted 00th January 2012

DOI: 10.1039/x0xx00000x

www.rsc.org/

J.M. Nicovich,[a] S. Mazumder,[a] P.L. Laine,[b,e] P.H. Wine,[*a,b] Y. Tang,[c] A.J.C. Bunkan,[d] and C.J. Nielsen[*d]

The rate coefficients for the reactions of $Cl(^2P_J)$ with methylamine (R1), dimethylamine (R2) and trimethylamine (R3) have been measured using the laser flash photolysis – resonance fluorescence technique as a function of temperature (274−435 K) and pressure (25−400 Torr N_2). The experimental data are well-represented by the following temperature- and pressure-independent rate coefficients ($10^{10} \times k$/ cm^3 molecule^{-1} s^{-1}): k_{R1} = 2.90 ± 0.44, k_{R2} = 3.89 ± 0.58, k_{R3} = 3.68 ± 0.55; the uncertainties are estimates of accuracy at the 95% confidence level. Potential energy surfaces (PES) for the reactions have been characterized at the MP2/cc-pVTZ level and improved single point energies of stationary points obtained in CCSD(T)-F12a calculations. The PES for all reactions are characterized by the formation of pre and post reaction complexes and submerged barriers. The calculated rate coefficients are in good agreement with experiment; the overall rate coefficients are relatively insensitive to variations of the barrier heights within typical chemical accuracy, but the branching ratios vary significantly.

Introduction

Several reviews of the atmospheric occurrence, thermodynamic properties and chemistry of amines have recently appeared.[1-4] In spite of around 150 different amines having been identified in the atmosphere,[1] they were almost left out of atmospheric and environmental sciences due to their low ppbV-range mixing ratios and their short lifetimes.[5] It has now been demonstrated from modeling of field observations,[6] and from controlled experiments in the CLOUD chamber at CERN,[7] that amines are important in new particle formation through their gas phase acid-base reaction with sulphuric acid. A recent matrix isolation study shows that trimethylamine and sulfuric acid may even form a 1:1 complex of ionic character, in which a proton is nearly completely transferred: $(CH_3)_3NH^+\cdots^-OSO_3H$.[8]

The primary tropospheric sink for amines is generally accepted to be reaction with the OH radical. It has been reported that levels of Cl atoms in the marine boundary layer can be 1−10 percent of OH levels,[9] and findings suggest a significant Cl production rate even in the middle of the continental United States.[10] Laboratory and theoretical research demonstrates that heterogeneous reaction of N_2O_5 with HCl(aq) may represent a significant source of tropospheric $ClNO_x$ species that can rapidly photolyze under daytime conditions to generate Cl atoms.[11] Hence, it appears that reaction with Cl could be a significant tropospheric sink for any trace gas that reacts with Cl significantly more rapidly than with OH. There are no kinetic data for Cl + amine reactions reported in the literature, although one reaction dynamics study of Cl + CH_3NH_2 has been published showing yields of the two hydrogen abstraction products to be 48% $^{\bullet}CH_2NH_2$ and 52% $^{\bullet}NHCH_3$ at a collision energy of ~2000 cm^{-1}.[12] Since it is a reasonable expectation that Cl + amine reactions are very fast, laboratory studies to quantify the kinetics of these reactions are needed.

[a]*School of Chemistry & Biochemistry, Georgia Institute of Technology, Atlanta, GA 30332-0400, USA. E-mail: paul.wine@chemistry.gatech.edu*
[b] *School of Earth & Atmospheric Sciences, Georgia Institute of Technology, Atlanta, GA 30332-0340, USA.*
[c]*School of Environmental and Municipal Engineering, Qingdao Technological University, Fushun Road 11. 266033 Qingdao, Shandong, P.R. China.*
[d]*Centre for Theoretical Computational Chemistry, Department of Chemistry, University of Oslo, P.O.Box 1033 Blindern, 0316 Oslo, Norway. E-mail: c.j.nielsen@kjemi.uio.no*
[e]*Present address: Portnoy Environmental Inc. (PEI), 1414 Sam Houston Parkway N., Suite 170, Houston, TX 77043, USA.*
†Electronic supplementary information (ESI) available: Figures of reactants, products and stationary points on the reaction surfaces. Tables with rate coefficients, energies of reactants, products and stationary points on the reaction surfaces. See DOI: 10.1039.xxxxxxxxxx

In this paper, we report a combined experimental and theoretical study of the reactions of Cl atoms with mono-, di- and tri-methyl amine.

$$Cl + CH_3NH_2 \rightarrow \text{products} \quad (R1)$$
$$Cl + (CH_3)_2NH \rightarrow \text{products} \quad (R2)$$
$$Cl + (CH_3)_3N \rightarrow \text{products} \quad (R3)$$

Experimental determinations of temperature- and pressure-dependent rate coefficients for R1–R3 are reported for the first time, as are theoretical analyses of reaction potential energy surfaces and kinetics. The potential influence of R1–R3 on the atmospheric chemistry of the studied amines is qualitatively assessed.

Experimental Approach

The kinetics of Cl reactions with CH_3NH_2, $(CH_3)_2NH$, and $(CH_3)_3N$ have been studied under pseudo-first order conditions with the amine as the excess reagent using the laser flash photolysis (LFP) – resonance fluorescence (RF) technique. In the LFP−RF approach, Cl atoms are produced on a nanosecond time scale via LFP of a suitable Cl-containing precursor. A chlorine resonance lamp, which consists of an electrodeless microwave discharge through a flowing gas mixture containing a trace of Cl_2 in helium, continuously excites vacuum-UV fluorescence in the photolytically produced Cl atoms. The fluorescence signal is monitored by a solar blind photomultiplier and signals are processed using photon-counting techniques in conjunction with multichannel scaling. As long as the Cl atom concentration is relatively low (less than 10^{12} atoms per cm^3 under typical operating conditions), the fluorescence signal is proportional to the Cl atom concentration.

A schematic diagram of the LFP−RF apparatus is published elsewhere.[13] The apparatus is similar in configuration to those employed in a number of earlier studies of chlorine atom kinetics carried out at Georgia Tech.[14-19] Details of the experimental approach that are specific to this study are provided below.

A jacketed Pyrex® reaction cell with an internal volume of 150 cm^3 was used in all experiments. The cell was maintained at a constant temperature by circulating ethylene glycol from a thermostated bath through the outer jacket. A copper-constantan thermocouple was inserted into the reaction zone through a vacuum seal, thus allowing measurement of the gas temperature under the precise pressure and flow rate conditions of the experiment. The temperature variation in the reaction volume, i.e., the volume from which fluorescence could be detected, was less than 2 K at the highest temperature employed in the study (435 K) and less than 1 K at the lowest temperature employed (274 K).

Atomic chlorine was produced by 248 nm laser flash photolysis of phosgene, Cl_2CO.

$$Cl_2CO + h\nu\,(248\text{ nm}) \rightarrow 2\,Cl + CO \quad (R4)$$

A GAM EX50 KrF excimer laser served as the 248 nm light source; its pulse width is ~20 ns and fluences employed in the study ranged from 3 to 67 mJ cm^{-2} $pulse^{-1}$.

All details concerning the operation of the resonance lamp and signal processing electronics are published elsewhere.[14-19] For each chlorine atom decay rate measured, signals from a large number of laser shots (100−20000) were averaged to obtain a well-defined pseudo-first order temporal profile over (typically) three e-folding times of chlorine atom decay.

Both excited spin-orbit state chlorine atoms ($^2P_{1/2}$) and ground state chlorine atoms ($^2P_{3/2}$) can be produced by the ultraviolet photo-dissociation of phosgene; the fraction of excited Cl($^2P_{1/2}$) has been reported to be <10% at 248 nm.[20] The RF detection scheme is sensitive to both spin orbit states. To ensure rapid deactivation of Cl($^2P_{1/2}$) atoms, approximately 0.5 Torr CO_2 was added to each Cl_2CO/amine/N_2 reaction mixture. Since the rate coefficient for deactivation of Cl($^2P_{1/2}$) by CO_2 is $(1.2 \pm 0.3) \times 10^{-11}$ cm^3 $molecule^{-1}$ s^{-1},[21-23] the time scale for spin-orbit state equilibration was always very rapid compared to the time scale for chemical reaction of Cl atoms.

In order to avoid accumulation of photochemically generated reactive species, all experiments were carried out under "slow flow" conditions. The linear flow rate through the reactor was typically 3 cm s^{-1} (1.4−9 cm s^{-1} was the complete range), while the laser repetition rate was typically 6 Hz (3−7 Hz was the complete range). Since the direction of flow was perpendicular to the photolysis laser beam, no volume element of the reaction mixture was subjected to more than a few laser shots. Phosgene (Cl_2CO) and amines were introduced into the reaction cell from 12-liter Pyrex® bulbs containing dilute mixtures in N_2, while CO_2 and N_2 were flowed directly from their high pressure storage cylinders. All gas flows were controlled by needle valves and measured using calibrated mass flow meters. The amine/N_2 gas mixture, CO_2, and additional N_2 were premixed before entering the reaction cell whereas the Cl_2CO/N_2 mixture was injected into reaction mixture flow (typically) 2 cm upstream from the reaction zone; this approach minimized interferences from hydrolysis of Cl_2CO on reactor walls and dark reaction of amines with the HCl product of Cl_2CO hydrolysis. At 298 K, kinetics results were found to be independent of injector position over the range 2−10 cm upstream from the reaction zone, and also independent of the fraction of total flow attributable to the Cl_2CO/N_2 mixture over the ranges 2−18% for R1, 0.5−13% for R2, and 0.5−12% for R3. These observations demonstrate that mixing of Cl_2CO into the overall flow was complete by the time the flow reached the reaction zone.

Concentrations of each component in the reaction mixture were determined from the corresponding bulb concentrations, the mass flow rates and the total pressures. The bulb concentrations of each amine were measured frequently by UV photometry at 213.9 nm using a zinc penray lamp as the light source. The absorption cross sections employed to convert measured absorbances to concentrations were determined as part of this study and are, in unit of 10^{-18} cm^2 $molecule^{-1}$, 2.35 for CH_3NH_2, 1.27 for $(CH_3)_2NH$ and 4.39 for $(CH_3)_3N$. The

cross section we determined for CH_3NH_2 is about 25% larger than a single literature value.[24]

The gases used in this study had the following stated minimum purities: CO_2, 99.99%; Cl_2CO, 99.9%; CH_3NH_2, 98%; $(CH_3)_2NH$, 99%; and $(CH_3)_3N$, 99%. The above purities all refer to the liquid phase in the high-pressure storage cylinders. The N_2 used in this study was the gas obtained as seep-off from a high-pressure liquid nitrogen cylinder. Nitrogen and CO_2 were used as supplied while the other gases were degassed repeatedly at 77 K before being used to prepare mixtures with N_2.

Computational methods and details

Electronic structure calculations

Geometries and frequencies of the stationary points on the amine + chlorine atom potiential energy surfaces were calculated using second order Møller-Plesset perturbation theory (MP2) with Dunning's correlation consistent cc-pVTZ basis set.[25] The pre- and post-reaction adducts were localized by calculating the reaction path in mass weighted coordinates (IRC).

Improved single point energies of the stationary points were calculated using explicitly correlated Coupled Cluster Singles and Doubles with perturbative triples, CCSD(T)-F12a,[26, 27] with Dunnings triple-zeta basis set augmented with diffuse functions, aug-cc-pVTZ.[28] The MP2 calculations were performed using Gaussian09,[29] while the explicitly correlated coupled cluster calculations were performed in Molpro 2012.1.[30, 31]

Calculation of rate coefficients

The kinetics of the different methyl amine + chlorine atom systems are governed by both the formation of a pre-reaction adduct and one or more tight transition states. To account for both inner and outer transition states, the steady state approximation was used at the microcanonical level, which gives an effective number of states for the overall reaction:

$$N(E)_{eff} = \frac{N_{Outer} \cdot \left(N_{TSN} + N_{TSC}\right)}{N_{TSN} + N_{TSC} + N_{Outer}} \quad \text{(E1)}$$

where N_{Outer}, N_{TSC} and N_{TSN} represents the number of states in the outer transition state, and the transition states for hydrogen abstraction from the C and N atom respectively ($N_{\mathrm{TSN}} = 0$ for TMA). In equation E1 it is assumed that the reaction occurs in the low pressure limit and that the pre-reaction complexes therefore do not undergo any collisions with the bath gas molecules. Since all barriers are significantly below zero, the possibility of tunnelling is included in the model. In the case of TMA + chlorine this model is identical to the two-transition state model proposed by Greenwald *et al*.[32]

It is further assumed that the post-reaction complexes dissociate rapidly, i.e. no back reaction is considered, and the thermal rate coefficients can then be calculated by Boltzmann weighting the effective number of states:

$$\int_0^\infty \frac{N(E) \cdot \exp(-E/k_B T)}{h \cdot Q_R(T)} dE \quad \text{(E2)}$$

The number of open states for the inner transition states was calculated using a rovibrational Beyer-Swinehart algorithm,[33] with ro-vibrational data from the MP2/cc-pVTZ calculations, while the number of states for the outer transition states was estimated using a capture model equivalent to Langevin-theory (see Smith[34] and references therein), but with the replacement of the ion-induced dipole potential with the sum of the London and the Debye forces.

$$V(R) = -\frac{3 I_A I_B}{2(I_A + I_B)} \cdot \frac{\alpha_A \alpha_B}{R^6} - \frac{\mu_A^2 \alpha_B}{4\pi\varepsilon_0 R^6} \quad \text{(E3)}$$

Experimental values for the dipole moments, μ_i, polarizabilities, α_i, and the first ionisation potentials, I_i, are summarized in Table S1 (Electronic Supplementary Information, ESI) and stem from the NIST database.[35]

The two spin-orbit states $^2P_{3/2}$ (lowest) and $^2P_{1/2}$ of Cl having degeneracies of 4 and 2, respectively, and separated by 882 cm^{-1} were included in the calculation of the electronic partition function. Since spin-orbit coupling present in the Cl atom becomes smaller during the reaction it will contribute to the potential energy surface by effectively lowering the non-relativistic energy of the reactants by 1/3 of the SO coupling constant of Cl (3.5 kJ mol^{-1}) assuming negligible SO coupling in the transition state.

Results

Kinetic experiments

As mentioned above, all experiments were carried out under pseudo–first order conditions with [amine] >> $[Cl]_0$. Hence, in the absence of side reactions that remove or produce $Cl(^2P_J)$ atoms, the $Cl(^2P_J)$ temporal profile following the laser flash is described by the following relationship:

$$\ln\{[Cl]_0/[Cl]_t\} = \ln\{S_0/S_t\} = (k_{Ri}[\text{amine}] + k_{R5})\, t = k\, t \quad \text{(E4)}$$

In equation (E4), S_0 is the RF signal at a time immediately after the laser fires, S_t is the RF signal at a later time t; k_i (i = 1, 2 or 3) is the total bimolecular rate coefficient for all $Cl(^2P_J)$ + amine reaction channels that are irreversible on the experimental time scale; k is the pseudo–first order $Cl(^2P_J)$ fluorescence signal decay rate coefficient; and k_{R5} is the first-order rate coefficient for background $Cl(^2P_J)$ atom loss:

$$Cl(^2P_J) \rightarrow \text{loss by diffusion from the detector field of view and/or reaction with background impurities.} \quad \text{(R5)}$$

k_{R5} was directly measured by observing the RF temporal profile in the absence of added amine for each set of reaction conditions; while not strictly first order, the parameterization of k_{R5} as a first order process is an excellent approximation for the first 5 ms after the laser flash, which is the relevant time scale for analysis of all kinetic data.

The bimolecular rate coefficients of interest, k_{Ri}(P,T), i = 1−3, are obtained from the slopes of plots of k' versus [amine] for data obtained at constant temperature and total pressure. Although numerous possible impurities in the methyl amine samples can react rapidly with atomic chlorine, we can assume impurity reactions are of negligible importance because the rate coefficients for reactions R1−R3 are measured to be very fast (see below) and, as reported above, the amine purities were ≥ 98%.

Overall, the observed kinetics are consistent with the behavior predicted by equation (E4), i.e., observed Cl(^{2}P$_J$) temporal profiles are exponential and observed k are found to increase linearly with increasing [amine]. Furthermore, observed kinetics were found to be independent of significant variations in laser fluence, confirming the expectation that radical concentrations were low enough to render radical−radical side reactions too slow to be a significant kinetic interference on the time scale of Cl(^{2}P$_J$) decay. Typical Cl(^{2}P$_J$) temporal profiles are shown in Figure 1 and typical plots of k versus [amine] are shown in Figure 2.

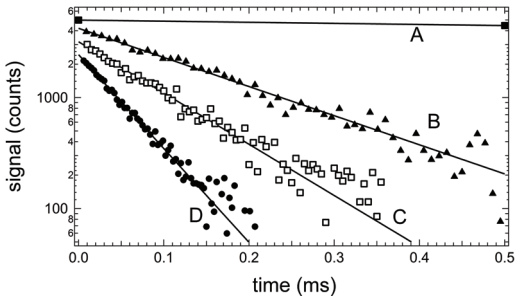

Figure 1. Typical resonance fluorescence temporal profiles observed in kinetic studies of R1–R3. Experimental conditions: T = 296 K, P = 25 Torr, linear flow rate through reactor = 3.0 cm s^{-1}. Concentrations (10^{11} cm^{-3}): [Cl_2CO] = (A) 481, (B) 391, (C) 378 and (D) 481; [CO_2] = 210000; [Cl]$_0$ = (A) 3, (B) 0.8, (C) 0.8, (D) 2; [CH_3NH_2] = (A) 0, (B) 212, (C) 364 and (D) 678. Number of laser shots averaged = (A) 20, (B) 6000, (C) 9000 and (D) 11000. Solid lines are obtained from nonlinear least–squares analyses of the Cl(^{2}P$_J$) fluorescence signal versus time data and give the following pseudo–first–order decay rates (k') in units of s^{-1}: (A) 76, (B) 6050, (C) 10600 and (D) 19500. For clarity, traces (A), (B) and (C) are scaled upwards by factors of 3.0, 2.4 and 2.0, respectively. Most of the data used to determine the decay rate for trace (A) were obtained at longer times than those shown in the Figure.

For all three Cl + amine reactions studied, bimolecular rate coefficients were, within experimental uncertainties, found to be independent of pressure over the range 25–400 Torr N_2. Such observational evidence supports the idea that the dominant pathway for Cl(^{2}P$_J$) + amine reactions over the full range of temperature and pressure investigated is H–transfer. Measured bimolecular rate coefficients for reactions R1−R3 are summarized in Tables S2−S4 (Electronic Supplementary Information, ESI).

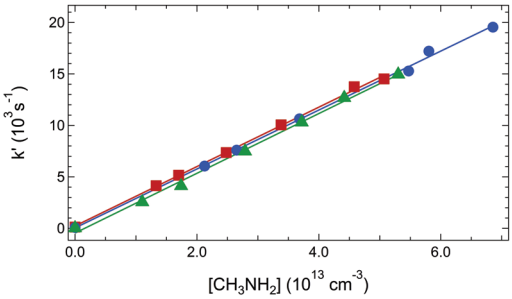

Figure 2. Plots of k versus [CH_3NH_2] for data obtained at different temperatures and pressures. Solid lines are obtained from linear least–squares analyses and lead to the bimolecular rate coefficients reported in Table S2 (ESI). Blue: 296 K, 25 Torr. Green: 296 K, 200 Torr. Red: 419 K, 25 Torr.

Because the precisions of tabulated k_{Ri} values are quite good (2σ < 5% at 298 K and 2σ < 11% at other temperatures), we estimate that the absolute uncertainty of reported values for k_{Ri} is ±10% at 298 K and ±16% at other temperatures. Since interfering side reactions appear to be of negligible importance (see above), the primary source of systematic error appears to be associated with amine concentration determinations.

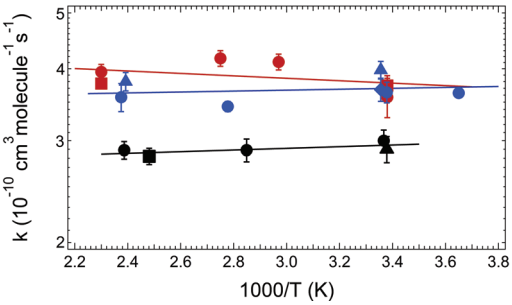

Figure 3. Arrhenius plots for Cl(^{2}P$_J$) reactions with CH_3NH_2 (R1, black), $(CH_3)_2NH$ (R2, red), and $(CH_3)_3N$ (R3, blue). Solid lines are obtained from linear least squares analyses of the unweighted ln k_{Ri} versus T^{-1} data; the best fit Arrhenius expressions in units of 10^{-10} cm^3 molecule^{-1} s^{-1} are k_{R1} = 2.63 exp(+33/T), k_{R2} = 4.46 exp(−49/T), and k_{R3} = 3.47 exp(+18/T). Error bars are 2σ, precision only.

Arrhenius plots for reactions R1−R3 are shown in Figure 3. The following best fit Arrhenius expressions are derived from linear least–squares analyses of the ln k_{Ri} versus T^{-1} data (units are 10^{-10} cm^3 molecule^{-1} s^{-1}):

$$k_{R1}(T) = (2.63 \pm 0.30) \exp\{(+33 \pm 38) / T\}$$
$$k_{R2}(T) = (4.46 \pm 1.45) \exp\{(-49 \pm 113) / T\}$$
$$k_{R3}(T) = (3.47 \pm 0.46) \exp\{(+18 \pm 78) / T\}$$

Uncertainties in the above expressions are 2σ and represent the precision of the Arrhenius parameters. Given that the statistical uncertainties in measured activation energies are larger than the activation energies themselves, the following temperature independent rate coefficients (obtained from computing

unweighted averages of experimental k_{Ri} values) are also considered adequate representations of the experimental data (units are 10^{-10} cm^{3}molecule^{-1}s^{-1}): k_{R1} = 2.90 ± 0.13, k_{R2} = 3.89 ± 0.46, and k_{R3} = 3.68 ± 0.35, where the uncertainties are two standard deviations of the average. Absolute uncertainties in these rate coefficients are estimated to be ±15% at the 95% confidence level.

Structures and Energies of Stationary Points

The stationary points on the potential energy surfaces (PES) of the Cl reactions with MA, DMA and TMA were located in MP2/cc-pVTZ calculations. Improved energies were obtained in CCSD(T)-F12a/aug-cc-pVTZ calculations; the results are summarized in Tables S5−S7 (ESI) and illustrated in Figure 4. Cartesian coordinates of reactants, products and stationary points on the PES obtained in MP2/cc-pVTZ calculations are given in Table S8 (ESI), which also includes illustrations of the stationary point structures. The minimum energy path (MEP) connecting reactants and products of the Cl reactions with MA, DMA and TMA were computed using the intrinsic reaction coordinate (IRC) method[36] at the MP2/cc-pVTZ level of theory. In addition to the saddle points of the hydrogen abstraction reactions we have located a pre-reaction van der Waals adduct on the MEP for all reactions. On the product side of the MEP there is a post-reaction van der Waals adduct between amino radicals and HCl. In summary, the general and prominent features of the amine + Cl reaction PES are strong pre-reaction complexes and saddle points with energies below that of the corresponding reactants.

Calculated rate coefficients

Results from the kinetics calculations are summarized in Table S9 (ESI), and the overall theoretical rate coefficients can be parameterized:

$$k_{R1}(T) = 2.13 \exp\{+99 / T\} \text{ or } 2.22\,(T/298\text{K})^{-0.037}$$
$$k_{R2}(T) = 2.89 \exp\{-87 / T\} \text{ or } 2.87\,(T/298\text{K})^{0.250}$$
$$k_{R3}(T) = 4.38 \exp\{-105 / T\} \text{ or } 2.98\,(T/298\text{K})^{0.301}$$

The calculated rate coefficients are in very good agreement with the experimental values with the largest deviations being around 35%. This good agreement is to a large extent caused by the fact that the reactions are very close to being collision controlled.

The sensitivity of the rate coefficients to the calculated energy barriers were tested by shifting the calculated barriers by 4 kJ/mol in opposite directions. The maximum change in overall rate coefficients was 7%, 1% and no change for MA, DMA and TMA respectively. The room temperature branching ratio for the MA reaction was found to be more sensitive to the barrier heights as lowering the barrier for C-abstraction and raising the barrier for N-abstraction gave 1C:99N while shifting the barriers in opposite directions gave 40C:60N. For the DMA no change was observed.

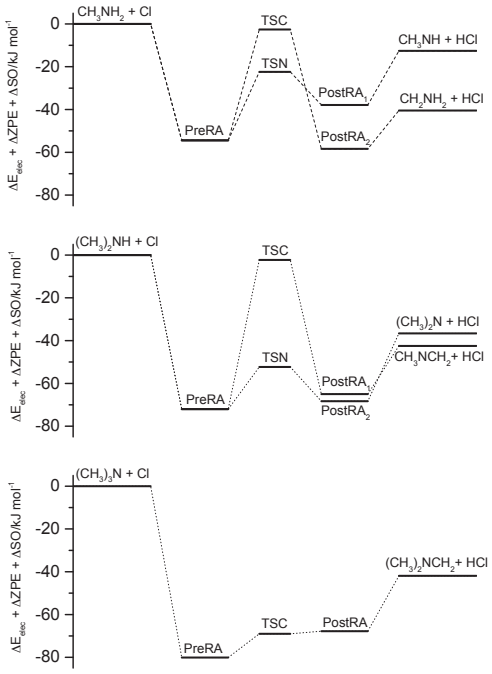

Figure 4. Reletive energies of stationary points on the potential energy surfaces of the CH_3NH_2 + Cl, $(CH_3)_2NH$ + Cl and $(CH_3)_3N$ + Cl reactions. Results from CCSD(T)-F12a/aug-cc-pVTZ//MP2/cc-pVTZ calculations.

Discussion

Literature Comparisons

Rudić *et al*.[12] carried out a theoretical study of the MA + Cl reaction employing a variant of G2-model chemistry,[37] and found essentially the same PES as derived in the present study. In particular, they identified the strongly bound pre-reactive complex as a 2-center-3-electron bond involving the nitrogen lone pair and the unpaired electron on Cl. The magnitude of the Cl–N bond strengths calculated in this study are slightly larger than the one measured for pyridine,[38] which can be attributed to the methyl groups donating electron density to the N lone pair.

The MA + Cl reaction dynamics study shows a roughly 50:50 branching in the initial abstraction.[12] It should be noted that the reactants are far from being thermalized in the study: the translational collision energy is about 2000 cm^{-1}, and there is very little rotational or vibrational energy in the methylamine reactant (2000 cm^{-1} corresponds to a translational temperature of ~ 2900 K). The present calculations show an increase in the C-H abstraction yield from 0.09 at 300 K to 0.22 at 600 K, so the 50 % yield reported in the reaction dynamics study[12]

appears to be in reasonable agreement with the theoretical findings of this study.

Implications for Atmospheric Chemistry of Amines

Consideration of the rate coefficients reported in this study in conjunction with rate coefficients for OH + amine reactions that were reported recently by Onel *et al*.,[39] suggests that the Cl rate coefficients are faster at 298 K by factors of 16, 6, and 6 for MA, DMA, and TMA, respectively, and that these rate coefficient ratios change very little as a function of temperature. In the marine boundary layer, Cl concentrations are typically 1–10 percent of OH concentrations[9] Hence, it appears that reaction with Cl is a minor but significant sink for amines in marine environments.

The calculated branching ratios in the MA and DMA reactions with Cl suggest that N-H abstraction dominates in the chlorine reactions in contrast to the corresponding OH reactions, where C-H abstraction dominates.[40-42] In areas with elevated chlorine atom concentrations the Cl reactions may therefore contribute significantly to nitramine and nitrosamine formation (*i.e.* RR'N + NO_2 → RR'NNO_2). An experimental determination of the branching ratios for the MA and DMA + Cl reactions is clearly needed.

Conclusions

The rate coefficients for the chlorine atom reactions with methylamine, dimethylamine and trimethylamine have been determined using the laser flash photolysis – resonance fluorescence technique. The reactions are extremely fast with nearly temperature independent rate coefficients close to the gas kinetic collision limit. Quantum chemical calculations show that the reactions are dominated by strongly bound pre-reaction complexes and submerged barriers, and statistical rate theory confirms that the reactions are collision controlled. Reaction with Cl appears to make a small but non-negligible contribution to destruction of amines in marine atmospheric environments. Unlike OH reactions with mono- and di-methyl amine, the Cl reactions are predicted theoretically to proceed predominantly by abstraction of hydrogen from the N atom, thus making Cl + amine reactions a potentially important source of atmospheric nitramines and nitrosamines.

Acknowledgements

This work is part of the technology qualification of amines for the CO_2 Capture Mongstad Project (CCM) funded by the Norwegian state through Gassnova SF. Additional support to the University of Oslo from the Research Council of Norway through a Centre of Excellence Grant (Grant No. 179568/V30) is acknowledged. Additional support to Georgia Tech from NASA (Grant No. NNX12AE02G) is also acknowledged.

Notes and references

1. X. Ge, A. S. Wexler and S. L. Clegg, *Atmos. Environ.*, 2011, **45**, 524-546.
2. X. Ge, A. S. Wexler and S. L. Clegg, *Atmos. Environ.*, 2011, **45**, 561-577.
3. C. J. Nielsen, H. Herrmann and C. Weller, *Chem. Soc. Rev.*, 2012, **41**, 6684-6704.
4. D. Lee and A. S. Wexler, *Atmos. Environ.*, 2013, **71**, 95-103.
5. R. Atkinson, *Chemical Reviews*, 1986, **86**, 69-201.
6. P. Paasonen, T. Olenius, O. Kupiainen, T. Kurten, T. Petaja, W. Birmili, A. Hamed, M. Hu, L. G. Huey, C. Plass-Duelmer, J. N. Smith, A. Wiedensohler, V. Loukonen, M. J. McGrath, I. K. Ortega, A. Laaksonen, H. Vehkamaki, V. M. Kerminen and M. Kulmala, *Atmos. Chem. Phys.*, 2012, **12**, 9113-9133.
7. J. Almeida, S. Schobesberger, A. Kurten, I. K. Ortega, O. Kupiainen-Maatta, A. P. Praplan, A. Adamov, A. Amorim, F. Bianchi, M. Breitenlechner, A. David, J. Dommen, N. M. Donahue, A. Downard, E. Dunne, J. Duplissy, S. Ehrhart, R. C. Flagan, A. Franchin, R. Guida, J. Hakala, A. Hansel, M. Heinritzi, H. Henschel, T. Jokinen, H. Junninen, M. Kajos, J. Kangasluoma, H. Keskinen, A. Kupc, T. Kurten, A. N. Kvashin, A. Laaksonen, K. Lehtipalo, M. Leiminger, J. Leppa, V. Loukonen, V. Makhmutov, S. Mathot, M. J. McGrath, T. Nieminen, T. Olenius, A. Onnela, T. Petaja, F. Riccobono, I. Riipinen, M. Rissanen, L. Rondo, T. Ruuskanen, F. D. Santos, N. Sarnela, S. Schallhart, R. Schnitzhofer, J. H. Seinfeld, M. Simon, M. Sipila, Y. Stozhkov, F. Stratmann, A. Tome, J. Trostl, G. Tsagkogeorgas, P. Vaattovaara, Y. Viisanen, A. Virtanen, A. Vrtala, P. E. Wagner, E. Weingartner, H. Wex, C. Williamson, D. Wimmer, P. Ye, T. Yli-Juuti, K. S. Carslaw, M. Kulmala, J. Curtius, U. Baltensperger, D. R. Worsnop, H. Vehkamaki and J. Kirkby, *Nature*, 2013, **502**, 359-363.
8. M. Rozenberg, A. Loewenschuss and C. J. Nielsen, *J. Phys. Chem. A*, 2014, **118**, 1004-1011.
9. O. W. Wingenter, B. C. Sive, N. J. Blake, D. R. Blake and F. S. Rowland, *J. Geophys. Res. Atmos.*, 2005, **110**, D20308.
10. J. A. Thornton, J. P. Kercher, T. P. Riedel, N. L. Wagner, J. Cozic, J. S. Holloway, W. P. Dube, G. M. Wolfe, P. K. Quinn, A. M. Middlebrook, B. Alexander and S. S. Brown, *Nature*, 2010, **464**, 271-274.
11. J. D. Raff, B. Njegic, W. L. Chang, M. S. Gordon, D. Dabdub, R. B. Gerber and B. J. Finlayson-Pitts, *Proc. Natl. Acad. Sci. U.S.A.*, 2009, **106**, 13647-13654.
12. S. Rudic, C. Murray, J. N. Harvey and A. J. Orr-Ewing, *Phys. Chem. Chem. Phys.*, 2003, **5**, 1205-1212.
13. B. J. Finlayson-Pitts and J. N. Pitts, Jr., *Chemistry of the upper and lower atmosphere*, Academic Press, San Diego, 2000, p.146.
14. R. E. Stickel, J. M. Nicovich, S. Wang, Z. Zhao and P. H. Wine, *J. Phys. Chem.*, 1992, **96**, 9875-9883.
15. J. M. Nicovich, S. Wang and P. H. Wine, *Int. J. Chem. Kinet.*, 1995, **27**, 359-368.
16. J. J. Orlando, C. A. Piety, J. M. Nicovich, M. L. McKee and P. H. Wine, *J. Phys. Chem. A*, 2005, **109**, 6659-6675.
17. J. M. Nicovich, S. Parthasarathy, F. D. Pope, A. T. Pegus, M. L. McKee and P. H. Wine, *J. Phys. Chem. A*, 2006, **110**, 6874-6885.
18. Z. Zhao, D. T. Huskey, J. M. Nicovich and P. H. Wine, *Int. J. Chem. Kinet.*, 2008, **40**, 259-267.
19. M. Marinkovic, M. Gruber-Stadler, J. M. Nicovich, R. Soller, M. Mülhäuser, P. H. Wine, L. Bache-Andreassen and C. J. Nielsen, *J. Phys. Chem. A*, 2008, **112**, 12416-12429.
20. A. I. Chichinin, *Chem. Phys. Lett.*, 1993, **209**, 459-463.
21. S. A. Sotnichenko, V. C. Bokun and A. I. Nadkhin, *Chem. Phys. Lett.*, 1988, **153**, 560-568.
22. A. I. Chichinin, *Khim. Fiz.*, 1996, **15**, 49-63.
23. Y. Matsumi, K. Izumi, V. Skorokhodov, M. Kawasaki and N. Tanaka, *J. Phys. Chem. A*, 1997, **101**, 1216-1221.
24. M. J. Hubin-Franskin, J. Delwiche, A. Giuliani, M. P. Ska, F. Motte-Tollet, I. C. Walker, N. J. Mason, J. M. Gingell and N. C. Jones, *J. Chem. Phys.*, 2002, **116**, 9261-9268.
25. T. H. Dunning, Jr., *J. Chem. Phys.*, 1989, **90**, 1007-1023.
26. T. B. Adler, G. Knizia and H.-J. Werner, *J. Chem. Phys.*, 2007, **127**, 221106.
27. G. Knizia, T. B. Adler and H.-J. Werner, *J. Chem. Phys.*, 2009, **130**, 054104.
28. R. A. Kendall, T. H. Dunning, Jr. and R. J. Harrison, *J. Chem. Phys.*, 1992, **96**, 6796-6806.

29. M. J. Frisch, G. W. Trucks, H. B. Schlegel, G. E. Scuseria, M. A. Robb, J. R. Cheeseman, G. Scalmani, V. Barone, B. Mennucci, G. A. Petersson, H. Nakatsuji, M. Caricato, X. Li, H. P. Hratchian, A. F. Izmaylov, J. Bloino, G. Zheng, J. L. Sonnenberg, M. Hada, M. Ehara, K. Toyota, R. Fukuda, J. Hasegawa, M. Ishida, T. Nakajima, Y. Honda, O. Kitao, H. Nakai, T. Vreven, J. Montgomery, J. A.; , J. E. Peralta, F. Ogliaro, M. Bearpark, J. J. Heyd, E. Brothers, K. N. Kudin, V. N. Staroverov, R. Kobayashi, J. Normand, K. Raghavachari, A. Rendell, J. C. Burant, S. S. Iyengar, J. Tomasi, M. Cossi, N. Rega, J. M. Millam, M. Klene, J. E. Knox, J. B. Cross, V. Bakken, C. Adamo, J. Jaramillo, R. Gomperts, R. E. Stratmann, O. Yazyev, A. J. Austin, R. Cammi, C. Pomelli, J. W. Ochterski, R. L. Martin, K. Morokuma, V. G. Zakrzewski, G. A. Voth, P. Salvador, J. J. Dannenberg, S. Dapprich, A. D. Daniels, O. Farkas, J. B. Foresman, J. V. Ortiz, J. Cioslowski and D. J. Fox, *Gaussian 09, Revision B.01*, (2009) Gaussian, Inc., Wallingford CT.
30. H.-J. Werner, P. J. Knowles, G. Knizia, F. R. Manby and M. Schuetz, *Wiley Interdiscip Rev Comput Mol Sci*, 2012, **2**, 242-253.
31. H.-J. Werner, P. J. Knowles, G. Knizia, F. R. Manby, M. Schütz, P. Celani, T. Korona, R. Lindh, A. Mitrushenkov, G. Rauhut, K. R. Shamasundar, T. B. Adler, R. D. Amos, A. Bernhardsson, A. Berning, D. L. Cooper, M. J. O. Deegan, A. J. Dobbyn, F. Eckert, E. Goll, C. Hampel, A. Hesselmann, G. Hetzer, T. Hrenar, G. Jansen, C. Köppl, Y. Liu, A. W. Lloyd, R. A. Mata, A. J. May, S. J. McNicholas, W. Meyer, M. E. Mura, A. Nicklass, D. P. O'Neill, P. Palmieri, D. Peng, K. Pflüger, R. Pitzer, M. Reiher, T. Shiozaki, H. Stoll, A. J. Stone, R. Tarroni, T. Thorsteinsson and W. M., *MOLPRO, version 2012.1, a package of ab initio programs*, (2012).
32. E. E. Greenwald, S. W. North, Y. Georgievskii and S. J. Klippenstein, *J. Phys. Chem. A*, 2005, **109**, 6031-6044.
33. T. Beyer and D. F. Swinehart, *Commun. ACM*, 1973, **16**, 379-379.
34. I. W. M. Smith, *Angew. Chem. Int. Ed. Engl.*, 2006, **45**, 2842-2861.
35. NIST Computational Chemistry Comparison and Benchmark Database. NIST Standard Reference Database Number 101, R. D. Johnson III, Release 16a, August 2013. http://cccbdb.nist.gov/
36. C. Gonzalez and H. B. Schlegel, *J. Phys. Chem.*, 1990, **94**, 5523-5527.
37. L. A. Curtiss, K. Raghavachari, G. W. Trucks and J. A. Pople, *J. Chem. Phys.*, 1991, **94**, 7221-7230.
38. Z. Zhao, D. T. Huskey, K. J. Olsen, J. M. Nicovich, M. L. McKee and P. H. Wine, *Phys. Chem. Chem. Phys.*, 2007, **9**, 4383-4394.
39. L. Onel, L. Thonger, M. A. Blitz, P. W. Seakins, A. J. C. Bunkan, M. Solimannejad and C. J. Nielsen *J. Phys. Chem. A* 2013, **117**, 10736-10745.
40. C. R. C. Lindley, J. G. Calvert and J. H. Shaw, *Chem. Phys. Lett.*, 1979, **67**, 57-62.
41. C. J. Nielsen, B. D'Anna, M. Karl, M. Aursnes, A. Boreave, R. Bossi, A. J. C. Bunkan, M. Glasius, A.-M. K. Hansen, M. Hallquist, K. Kristensen, T. Mikoviny, M. M. Maguta, M. Müller, Q. Nguyen, J. Westerlund, K. Salo, H. Skov, Y. Stenstrøm and A. Wisthaler, *Summary Report: Photo-oxidation of Methylamine, Dimethylamine and Trimetahylamine. Climit project no. 201604* NILU OR 2/2011, ISBN 978-82-425-2357-0, NILU, 2011.
42. L. Onel, M. Blitz, M. Dryden, L. Thonger and P. Seakins, *Environmental Science & Technology*, 2014, DOI:10.1021/es502398r.

Paper III

Bunkan, A. J. C; Hetzler, J; Mikoviny, T; Wisthaler, A; Nielsen, C. J.; Olzmann, M. Experimental and theoretical study of the OH radical reactions with *N*-methylformamide and *N,N*-dimethylformamide.
Manuscript in preparation

Paper IV

Bunkan, A. J. C.; Tang, Y. and Sellevåg, S. R. and Nielsen, C. J. Atmospheric Gas Phase Chemistry of CH_2=NH and HNC. A First-Principles Approach. *The Journal of Physical Chemistry A* **2014**, 118, 5279-5288.

Paper V

Maguta, M. M.; Aursnes, M. Bunkan, A. J. C.; Edelen, K.; Mikoviny, T; and Nielsen, C. J.; Stenstrøm, Y; Tang, Y; Wisthaler, A. Atmospheric Fate of Nitramines: An Experimental and Theoretical Study of the OH Reactions with CH_3NHNO_2 and $(CH_3)_2NNO_2$. *The Journal of Physical Chemistry A* **2014**, *118*, 3450-3462.

Paper VI

Bunkan, A. J. C.; Liang, C.-H.; Pilling, M. J.; Nielsen, C. J. Theoretical and experimental study of the OH radical reaction with HCN. *Molecular Physics* **2013**, *111*, 1589-1598.